UPPSALA
UNIVERSITET

Digital Comprehensive Summaries of Uppsala Dissertations from the Faculty of Science and Technology 1383

Magnetization dynamics on the nanoscale

From first principles to atomistic spin dynamics

JONATHAN PHILIPPE CHICO CARPIO

ACTA
UNIVERSITATIS
UPSALIENSIS
UPPSALA
2016

ISSN 1651-6214
ISBN 978-91-554-9598-5
urn:nbn:se:uu:diva-287415

Dissertation presented at Uppsala University to be publicly examined in Sieghbahnsalen, Ångströms laboratoriet Lägerhyddsvägen 1, Uppsala, Tuesday, 14 June 2016 at 10:15 for the degree of Doctor of Philosophy. The examination will be conducted in English. Faculty examiner: Professor Samir Lounis (Peter Grünberg Institute (PGI), Forschungszentrum Jülich GmbH).

Abstract
Chico Carpio, J. P. 2016. Magnetization dynamics on the nanoscale. From first principles to atomistic spin dynamics. *Digital Comprehensive Summaries of Uppsala Dissertations from the Faculty of Science and Technology* 1383. 115 pp. Uppsala: Acta Universitatis Upsaliensis. ISBN 978-91-554-9598-5.

In this thesis first-principles methods, based on density functional theory, have been used to characterize a wide range of magnetic materials. Special emphasis has been put on pairwise magnetic interactions, such as Heisenberg exchange and Dzyaloshinskii-Moriya interactions, and also on in the Gilbert damping parameter. These parameters play a crucial role in determining the magnetization dynamics of the considered materials.

Magnetic interaction parameters, has been calculated for several materials based on Co/Ni/Co heterostructures deposited on non-magnetic heavy metals where. The aim was to clarify how the composition of the underlayers affect the magnetic properties, in particular the Dzyaloshinskii-Moriya interactions. The DMI was found to be strongly dependent on the material of the underlayer, which is consistent with previous theoretical works. Such behaviour can be traced back to the change of the spin-orbit coupling with the material of the underlayer, as well as with the hybridization of the *d*- states of the magnetic system with the *d*- state of the non-magnetic substrate.

First-principles calculations of the Gilbert damping parameter has been performed for several magnetic materials. Among them the full Heusler families, Co_2FeZ, Co_2MnZ with Z=(Al, Si, Ga, Ge). It was found that the first-principles methods, reproduce quite well the experimental trends, even though the obtained values are consistently smaller than the experimental measurements. A clear correlation between the Gilbert damping and the density of states at the Fermi energy was found, which is in agreement with previous works. In general as the density of states at the Fermi energy decreases, the damping decreases also.

The parameters from first principles methods, have been used in conjunction with atomistic spin dynamics simulations, in order to study ultra-narrow domain walls. The domain wall motion of a monolayer of Fe on W(110) has been studied for a situation when the domain wall is driven via thermally generated spin waves from a thermal gradient. It was found that the ultra-narrow domain walls have an unexpected behaviour compared to wide domain walls in the continuum limit. This behaviour have been explained by the fact that for ultra-narrow domain walls the reflection of spin waves is not negligible.

Furthermore, the dynamics of topologically protected structures, such as topological excitations in a kagome lattice and edge dislocations in FeGe has been studied. For the FeGe case, the description of the thermally driven dynamics of the edge dislocations, was found to be a possible explanation for the experimentally observed time dependence of the spiral wavelength. In the kagome lattice, it was also found that due to its topological properties, topological excitations can be created in it.

Jonathan Philippe Chico Carpio, Department of Physics and Astronomy, Materials Theory, Box 516, Uppsala University, SE-751 20 Uppsala, Sweden.

ISSN 1651-6214
ISBN 978-91-554-9598-5
urn:nbn:se:uu:diva-287415 (http://urn.kb.se/resolve?urn=urn:nbn:se:uu:diva-287415)

To my family

List of papers

This thesis is based on the following papers, which are referred to in the text by their Roman numerals.

I **Chico, J.**, Etz, C., Bergqvist, L., Eriksson, O., Fransson, J., Delin, A. and Bergman, A.
Thermally driven domain-wall motion in Fe on W(110)
Physical Review B, **90**, 014434, July 2014

II Edström, A., **Chico, J.**, Jakobsson, A., Bergman, A., and Rusz J.
Electronic structure and magnetic properties of L10 binary alloys
Physical Review B, **90**, 014402, July 2014

III Pereiro, M., Yudin, D., **Chico, J.**, Etz, C., Eriksson, O. and Bergman, A.
Topological excitations in a kagome magnet
Nature Communications, **5**, 4815, September 2014

IV Dürrenfeld, P. Gerhard J., F. **Chico, J.**, Dumas, R. K., Ranjbar, M., Bergman, A., Bergqvist, L., Delin, A., Gould, C., Molenkamp, L. W. and Åkerman, J.
Tunable damping, saturation magnetization, and exchange stiffness of half-Heusler NiMnSb thin films
Physical Review B, **92**, 214424, December 2015

V Dussaux, A., Schoenherr, P., Koumpouras, K., **Chico, J.**, Chang, K., Lorenzelli, L., Kanazawa, N., Tokura, Y., Garst, M., Bergman, A., Degen, C.L. and Meier, D.
Local dynamics of topological magnetic defects in the itinerant helimagnet FeGe
Submitted Nature Communications.

VI **Chico, J.**, Keshavarz H., S., Kvashnin, Y., Pereiro, M., Di Marco I., Etz, C., Bergman, A. and Bergqvist, L.
First principles studies of the Gilbert damping and exchange interactions for half-metallic Heuslers alloys
Submitted PRB

VII **Chico, J.**, Koumpouras, K., Bergqvist, L. and Bergman, A.
First principle studies of Co/Ni/Co heterostructures on heavy metal substrates.
In preparation

VIII Koumpouras, K., **Chico, J.**, Bergqvist, L. and Bergman, A.
Helical spiral states in the MnZSn half-Heuslers with Z=(Tc, Ru, Rh, Os, Ir, Pt). A first principles study
In preparation

IX **Chico, J.**, Koumpouras, K., Bergqvist, L. and Bergman, A.
Relativistic effects in domain wall dynamics in magnetic heterostrcutures.
In preparation

X Pan, F., **Chico, J.**, Hellsvik, J., Delin, A., Bergman, A. and Bergqvist, L.
A systematic study of Gilbert damping and exchange stiffness at finite temperatures in doped permalloy from first principles calculations
Submitted PRB

During the work in this thesis the following works were also made, but are not included in the thesis.

XI Borlenghi, S., Iubini, S., Lepri, S., **Chico, J.**, Bergqvist, L., Delin, A. and Fransson, J.
Energy and magnetization transport in nonequilibrium macrospin systems
Physical Review E, **92**, 012116, July 2015

XII Arnalds, U. B., **Chico, J.**, Stopfel, H., Kapaklis, V., Bärenbold, O., Verschuuren, M. A., Wolff, U., Neu, V., Bergman, A. and Hjörvarsson, B.
A new look on the two-dimensional Ising model: thermal artificial spins
New Journal of Physics, **18**, 023008, January 2016

Reprints were made with permission from the publishers.

Contents

1 Introduction 9

2 Magnetization dynamics 12
2.1 Basics on Magnetism 12
2.2 Heisenberg Model 15
2.2.1 Magnetic ordering 15
2.2.2 Extended Heisenberg model 16
2.3 Landau-Lifshitz equations 17
2.3.1 Micromagnetism 19

3 Density Functional Theory 21
3.1 Kohn-Sham equations 22
3.1.1 Exchange correlation potentials 23
3.1.2 Relativistic DFT 26
3.2 Plane wave methods 27
3.3 Korringa-Kohn-Rostoker approach 28
3.3.1 The Dyson equation 30
3.3.2 Multiple Scattering Theory 32
3.3.3 Coherent Potential Approximation 35

4 Calculation of exchange interactions 37
4.1 LKAG Formalism 38
4.1.1 Exchange interactions for magnetic heterostructures 39
4.1.2 From first principles to micromagnetism 41
4.1.3 Dzyaloshinskii-Moriya interactions 43

5 Magnetocrystalline anisotropy 49
5.1 Origins of the magnetic anisotropy 49
5.1.1 Shape anisotropy 49
5.1.2 Spin-orbit coupling and MAE 50
5.2 Calculating MAE from first principles 51
5.2.1 Total energy calculations 51
5.2.2 Force theorem method 52
5.2.3 Torque method 52

6 The Gilbert damping parameter 56
6.1 Overview of theoretical methods 56
6.1.1 Breathing Fermi surface model 57

6.1.2 Torque correlation model 59

7 Atomistic spin dynamics 64
7.1 Temperature effects 67
7.1.1 Monte Carlo methods 67
7.1.2 Langevin Dynamics 69
7.1.3 Thermally driven dynamics in FeGe 70
7.2 Spin Waves 72
7.2.1 Adiabatic magnon spectra 73
7.2.2 Dynamical structure factor 74
7.3 Domain wall dynamics 77
7.3.1 Thermally driven domain wall motion on Fe/W(110) 80
7.3.2 Current driven domain wall motion 84
7.4 Topology in magnetism 87
7.4.1 Kagome lattice 89

8 Conclusions and Outlook 93

9 Summary in Swedish 95

10 Acknowledgments 97

A SHE torques in the LLG equation 98

References 101

1. Introduction

By 2007 the amount of man made information in the world was estimated to be 2.9×10^{20} bytes[1], even more remarkable on 2013 it was believed that 90% of the data in the world was created in the last two years[2]. Never before has it been so easy to create, modify, store and transmit data as it it today.

The reason behind this unprecedented surge is the development of electronic technology during the second half of the 20th century, which fundamentally changed mankind's relation with information. The advent of electronics allowed the creation of devices which have shifted society from a primordially industry based economy to an information based economy, starting the so-called information age.

The success of electronic applications comes from their ability to use electronic currents within devices to perform logical operations, of this way it is possible to do calculations at a much faster rate than it is possible with mechanical means. As the use of electronics has become widespread the demands placed on them have increased, this has lead to a constant effort for the development of faster, smaller and more energy efficient applications.

The basic unit of these devices is the transistor, which due to technological advances have experienced a constant increase in performance, and decrease in size. However, the transmission of information via an electronic current has limitations. Electronic currents dissipate energy as they are transmitted in the form of heat due to their scattering inside materials. Energy is also lost in capacitors and semiconductor devices due to current leakage. Furthermore electronic transistors have as an ultimate size the atomic limit which puts a hard limitation on how small devices can be. These issues among others, represent some of the problems faced in the design of new electronic devices. Such considerations have lead manufacturers to re-think which is the most efficient way to design new applications. An example of this is the fact that during the last years the speed of each core in a CPU has not increased as fast as previously, as the amount of power needed for even faster computers could lead to overheating of the system, instead more computing cores are added to a single CPU.

While the change of design philosophy has helped manufacturers to overcome many of the problems of electronics, researchers have been actively studying other means to transmit information more efficiently giving rise to new disciplines. A very promising alternative is *spintronics* which use not only the electron charge but also in the spin as a means to transmit information, and *magnonics* which instead use the excitations of magnetic materials (*spin waves*/*magnons*) as information carriers.

Spintronics has been extensively studied in the last decades due to its potential applications for information storage. Its importance is exemplified in the Giant Magneto-Resistance (GMR) effect [3, 4] which earned Albert Fert and Peter Grünberg the Physics Nobel Prize on 2007. The GMR effect describes how the electrical resistance of a magnetic multilayer changes depending on the relative orientation of the magnetization between the layers, with a parallel orientation resulting in a low resistance and an anti-parallel orientation resulting in a high resistance state.

Magnonics has also been studied in great detail as it has a key advantage over electronics, it does not rely on the motion of electron themselves. Instead it uses the magnetic excitations in a material to transmit information. These excitations can be transmitted with low losses and it has been shown that it is possible to create diodes and transistors with them [5–7].

The interest in magnonics and spintronics devices has lead to a renaissance in the field of *magnetic domain walls*. This interest stems from the possible applications that controlled domain wall motion could have for devices such as Magnetic Random Access Memories (MRAMs), including the proposed racetrack memory[8], in which magnetic domains with a given orientation would be used to represent either a 0 or a 1. In order to be able to read and write in such a device, controlled motion of the domain wall is necessary. Both spin polarized electronic currents [9–19] and magnonic currents [20–22] can move domain walls at very high speeds which makes them specially attractive for practical applications.

The renewed interested in domain wall dynamics has motivated the search of new materials for potential applications. Suitable materials must allow for both a high information density as well as fast domain wall motion. Materials with high anisotropy such as perpendicular magnetic anisotropy (PMA) materials, are promising candidates as they would allow for higher information densities [8]. Recent studies have also shown that relativistic effects such as the Dyzaloshinskii-Moriya interaction (DMI) can profoundly influence the domain wall dynamics [23–25].

One of the leading approaches to study domain wall dynamics is numerical simulations. Micromagnetic simulations are one of the most used tools to describe the dynamics of magnetic materials. Here the magnetization of a material is considered as a continuous variable, and due to the size of the systems that can be studied the dipolar interaction is the dominant term. However, to study system at a smaller length scale, when the exchange interactions dominates over dipolar interactions, a micromagnetic simulation might not be the most appropriated method. Instead approaches such as atomistic spin dynamics, in which each of the atomic moments of a system are considered, can be better suited.

By combining *ab initio* methods and atomistic spin dynamics it is possible to describe the material specific domain wall motion generated by a wide range of stimuli. Density Functional Theory (DFT) allows the characteriza-

tion of a system with great accuracy, thus allowing a direct comparison with experimental situations, possibly even permitting the prediction of possible candidates for practical applications.

A quantity that has also received a large amount of attention from the theoretical standpoint is the Gilbert damping. It controls the dissipation rate of energy and angular momentum from the magnetic subsystem to the lattice. Usually, from the magnetization dynamics standpoint, this is either a free parameter, or it is obtained from ferromagnetic resonance FMR experiments [26]. However, thanks to methods as the breathing Fermi surface (BFS) [27] and the torque correlation model (TCM) [28], it is now possible to calculate the damping from first principles methods. This has opened new venues of research, as the capacity of predicting the damping can be of great importance to determine promising materials in the field of magnonics.

In this thesis first principle methods will be used to characterize the properties of magnetic materials, with special emphasis on the interatomic exchange interactions and the Gilbert damping. These will be used in conjunction with atomistic spin dynamics simulations, this with the objective of being able to accurately describe the dynamics of a diverse class of materials. Special emphasis is placed in relativistic effects such as the Dzyaloshinskii-Moriya interaction, the magnetocrystalline anisotropy and the Gilbert damping, due to their importance in the description of magnetic textures such as domain walls and skyrmions and their dynamics.

The thesis is organized in the following manner, in Chapter 2 the basics of magnetism will be introduced. In Chapter 3 the background of density functional theory will be introduced, while paying special care to the description of the Korringa-Kohn-Rostoker method [29, 30], which is used throughout the thesis. The different methods to calculate the exchange interactions will be presented in Chapter 4, with emphasis on the Liechtenstein, Katsnelsson, Antropov and Gubanov (LKAG) [31, 32] formalism. Chapter 5 deals with the methodology to calculate the magnetocrystalline anisotropy. Chapter 6 provides information on the formalism used to calculate the damping parameter from first principles methods. The theory of atomistic spin dynamics and several applications such as domain wall dynamics will be discussed in Chapter 7. Lastly, in Chapter 8 some conclusions and outlook for this thesis will be presented. Throughout the different chapters in this thesis, key results from the included publications will be used to exemplify the theoretical treatments presented in them.

2. Magnetization dynamics

2.1 Basics on Magnetism

The phenomena of magnetism has been known since ancient times. Its influence on the development of devices has been far reaching, revolutionizing the world with inventions ranging from the magnetic compass to modern hard drives. However, the magnetic properties of materials were used throughout history well before an understanding of the origin of magnetism was reached.

It was not until the the 19th century, that the basis of electromagnetic theory was developed. It was James Clerk Maxwell who compiled and realized a coherent theoretical framework which encompassed all the previously work done in electromagnetism. This compilation is known as the Maxwell equations

$$\nabla \cdot \mathbf{E} = \frac{\rho}{\varepsilon_0} \tag{2.1.1a}$$

$$\nabla \cdot \mathbf{B} = 0 \tag{2.1.1b}$$

$$\nabla \times \mathbf{E} = -\frac{\partial \mathbf{B}}{\partial t} \tag{2.1.1c}$$

$$\nabla \times \mathbf{B} = \mu_0 \left(\mathbf{j} + \varepsilon_0 \frac{\partial \mathbf{E}}{\partial t} \right). \tag{2.1.1d}$$

The Maxwell equations in free space (Eq. 2.1.1) show the relations between charged particle densities ρ, current densities $\mathbf{j}$ and magnetic $\mathbf{B}$ and electric $\mathbf{E}$ fields. They form the basis of classical electrodynamics and are completely consistent with special relativity. The Maxwell equations describe how magnetic and electric fields can be created by charged particles and how charged particles react in the presence of these fields. They describe electromagnetic phenomena in a very precise way and represent one of the greatest achievements in physics.

Nonetheless, the spontaneous magnetization present in some materials cannot be accounted for only using the Maxwell equations. In order to account for magnetic fields in a material an electronic current must be constantly flowing through it. An estimation of the magnitude of the current needed to, for example, generate the magnetization of iron $M = 1.76 \times 10^6 \frac{\mathrm{A}}{\mathrm{m}}$ implies that there needs to be a perpetually circulating surface current of the same magnitude, which seems implausible [33]. Furthermore, this consideration cannot explain magnetism in insulating materials.

Another argument against a classical explanation of magnetism in a material was proposed by Bohr and van Leeuwen in the 1930's [34]. They started by writing the Hamiltonian of N classical particles with charge e, and mass m under the influence of a magnetic field, determined by the vector potential $\mathbf{A}$

$$\mathscr{H} = \sum_{i=1}^{N} \frac{1}{2m}\left(\mathbf{p}_i - \frac{e}{c}\mathbf{A}_i\right)^2 + V\left(\mathbf{q}_1, \mathbf{q}_2, \cdots, \mathbf{q}_N\right), \tag{2.1.2}$$

where c is the speed of light, the $\mathbf{q}_i$'s are the canonical coordinates, $\mathbf{p}_i$ is the momenta of the i-th particle and V represents the interaction potential between the particles. From the Hamiltonian (Eq. 2.1.2) the magnetization of the system can be obtained through the classical partition function Z (Eq. 2.1.3) and the relation between the magnetization and the Helmholtz free energy (Eq. 2.1.4).

$$Z = \int \mathrm{e}^{-\beta\mathscr{H}} \mathrm{d}\mathbf{q}_1 \mathrm{d}\mathbf{q}_2 \cdots \mathrm{d}\mathbf{q}_N \mathrm{d}\mathbf{p}_1 \mathrm{d}\mathbf{p}_2 \cdots \mathrm{d}\mathbf{p}_N \tag{2.1.3}$$

$$\mathbf{M} = k_\mathrm{B} T \frac{\partial}{\partial \mathbf{H}} \ln Z, \tag{2.1.4}$$

with $\beta = \frac{1}{k_\mathrm{B} T}$, $\mathrm{k_B}$ is the Boltzmann constant, T the temperature and $\mathbf{H}$ the magnetic field.

To simplify the calculation of the partition function one can perform the following transformation $\mu_i = \mathbf{p}_i - \frac{e}{c}\mathbf{A}_i$. It is important to notice that as the integral over the momenta $\mathbf{p}_i$ is over all $\mathscr{R}^3$, the integral over μ_i has the same integration limits

$$Z = \int \mathrm{e}^{-\beta V} \int \exp\left(-\frac{\beta}{2m}\sum_i \mu_i^2\right) \mathrm{d}\mu_1 \mathrm{d}\mu_2 \cdots \mathrm{d}\mu_N \mathrm{d}\mathbf{q}_1 \mathrm{d}\mathbf{q}_2 \cdots \mathrm{d}\mathbf{q}_N. \tag{2.1.5}$$

Performing the integration over the μ_i's results in Z being independent of $\mathbf{H}$, which means that the partial derivative in Eq. 2.1.4 vanishes. Therefore, by just considering a system of classical charged particles moving inside a solid, one cannot explain the spontaneous magnetization that some materials exhibit. Hence, to obtain an explanation of magnetism at fundamental level it is necessary to go beyond classical physics and instead use *relativistic quantum mechanics*. Magnetism is based on the spin of the electron a fundamental quantity that has no classical equivalent.

The spin is a property of quantum mechanical objects, and it is considered as an intrinsic angular momentum since it has similar properties to the angular momentum operator in quantum mechanics and can be described by the same type of algebra. In quantum mechanics the spin is associated to a spin operator $\mathbb{S}$ and to the spin quantum number s, and allows for the classification

of quantum objects in *bosons*, particles with integer spin, and *fermions* particles with half-integer spin. Bosons and fermions differ also in the fact that fermions must obey the Pauli exclusion principle, i.e. no two fermions can have the exact same quantum numbers, while bosons do not experience such restriction.

Electrons are fermions, with spin quantum number which can have the values $s = \pm\frac{1}{2}$. Hence, the Pauli exclusion principle and the Coulomb interaction will determine the ground state of a multi-electron atom, thus ultimately leading to a magnetic or non-magnetic solution. Nevertheless, Hund formulated a series of empirical rules that allow the determination of the electronic configuration of the ground state of a free atom. Hund's rules can be formulated in the following way

- The state that minimizes the energy is that which maximizes the sum of the s values for all the electrons in the open sub shell.
- For a given multiplicity, i.e. a given s, the angular momentum quantum number, l, related to the operator $\mathbb{L}$ must be maximized as it has the lowest energy.
- If the outermost sub shell of the atom is half-filled or less, then the minimum energy state is the one with the lowest total angular momentum j, associated with the operator $\mathbb{J} = \mathbb{L} + \mathbb{S}$. If the shell is more than half-filled, the minima is achieved with the highest value of j.

Hitherto, the determination of the atom's ground state also sets the total angular momentum, which in turn can be used to calculate the *magnetic moment* of the atom

$$\mu = \mu_l + \mu_s = g_l \mu_B \frac{l}{\hbar} + g_s \mu_B \frac{s}{\hbar}$$

$$\mu = g_j \mu_B \frac{j}{\hbar} \tag{2.1.6}$$

$$g_j = -\frac{3j(j+1) - l(l+1) + s(s+1)}{2j(j+1)}, \tag{2.1.7}$$

where $g_l = -1$ and $g_s \approx -2.0023$ are the angular and electronic gyromagnetic factors, $\hbar$ is the Planck constant, μ_B is the Bohr mangeton, g_j is the Landé g-factor, μ_s is the spin moment and μ_l is the orbital moment.

In order to describe the magnetic properties of a solid, more information is needed. Electrons in a material interact with each other, hybridize and give rise to the formation of electronic bands, thus making the free atom description incomplete. Also the electron-electron interactions give rise to different magnetic ground states and a multitude of phenomena when the material is subjected to external stimuli such as temperature.

2.2 Heisenberg Model

The number of atoms in a solid is very large, making any analytical solution to the quantum mechanical problem impossible. Therefore, to explain the magnetic properties of a system approximations and models must introduced. Generally the models must be able to reproduce the different types of magnetic order experimentally observed as well as macroscopic phenomena such as phase transitions.

One of the most used statistical models in magnetism is the *Heisenberg model*. The quantum treatment of this model, is in general a very challenging task. Hence for systems which have large magnetic moments, the semiclassical treatment of this model is instead used. In this model the magnetic moments, $\mathbf{m}_i$, of a material are approximated as vectors in $\mathscr{R}^3$ and the interaction among them is considered in the following way

$$\mathscr{H} = -\sum_{\langle i,j \rangle} J_{ij} \hat{m}_i \cdot \hat{m}_j, \tag{2.2.1}$$

where $\hat{m}_i$ is the direction of the $i-$th magnetic moment and the J_{ij}'s are the interaction strength between the i-th and j-th magnetic moments, and is called the *exchange interaction*, since if stems from the change in energy when two electrons are interchanged, the symbol $\langle \cdots \rangle$ means that the summation is considered only between nearest neighbours. Then it is possible to define the total magnetization $\mathbf{M}$ of a sample with N magnetic atoms as the sum of the individual magnetic moments, $\mathbf{m}_i$, such that $\mathbf{M} = \frac{1}{N}\sum_i^N \mathbf{m}_i$.

2.2.1 Magnetic ordering

The Heisenberg model allows the description of different types of magnetic order observed experimentally, which are characterized by the relative orientation of the moments with respect to each other. Some types of magnetic ground states which can be described through the nearest neighbour Heisenberg model are the *ferromagnetic*, *antiferromagnetic* and *ferrimagnetic* states.

Ferromagnetic order refers to the state in which all the magnetic moments are aligned parallel to each other (Fig. 2.1**a**), this is the type which is closest to the intuitive notion of magnetism, as it is the one present in many permanent magnets, i.e. such as a regular fridge magnet. On the other hand, antiferromagnetic materials have their magnetic moments arranged anti-parallel to each other resulting in a zero net magnetic moment (Fig. 2.1**b**). Ferrimagnetic order is similar to the antiferromagnetic case as the magnetic moments of a solid are antiparallel to each other, but the net magnetization is non-zero, resulting from the magnetic moments in one of the sublattices being larger than the ones in the other (Fig. 2.1**c**). To obtain more complex states, such as non-collinear structures (Fig. 2.1**d**) the model needs to be extended, how to achieve this will be discussed in the following sections.

Figure 2.1. Distinct types of magnetic order which might occur in a material. They are characterized depending on the relative orientation of the magnetic moments present in it.

From Eq. 2.2.1 the previously mentioned magnetic configurations can be obtained depending on the sign of the J_{ij}'s. If $J_{ij} > 0$ the energy would be minimized if the magnetic moments are parallel to each other, that is a ferromagnetic ground state (Fig. 2.1**a**). On the other hand, if $J_{ij} < 0$ the moments prefer to be aligned anti-parallel to each other, resulting in an anti-ferromagnetic or ferrimagnetic state depending on the magnitude of the moments (Fig. 2.1**b**-2.1**c**).

Moreover, the magnetic order is strongly dependent on the temperature. Experimentally it is known that a ferromagnet gradually looses its magnetization as temperature increases, especially at low temperatures where the magnetization follows the Bloch $T^{\frac{3}{2}}$ law. For a magnetic material the magnetization vanishes at a certain critical temperature; T_c (Curie temperature for ferromagnets). From the Heisenberg model such behaviour can be described if one considers that temperature acts as a source of disorder. As temperature increases the alignment between the moments is broken and the total magnetization becomes lower than the saturation magnetization. Eventually the disorder generated by the temperature becomes so large that all the moments are aligned in different directions and the systems is in a completely disordered state, i.e. a *paramagnetic state*, which is also present in some materials even at very low temperatures.

In principle the temperature dependent behaviour of the magnetization can be obtained by calculating the partition function and finding the free energy of the system. Nevertheless, due to the high number of magnetic moments in the system an analytical solution is impossible, and usually approximations such as Mean Field theory [35], Random Phase Approximation (RPA) [36, 37] or numerical methods such as Monte Carlo techniques [38] are used, some of which will be described in Chapter 7.1.

2.2.2 Extended Heisenberg model

The Heisenberg model has been used very successfully to describe magnetic materials. Nonetheless, nearest neighbour exchange interactions are not enough to explain certain phenomena such as non-collinear magnetism. Also, exchange interactions can be long ranged in certain materials, such as metals, which exhibit the Ruderman-Kittel-Kasuya-Yosida (RKKY) interaction [39–

41]. Therefore in most cases the Heisenberg model is expanded to include more interactions

$$\mathscr{H} = \underbrace{-\sum_{ij} J_{i\neq j}\hat{m}_i \cdot \hat{m}_j}_{\text{Heisenberg exchange}} + \underbrace{\sum_{i,j} \mathbf{D}_{ij} \cdot (\hat{m}_i \times \hat{m}_j)}_{\text{Dzyalonshinskii-Moriya}} \underbrace{- K \sum_i (\hat{m}_i \cdot \hat{\mathbf{e}}_\mathrm{K})^2}_{\text{uniaxial anisotropy}} \\ \underbrace{-\frac{1}{2}\sum_{i\neq j} Q_{ij}^{\mu\nu} m_i^\mu m_j^\nu}_{\text{dipolar interaction}} \underbrace{- \sum_i \mathbf{B} \cdot \mathbf{m}_i}_{\text{Zeeman interaction}} \quad , \tag{2.2.2}$$

where $\mathbf{D}_{ij}$ is the antisymmetric Dzyalonshinskii-Moriya interaction [42, 43], K is the uniaxial anisotropy constant with the magnetic easy axis is oriented along $\hat{\mathbf{e}}_\mathrm{K}$, $Q_{ij}^{\mu\nu}$ the dipolar tensor with μ, ν being the Cartesian components and $\mathbf{B}$ is an external magnetic field. It is also worth mentioning that the summations in Eq. 2.2.2 are not over neighbouring moments any more, which means that one can obtain more complex magnetic ground states (Fig. 2.1**d**).

From, now on in this thesis the extended Heisenberg model will be referred only as the Heisenberg model. The development of first principle methods, such as density functional theory, allows for the calculation of material specific parameters belonging to the Heisenberg Hamiltonian, thus allowing the description of real materials. The theoretical treatment behind this procedure will be discussed in Chapter 4 for the Heisenberg exchange and Dzyaloshinskii-Moriya vectors and in Chapter 5 for the anisotropy constants.

2.3 Landau-Lifshitz equations

While the Heisenberg Hamiltonian can be used to describe ground state properties, the description of the dynamics require a definition of an equation of motion. In order to obtain an equation of motion one can start by considering a magnetic material with magnetization, $\mathbf{M}$, in the presence of an external magnetic field $\mathbf{B}$. As follows from Eq. 2.2.2 the magnetization interacts with the Zeeman term, which exerts a force on the magnetic moment that tries to align it parallel to the direction of the field.

Consider a semi-classical approximation in which the magnetic moment is treated as a 3D vector with a constant length. In this case the moment has the same behaviour as the angular momentum, $\mathbf{L}$, from classical mechanics. Therefore, it follows the same time evolution as the angular momentum, where its time derivative is non-zero only if a torque, τ, is applied over the system

$$\tau = \frac{\mathrm{d}\mathbf{L}}{\mathrm{d}t}. \tag{2.3.1}$$

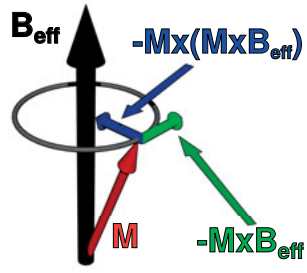

Figure 2.2. Sketch describing the precession $\mathbf{M} \times \mathbf{B}_{\text{eff}}$ and damping term $\mathbf{M} \times (\mathbf{M} \times \mathbf{B}_{\text{eff}})$ of the equation of motion of the magnetizaion under the effect of an effective field $\mathbf{B}_{\text{eff}}$.

Analogously, the magnetic field would exert a torque over the magnetization making it precess around the axis given by the direction of the field

$$\frac{\mathrm{d}\mathbf{M}}{\mathrm{d}t} = -\gamma \mathbf{M} \times \mathbf{B}, \tag{2.3.2}$$

where γ is the gyromagnetic ratio.

Although Eq. 2.3.2 describes the magnetization precessing around a magnetic field, the moment will never align itself with the field in this expression. Therefore, to get the correct dynamics of the system a dissipative term must be included such that the motion of the magnetization eventually aligns itself towards the field (Fig. 2.2). However, considering just the external field in Eq. 2.3.2 is not enough to describe the dynamics of the system, as it does not take into account the different interactions which would be present inside a material such as exchange interactions, finite size effects, etc. Therefore, it becomes necessary to define an effective magnetic field $\mathbf{B}_{\text{eff}}$, which contains all these considerations. Hence, the equation of motion for the magnetization of a material can be written as

$$\frac{\mathrm{d}\mathbf{M}}{\mathrm{d}t} = -\gamma \mathbf{M} \times \mathbf{B}_{\text{eff}} - \gamma \frac{\lambda}{M_s} \mathbf{M} \times (\mathbf{M} \times \mathbf{B}_{\text{eff}}) \tag{2.3.3}$$

with M_s being the saturation magnetization of the system and λ is a damping parameter describing the dissipation of energy from the magnetic system. This equation is the *Landau-Lifshitz* (LL) equation [44], which describes the precessional motion of the magnetization when subjected to a torque with a phenomenological relaxation term.

The Landau-Lifshitz equation works well to describe the dynamics of a system in the low damping limit, nevertheless to be able to describe the dynamics of materials with high damping, Gilbert [45], modified the equation and introduced a damping term which depends on the time derivative of the

magnetization itself

$$\frac{\mathrm{d}\mathbf{M}}{\mathrm{d}t} = -\gamma \mathbf{M} \times \mathbf{B}_{\mathrm{eff}} + \frac{\alpha}{M_s} \mathbf{M} \times \frac{\mathrm{d}\mathbf{M}}{\mathrm{d}t}, \tag{2.3.4}$$

where α is the Gilbert damping. Equation 2.3.4 is the *Landau-Lifshitz-Gilbert* (LLG) equation, which is mathematically identical to the Landau-Lifshitz equation if one redefines the gyromagnetic ratio as $\gamma = \frac{\gamma}{1+\alpha^2}$ and $\lambda = \frac{\gamma\alpha}{1+\alpha^2}$, leading to

$$\frac{\mathrm{d}\mathbf{M}}{\mathrm{d}t} = -\frac{\gamma}{1+\alpha^2} \left(\mathbf{M} \times \mathbf{B}_{\mathrm{eff}} + \frac{\alpha}{M_s} \mathbf{M} \times [\mathbf{M} \times \mathbf{B}_{\mathrm{eff}}] \right). \tag{2.3.5}$$

The Landau-Lifshitz-Gilbert equation (Eq. 2.3.5) has been extensively used to describe the magnetization dynamics to a great degree of success [46]. Nevertheless, in this original description no temperature effects are included. The great importance of temoerature effects led to Brown [47], and Kubo and Hashitsume [48] to introduce fluctuation terms in the LLG equation within a Langevin description, which allows the modelling of temperature effects in the magnetic subsystem. This will be described in detail in Chapter 7.1.

The phenomena that can be described the LLG equation depends intimately on the nature of the effective field $\mathbf{B}_{\mathrm{eff}}$, which can be obtained in a multitude of ways. One of the methods to model the effective field is the Heisenberg Hamiltonian (Eq. 2.2.2), in it the effective field is defined as $\mathbf{B}_{\mathrm{eff}} = -\frac{\partial \mathscr{H}}{\partial \mathbf{M}}$, or directly obtained from density functional theory. This is not the only method which can be used, as for example the *constrained fields* method can be considered [49, 50].

An analytical solution of Eq. 2.3.5 is not possible for most cases and therefore numerical solutions are needed to be able to tackle most systems.

2.3.1 Micromagnetism

The LLG equation presented in this section describes the time evolution of the magnetization of a system, and it is mostly used in the field of *micromagnetism*. In micromagnetism the magnetization is considered as a continuous variable in space, $\mathbf{M}(\mathbf{r},t)$, which depends on the spatial coordinate $\mathbf{r}$ and on time t. The Heisenberg Hamiltonian is then usually rewritten to a continuous form to parametrize the interactions present in the system. For example, the micromagnetic exchange energy for a time t can be written as

$$E_{\mathrm{xc}} = \int_{\Omega} \sum_{i,j,k} A_{jk} \frac{\partial M_i}{\partial x_j} \frac{\partial M_i}{\partial x_k} d\mathbf{r} \tag{2.3.6}$$

where A_{jk} is the *exchange stiffness constant*, which is a measurement of the exchange energy density of the system, the indexes i, j and k run through the $\{x,y,z\}$ Cartesian coordinates. In a similar way it is possible to write a

continuous analogous for the other terms presented in Eq. 2.2.2. The exchange stiffness is directly related to the Heisenberg exchange interaction, this will be discussed in detail in Chapter 4.1.2.

In this approach the size of the systems studied are usually in the order of $\sim 100\,\text{nm} - 100\,\mu\text{m}$. The sample itself is usually described using finite element or finite difference methods, and the size of the elements are usually in the subnanometer-nanometer scale. Furthermore, on these length-scales, the dipolar term is a dominant interaction.

Despite all the success of micromagnetism, it fails to treat systems at small length scales, where a continous description of the magnetization breaks down. For instance, real materials have a certain crystalline structure which is neglected and materials such as ferrimagnets have different sublattices which might exhibit different dynamics. Also in classical micromagnetism it is impossible to treat the dynamics of antiferromagnetic materials, since the magnetization at each point in the continuum model is zero. Such aspects cannot be appropriately described with traditional micromagnetic methods. Hence, in order to predict the magnetization dynamics of real materials, it becomes necessary to study the material properties by a combination of first principle methods (Chapter 4) and high resolution atomistic spin dynamics simulations (Chapter 7).

3. Density Functional Theory

The study of the properties of solids is an ancient pursuit. Mankind has tried to find better materials to make tools for centuries. But as science and technology advanced and the quest for better materials became more and more complicated a deeper understanding of our observations was needed. Since the material properties are dictated by the electronic structure of the system a deep understanding of it becomes necessary.

A solid is composed by atoms which arrange themselves in a certain crystalline structure. The nucleus and electrons are constantly interacting. These particles are quantum objects which can be described by the many body time independent Schrödinger equation

$$\mathscr{H}\Psi(\mathbf{r}_1,\cdots,\mathbf{r}_N,\mathbf{R}_1,\cdots,\mathbf{R}_M)=\Psi(\mathbf{r}_1,\cdots,\mathbf{r}_N,\mathbf{R}_1,\cdots\mathbf{R}_M)E, \tag{3.0.1}$$

where Ψ is the many body wave function, the $\mathbf{r}_i$'s are the positions of the electrons, while the $\mathbf{R}_i$'s are the positions of the ions, E is the total energy and $\mathscr{H}$ is the Hamiltonian of the system which is written in Rydberg atomic units, i.e when the reduced Planck's constant is set to $\hbar=1$, the electron charge $e^2=2$ and the electron mass $m_e=\frac{1}{2}$ as

$$\mathscr{H}=-\sum_i\frac{\nabla^2_{\mathbf{R}_i}}{M_i}-\sum_i\nabla^2_{\mathbf{r}_i}+\sum_{i\neq j}\frac{Z_iZ_j}{|\mathbf{R}_i-\mathbf{R}_j|}+\sum_{i\neq j}\frac{1}{|\mathbf{r}_i-\mathbf{r}_j|}-\sum_{i,j}\frac{2Z_i}{|\mathbf{r}_i-\mathbf{R}_j|}, \tag{3.0.2}$$

where M is the mass of the ions and Z is the atomic number of the ions. The first two terms in Eq. 3.0.2 are the kinetic energy of the ions and electrons receptively, while the other terms give the ion-ion, electron-electron and ion-electron Coulomb interactions respectively.

The number of atoms in a solid is very large which makes an analytical solution of the the many-body Schrödinger equation impossible. Therefore, approximations must be introduced to be able to solve the problem. One of the most used approximations in solid state physics is the Born-Oppenheimer approximation. In this approximation the electronic and ionic degrees of freedom are decoupled, this is an example of an *adiabatic approximation*. Such separation is possible because the velocities of the ions and electrons in the solid are very different, which results from the ionic masses being much larger than the mass of the electron $M\gg m_e$.

Therefore, one can consider the ions as being fixed, resulting in the ionic kinetic term being zero and the ion-ion and ion-electron terms depending parametrically on the ionic positions $\mathbf{R}_i$. Meaning that the Hamiltonian 3.0.2 can be written as following

$$\mathscr{H} = \sum_i \left[-\nabla^2_{\mathbf{r}_i} + V_{ext}(\mathbf{r}_i)\right] + \sum_{i \neq j} \frac{1}{|\mathbf{r}_i - \mathbf{r}_j|}, \tag{3.0.3}$$

where $V_{ext}(\mathbf{r}_i)$ is the potential generated from the background ion-ion and ion-electron interactions. Although, this approximation greatly simplifies the problem, it is still impossible to obtain an analytical solution for a solid.

Thus, treating the many-body problem in solids is an extremely complicated problem, but a significant breakthrough came thanks to the work of Hohenberg and Kohn [51], which proposed that instead of using the wave function of the electron as the primary object, the electron density of the system $n(\mathbf{r})$ would be used. Such considerations form the foundation of *Density Functional Theory* (DFT) which is based on the Hohenberg-Kohn theorems that state

Theorem 1 (see Martin [52](p122)) *"For any system of interacting particles in an external potential $V_{ext}(\mathbf{r})$, the density is uniquely determined."*

Theorem 2 (see Martin [52](p122)) *"A universal functional for the energy $E[n]$ in terms of the density $n(\mathbf{r})$ can be defined, valid for any external potential $V_{ext}(\mathbf{r})$. For any particular $V_{ext}(\mathbf{r})$, the exact ground state energy of the system is the global minimum value of this functional."*

The Hohenberg-Kohn theorems establish that if one knows the density of the system all its properties can be obtained, this is a consequence of the fact that the density replaces the role of the wavefunction. Hence, one can write the system's total energy as a functional of the electronic density

$$E[n(\mathbf{r})] = F[n(\mathbf{r})] + \int \mathrm{d}^3 r V_{ext}(\mathbf{r}) n(\mathbf{r}), \tag{3.0.4}$$

with $F[n(\mathbf{r})]$ being a functional which does not depend on the external potential $V_{ext}(\mathbf{r})$.

3.1 Kohn-Sham equations

It was Kohn and Sham [53] though who developed a practical scheme to map the many body problem to an effective single electron auxiliary system, which can be used to obtain the properties of the interacting system. The idea behind this scheme is to find an auxiliary non-interacting system such that it has the same density as the real case. In this case both of them would have the same total energy as prescribed by the Hohenberg-Kohn theorems. Therefore, the

effective one electron problem can be written in a set of equations known as the Kohn-Sham equations

$$\left[-\nabla^2 + V_{eff}(\mathbf{r})\right]\psi_i(\mathbf{r}) = \varepsilon_i \psi_i(\mathbf{r}) \tag{3.1.1}$$

where ψ_i are the Kohn-Sham orbitals, ε_i are the Kohn-Sham eigenvalues and V_{eff} is the effective potential. The electron density is then written as

$$n(\mathbf{r}) = \sum_{i=1}^{N} |\psi_i(\mathbf{r})|^2 \tag{3.1.2}$$

and the effective potential $V_{eff}(\mathbf{r})$ is expressed as

$$V_{eff}(\mathbf{r}) = V_{ext}(\mathbf{r}) + 2\int \mathrm{d}^3 r' \frac{n(\mathbf{r}')}{|\mathbf{r}-\mathbf{r}'|} + V_{xc}(\mathbf{r}), \tag{3.1.3}$$

in which the first term is the external potential generated by the ions, the second term is the Hartree energy term which describes the electron-electron interactions and the last term is the exchange-correlation potential which includes all the many-body effects.

It is important to mention that the Kohn-Sham eigenvalues have in general no physical meaning, they are not excitation energies, the only exception is the largest eigenvalue for a finite system, which corresponds to the negative of the ionization energy [54]. However, the eigenvalues are clearly mathematically defined as expressed in the Slater-Janak theorem [55].

Lastly one can write the total energy functional as a function of the electron density, the Kohn-Sham eigenvalues, ε_i, and the exchange-correlation energy, E_{xc}, in the following way

$$E[n(\mathbf{r})] = \sum_i \varepsilon_i - \int\int \mathrm{d}^3 r \mathrm{d}^3 r' \frac{n(\mathbf{r})\, n(\mathbf{r}')}{|\mathbf{r}-\mathbf{r}'|} + E_{xc}[n(\mathbf{r})]. \tag{3.1.4}$$

3.1.1 Exchange correlation potentials

It is important to note that while DFT is an exact theory, the Kohn-Sham formalism is not, in principle only the total energy of the system can be ensured to be correct. One important aspect is that the exchange correlation term is not known. Hence, approximations on the shape of the exchange-correlation term must be introduced. The two most used approximations are the local density approximation (LDA), first proposed by Kohn and Sham [56] and the generalized gradient approximation (GGA).

The local density approximation assumes that the exchange-correlation energy density $\varepsilon_{xc}[n(\mathbf{r})]$, obtained for an uniform electron gas with a density $n(\mathbf{r})$ works even in situations in which the electron gas is not uniform. This

assumption allows one to parametrize the exchange-correlation potential

$$V_{xc}^{LDA}(\mathbf{r}) = \varepsilon_{xc}[n(\mathbf{r})] + n(\mathbf{r}) \frac{\partial(\varepsilon_{xc}[n(\mathbf{r})])}{\partial n(\mathbf{r})} \tag{3.1.5}$$

$$E_{xc}^{LDA}[n(\mathbf{r})] = \int n(\mathbf{r}) \varepsilon_{xc}[n(\mathbf{r})] \mathrm{d}^3 r. \tag{3.1.6}$$

On the other hand the generalized gradient approximation assumes that the exchange-correlation density depends not only on the electronic density but also on the gradient of the density

$$E_{xc}^{GGA}[n(\mathbf{r})] = \int n(\mathbf{r}) \varepsilon_{xc}[n(\mathbf{r}), |\nabla n|] \mathrm{d}^3 r. \tag{3.1.7}$$

The GGA functionals can improve some of the problems resulting from LDA treatments, such as the fact that LDA usually underestimates the lattice constant of the material. However, GGA does not always an improvement, in particular LDA is better suited to describe the properties of itinerant magnetic systems than a GGA approach [57].

The treatment performed until now has not taken into account the spin degree of freedom, which is valid for non-magnetic systems, but as the objective here is to study magnetic systems, the formalism must be extended to include the spin of the electrons.

The inclusion of the spin in the non-relativistic Kohn-Sham scheme was done by von Barth and Hedin [58] in which the Kohn-Sham equations are generalized for magnetic systems. For a complete relativistic treatment of the system the Dirac equation or the Schrödinger-Pauli with spin-orbit coupling, must be considered instead of the Schrödinger-Pauli equation.

The spin degeneracy is lifted by the introduction of a spin dependent exchange-correlation potential. It requires that one replaces the density $n(\mathbf{r})$ by the generalized density matrix $\rho(\mathbf{r})$ in the following way

$$n(\mathbf{r}) \rightarrow \rho(\mathbf{r}) = \frac{n(\mathbf{r})}{2} \mathbb{1} + \frac{\mathbf{m}(\mathbf{r})}{2} \sigma, \tag{3.1.8}$$

with $\mathbb{1}$ being the 2×2 unit matrix, $\mathbf{m}(\mathbf{r})$ the magnetization density and $\sigma = (\sigma_x, \sigma_y, \sigma_z)$ the Pauli matrices. Therefore one must modify the wave functions to a spinor form

$$\psi_i(\mathbf{r}) = \begin{pmatrix} \alpha_i(\mathbf{r}) \\ \beta_i(\mathbf{r}) \end{pmatrix}, \tag{3.1.9}$$

with $\alpha_i(\mathbf{r})$ and $\beta_i(\mathbf{r})$ being the spin projections. Using the previously defined quantities one can write the density matrix $\rho(\mathbf{r})$ as:

$$\rho(\mathbf{r}) = \sum_{i=1}^{N} \begin{pmatrix} |\alpha_i(\mathbf{r})|^2 & \alpha_i(\mathbf{r}) \beta_i(\mathbf{r})^* \\ \alpha_i(\mathbf{r})^* \beta_i(\mathbf{r}) & |\beta_i(\mathbf{r})|^2 \end{pmatrix}. \tag{3.1.10}$$

The density matrix lets one write the electronic and magnetization densities:

$$n(\mathbf{r}) = \mathrm{Tr}[\rho(\mathbf{r})] = \sum_{i=1}^{N} |\psi_i(\mathbf{r})|^2 \tag{3.1.11a}$$

$$\mathbf{m}(\mathbf{r}) = \sum_{i=1}^{N} \psi_i(\mathbf{r})^{\dagger} \sigma(\mathbf{r}) \psi_i(\mathbf{r}) \tag{3.1.11b}$$

with N being the number of states in the system. The generalization to a spin dependent theory implies that one must also introduce spin dependent terms in the Hamiltonian, i.e. spin dependent kinetic energies and effective potentials, even though there is in reality no spin dependence on these terms, this is done to write the equation in a spinor form

$$\sum_{\beta=1}^{2} \left[-\delta_{\alpha\beta}\nabla^2 + V_{eff}^{\alpha\beta}(\mathbf{r}) \right] \psi_{i\beta}(\mathbf{r}) = \varepsilon_i \delta_{\alpha\beta} \psi_{i\beta}(\mathbf{r}), \quad \alpha = 1,2, \tag{3.1.12}$$

the Kohn-Sham equation can then be separated in a magnetic and a non-magnetic part

$$\varepsilon_i \psi_{i\alpha}(\mathbf{r}) = \sum_{i=1}^{2} \left[-\nabla^2 \delta_{\alpha\beta} + V_0(\mathbf{r})_{\alpha\beta} + (\mathbf{B}_{\mathrm{eff}}(\mathbf{r}) \cdot \sigma) \right] \psi_{i\beta}(\mathbf{r}), \tag{3.1.13}$$

where $V_0(\mathbf{r})_{\alpha\beta}$ is the non-magnetic part of the potential and $\mathbf{B}_{\mathrm{eff}}(\mathbf{r}) \cdot \sigma$ is the magnetic potential.

Many different parametrizations of the LSDA functional exists such as the ones proposed by Vosko, Wilk and Nusair [59], Perdew *et al.* [60], Perdew and Zunger [61] and Perdew and Wang [62] among others. However, all of these are just different parametrizations of the same functional. On the other hand, the GGA different parametrizations of the exchange correlation potential, such as the ones proposed by Langerth and Mehl [63] and Perdew, Burke and Ernzerhof [64] among others, are different functionals on themselves, that is there is no single GGA functional.

The treatment of correlations is a quite challenging problem in DFT, as strongly correlated electrons are not well treated under LSDA and GGA. As a result several methods have been developed to treat correlations. One prominent example is the LSDA+U approach, in which an on-site Hubbard term to treat the strong Coulomb interaction between correlated electrons. As part of the correlation term is already taken into account via the LSDA exchange-correlation potential, the so-called double counting term (DC) must be subtracted from the total energy. However, this term in general has no unique way to be defined, two approaches are generally used, the around mean-field (AMF) scheme introduced by Czyżyk and Sawatzky [65], and the fully localized limit (FLL) by Lichtenstein *et al.* [66].

A more sophisticated method to treat correlation effects is via dynamical mean-field theory (DMFT), where correlation effects are taken into account

by treating the electrons as a interacting with a bath in an impurity model, a detailed explanation of this method goes beyond the topics treated in this thesis and the reader is instead directed to Ref. [67] for more details.

3.1.2 Relativistic DFT

Relativistic effects have not been considered in the DFT treatment presented until now, hence properties that depend on relativistic effects cannot be treated with the regular Kohn-Sham treatment presented. Hence, to be able to properly take into account relativistic effects, a generalization of the Kohn-Sham treatment to a relativistic framework must be performed. This was first performed by Rajagopal and Callaway [68] and later by MacDonald and Vosko [69]. The generalization can by done by considering that the total energy of the system can be written as a functional of the four component current, $j^{\nu} = (n, \mathbf{j})$, with n being the probability density and $\mathbf{j}$ being the probability current, and n the electronic density, making use of the Gordon decomposition of the current one can then write

$$E_{\text{tot}}\left[j^{\nu}\right] = T_s\left[j^{\nu}\right] + E_{\text{ext}}\left[j^{\nu}\right] + E_H\left[j^{\nu}\right] + E_{\text{xc}}\left[j^{\nu}\right] \tag{3.1.14}$$

where T_s is the kinetic energy term, E_{ext} is the external potential term which includes both the ionic potential and a vector potential resulting from an external magnetic field, E_H is the Hartree term and E_{xc} is the exchange correlation potential. This can be done by writing the Dirac-Kohn-Sham equation

$$\left(c\hat{\alpha}\cdot\mathbf{p} + \beta c^2 + v_{\text{eff}}(\mathbf{r}) - \mathbf{m}(\mathbf{r})\cdot\mathbf{B}_{\text{eff}}(\mathbf{r})\right)\psi_i = \varepsilon_i\psi_i. \tag{3.1.15}$$

Here one can define the effective potential $v_{\text{eff}}(\mathbf{r})$ and the effective magnetic field $\mathbf{B}_{\text{eff}}(\mathbf{r})$as

$$v_{\text{eff}}(\mathbf{r}) = v(\mathbf{r}) + \int \frac{n_\sigma(\mathbf{r})}{|\mathbf{r}-\mathbf{r}'|}dr + \frac{\delta E_{\text{xc}}\left[n_\sigma(\mathbf{r}), \mathbf{m}(\mathbf{r})\right]}{\delta n_\sigma(\mathbf{r})} \tag{3.1.16}$$

$$\mathbf{B}_{\text{eff}}(\mathbf{r}) = \mathbf{B}_{\text{ext}}(\mathbf{r}) + \frac{\delta E_{\text{xc}}\left[n_\sigma(\mathbf{r}), \mathbf{m}(\mathbf{r})\right]}{\delta \mathbf{m}(\mathbf{r})} \tag{3.1.17}$$

where $v(\mathbf{r})$ is the external ionic potential and $\mathbf{B}_{\text{ext}}(\mathbf{r})$ is the external magnetic field.

Besides the fully relativistic Dirac equation, the scalar relativistic approach is often used. In this approach the Dirac equation can be rewritten and the spin-orbit coupling can be removed [70]. The spin orbit is then treated in a perturbational approach.

The relativistic description of DFT allows one to describe relativistic phenomena such as the anti-symmetric Dzyaloshinskii-Moriya interaction which will be described in Chapter 4, magneto-crystalline anisotropy discussed in

Chapter 5 and the Gilbert damping parameter that will be discussed in Chapter 6.

Up until now a theoretical description of the basic premises of DFT have been presented. For practical applications a methodology needs to be introduced to solve the Kohn-Sham equations, in the next section both plane waves based methods and the Korringa-Kohn-Rostoker (KKR) method will be discussed. The KKR method is used throughout this thesis to obtain numerical results for materials properties will be introduced.

3.2 Plane wave methods

One of the most used approaches to solve the Kohn-Sham equations is the plane wave method. This consist of expanding the Kohn-Sham wavefunctions as plane waves, following Ref [71], the plane waves can be defined as $\phi(\mathbf{r}) = \frac{1}{N} e^{i\mathbf{g}\cdot\mathbf{r}}$, with N being a normalization factor, [r the position in real space, and $\mathbf{g}$ a vector in reciprocal space.

Plane waves have the advantage that they are orthonormal, that is one can write

$$\int_{-\infty}^{\infty} d^3 r \phi_{\mathbf{g}}^{*}(\mathbf{r}) \phi_{\mathbf{g}'}(\mathbf{r}) = \delta\left(\mathbf{g} - \mathbf{g}'\right) \tag{3.2.1}$$

meaning that they can give rise to diagonal terms in the Hamiltonian, such as in the case of the momentum operator, simplifying calculations tremendously.

Also, making use of the Bloch theorem one can take advantage of the symmetry of the solid. Hence, by defining the reciprocal vector, $\mathbf{g}$, as $\mathbf{g} = \mathbf{k} + \mathbf{G}$, with $\mathbf{k}$ being the considered reciprocal space vector and $\mathbf{G}$ a reciprocal lattice vector defined as a linear combination of the fundamental vectors in reciprocal space $\mathbf{A}$, $\mathbf{B}$ and $\mathbf{C}$ (see for example [34])

$$\mathbf{G} = g_1\mathbf{A} + g_1\mathbf{B} + g_3\mathbf{C} \tag{3.2.2}$$

allowing one to expand the Bloch functions as

$$\psi_{\mathbf{k}}(\mathbf{r}) = \frac{1}{N} \sum_{\mathbf{G}} a_{\mathbf{G}}(\mathbf{k}) e^{i(\mathbf{k}+\mathbf{G})\cdot\mathbf{r}} \tag{3.2.3}$$

where $a_{\mathbf{G}}(\mathbf{k})$ are a series of coefficients which fulfil $\sum_{\mathbf{G}} = |a_{\mathbf{G}}(\mathbf{k})|^2 = 1$.

Making use of such expansion one can then calculate the matrix element of the Kohn-Sham Hamiltonian

$$\sum_{\mathbf{G}} \left\{ \left[(\mathbf{k}+\mathbf{G})^2 - \varepsilon_{\mathbf{k}} \right] \delta_{\mathbf{G}\mathbf{G}'} + \hat{V}\left(\mathbf{G}' - \mathbf{G}\right) \right\} a_{\mathbf{G}}(\mathbf{k}) = 0 \tag{3.2.4}$$

where $\hat{V}$ is the Fourier transform of the potential.

In this way the Kohn-Sham equation becomes a standard eigenvalue problem. However, due to the $\frac{1}{r^2}$ behaviour of the potential, an all electron treatment of the problem becomes very prohibitive from the computational standpoint, as large number of $\mathbf{G}$ vectors would be needed to ensure the proper description of the system. That is, due to the high energy of the core electrons, the large cut-off energy becomes so large that the basis size becomes unwieldy. Several approaches to treat these problems are generally used, such as, pseudopotential methods [72], and augmented plane waves [73] approaches.

3.3 Korringa-Kohn-Rostoker approach

The periodicity of solids bring forth one big advantage: instead of having to solve the Khon-Sham equation for the whole solid, it is only necessary to solve it in the Wigner-Seitz cell. Owing to the Bloch theorem, if the solution to the Kohn-Sham is known within one Wigner-Seitz cell, then the solution is also known for the whole solid. Hence, one can begin by considering an atom, n, at position, $\mathbf{R}_n$. If the potential shape is assumed to be spherical, one can write the wavefunction, $\psi(\mathbf{r})$ as

$$\psi(\mathbf{r}) = \sum_{l,m} C_{lm} R_{lm}(\mathbf{r}) Y_{lm}(\mathbf{r}) \tag{3.3.1}$$

where $R_{lm}(\mathbf{r})$ is the radial solution of the Schrödinger equation, $Y_{lm}(\mathbf{r})$ are the spherical harmonics, C_{lm} are a series of coefficients and l, m are the angular momentum and magnetic quantum numbers respectively. If one considers the spherical potential to be given the Muffin-Tin approximation (MT). That is spherically symmetric inside the muffin-tin radius R_{MT} and constant outside of it (see Fig. 3.1). A constraint is enforced in the solution for the wave function, as they must match in the intersect between the two regions.

In 1947 Korringa [29] proposed a wavefunction method to calculate the C_{lm} coefficients, based on the matching of incident and scattered wavefunctions from the potential centred in a give, unit cell. Later on, in 1954 Kohn and Rostoker [30] proposed an alternative derivation, in which the wavefunction was expressed by using the Green's function, $G(E,\mathbf{r},\mathbf{r}')$. This is done by rewriting the Schrödinger equation as the integral Lippmann-Schwinger equation [74]

$$\psi^n(\mathbf{r},E) = \psi^0(\mathbf{r},E) + \int_{\Omega_n} d^3r' G_0\left(E,\mathbf{r},\mathbf{r}'\right) V^n(\mathbf{r})\, \psi^n(\mathbf{r},E) \tag{3.3.2}$$

with $\psi^0(\mathbf{r},E)$ being the free electron wave function, Ω_n the volume of the n-th cell and $V^n(\mathbf{r})$ is the potential acting over the electron at site $\mathbf{R}_n$. The Green function is defined as

$$[E - \mathscr{H}]\, G\left(\mathbf{r},\mathbf{r}',E\right) = \delta\left(\mathbf{r}-\mathbf{r}'\right) \tag{3.3.3}$$

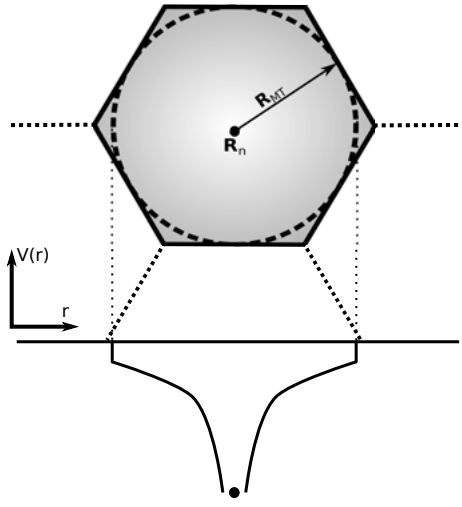

Figure 3.1. Sketch of the Muffint Tin potential centered around atom n in the Wigner-Seitz construction.

However, this classical interpretation of the KKR technique as a series of matching wavefunctions is for most part not used in present implementations. Instead, most modern implementations of the KKR method are based on Multiple Scattering Theory (MST). Here the basic idea is that each atom is treated as a scattering center for the electronic waves, with the scattering process being described by the scattering matrix. Also, the condition that the incident wave at each center is equal to the sum of all the outgoing waves for all the other scattering centres must be fulfilled [71].

The Green function contains the same information as the wavefunction. This can be be easily seen when one expresses the Green function in the Lehman representation, i.e. as a function of the eigenfunctions [71, 75]

$$G^{\pm}\left(\mathbf{r},\mathbf{r}',E\right)=\lim_{\varepsilon\to 0}\sum_{\nu}\frac{\psi_{\nu}\left(\mathbf{r}\right)\psi_{\nu}^{*}\left(\mathbf{r}'\right)}{E-E_{\nu}\pm i\varepsilon} \tag{3.3.4}$$

where the superscript +(-) refer to the retarded Green function, $G^{+}\left(\mathbf{r},\mathbf{r}',E\right)$, that is propagating states forward in time, or the advanced Green function $G^{-}\left(\mathbf{r},\mathbf{r}',E\right)$, ψ_{ν} refers to the eigenfuction for the state ν and E_{ν} is the eigenvalue associated with the eigenfuction ψ_{ν}. The factor ε is a positive real number to ensure the convergence of the expression.

Due to the relation between the eigenstates of the system and the Green function, it is possible to obtain all the information of the system encoded in the wavefunction via the Green function instead.

In general one can calculate the expectation value of an operator, $\mathbb{A}$, in the KKR formalism by using the relation

$$\langle\mathbb{A}\rangle=-\frac{1}{\pi}\mathrm{Im}\int_{-\infty}^{\infty}\mathrm{Tr}\left[\mathbb{A}G\left(\mathbf{r},\mathbf{r}',E\right)\right]f_{T}\left(E\right)dE \tag{3.3.5}$$

for example, the density of states $n(E)$ and the charge density $\rho(\mathbf{r})$ can be obtained in such manner

$$n(E) = -\frac{1}{\pi}\mathrm{Im}\int G\left(\mathbf{r},\mathbf{r}',E\right)d^3r = -\frac{1}{\pi}\mathrm{ImTr}\left[G(E)\right] \tag{3.3.6}$$

$$\rho(\mathbf{r}) = -\frac{1}{\pi}\mathrm{ImTr}\int_{-\infty}^{\infty} G\left(\mathbf{r},\mathbf{r}',E\right) f_T(E)\,dE \tag{3.3.7}$$

where $f_T(E) = \frac{1}{1+\exp\left(\frac{E-E_F}{k_B T}\right)}$ is the Fermi function, k_B is the Boltzmann constant and E_F is the Fermi energy.

Thus one can use the definitions above to calculate the density of states for real materials from first-principles. One example is the Heusler alloy Co_2MnsSi in the $L2_1$ crystal structure, as see in Fig. 3.2 as studied in detail in **paper VI**. The DOS allows one to identify several properties of the system such as the fact that this system is half-metallic, i.e. it is an insulator in one of the spin channels as demonstrated by the gap around the Fermi energy for the minority states. Also the effect that different potential constructions can have in the description of the electronic states is seen in the DOS. Here two different constructions of the potential were considered. First, the Atomic Sphere Approximation (ASA), where the potential is spherically symmetric, and is considered to act on a sphere with a volume equal to the volume of the Wigner-Seitz cell centred around a given atom. For closed packed structures this leads to an overlap of the sphere until the entire volume of the cell is filled. For open systems, empty spheres centred at the interstitials can be used to fill the volume. Another alternative to construct the potential, is the Full Potential (FP) scheme on the other hand treats both spherical and non-spherical parts of the potential. And thus is expected to give a more accurate description of the real potential.

3.3.1 The Dyson equation

Another important property of the Green function is how one can relate the un-perturbed Green function $G_0(E)$ with the Green function $G_1(E)$ resulting from a perturbation ΔV of the un-perturbed Hamiltonian $\mathscr{H}_0$. Hence one can write equations such as Eq. 3.3.3 for both the perturbed and unperturbed Green function

$$G_0^{-1}(E) = E - \mathscr{H}_0 \tag{3.3.8}$$

$$G_1^{-1}(E) = E - (\mathscr{H}_0 + \Delta V) \tag{3.3.9}$$

Substituting Eq 3.3.8 in Eq. 3.3.9 allows one to write

$$G_1^{-1}(E) = G_0^{-1}(E) - \Delta V \tag{3.3.10}$$

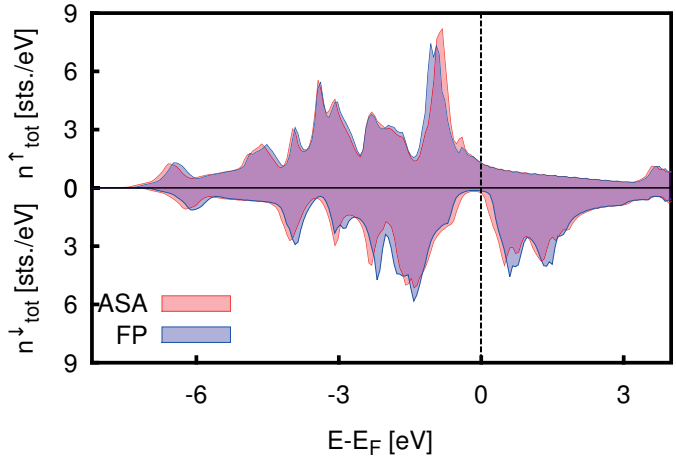

Figure 3.2. Density of states for Co_2MnSi, as studied in **paper VI**. Different treatments for the geomerty of the potential were considered, the atomic sphere approximation (ASA) and a full potential treatment (FP). The half-metallic character of the material is revealed by the gap in one of the spin channels.

then one can write the **Dyson equation** relating the Green function of the reference system to the one of the perturbed system

$$\begin{aligned} G_1(E) &= [1 - G_0(E)\Delta V]^{-1} G_0(E) \\ &= G_0(E)[1 - \Delta V G_0(E)]^{-1} \\ &= G_0 + G_0(E)\Delta V G_1(E). \end{aligned} \tag{3.3.11}$$

The Dyson equation can then by written as a series expansion as seen in Eq. 3.3.12. This capacity of the Dyson equation is one of the corner stones for interpreting the KKR method from the point of view of scattering theory, as each term in the expansion describes successive interaction events between the reference Green function G_0 and the perturbation ΔV.

$$G_1(E) = G_0(E) + G_0(E)\Delta V G_0(E) + G_0(E)\Delta V G_0(E)\Delta V G_0(E) + \cdots \tag{3.3.12}$$

With knowledge of the Dyson equation and the basic properties of Green's functions one can introduce the basic concepts of MST, which forms the basis of modern KKR methods. Compared with plane wave methods, KKR methods can be formulated to have profound advantages when dealing with systems in which translational symmetry is lost, either by impurities in solids [76–78] or for systems of reduced symmetry [79–84].

3.3.2 Multiple Scattering Theory

In order to be able to describe the scattering problem in a real solid, in which multiple scattering sites exist, one must first be able to describe the single scattering site problem using Green functions. The following treatment is based on Refs. [85, 86]. For this one considers the scattering of plane waves (the eigenfunctions of a free electron system) from a spherical atomic potential. Due to the symmetry of the system it is useful to represent the plane waves in the angular momentum representation.

$$\psi_{\mathbf{k}}(\mathbf{r}) = \sum_{l,m} 4\pi i^l j_l\left(\sqrt{E}r\right) Y_l^m(\mathbf{k}) Y_l^m(\mathbf{r}) \tag{3.3.13}$$

where Y_l^m are the spherical harmonics and j_l are spherical Bessel functions. One can also write the free space Green's function in the angular momentum representation

$$G\left(\mathbf{r},\mathbf{r}',E\right) = \sum_{l,m} Y_l^m(\mathbf{r}) G_l\left(\mathbf{r},\mathbf{r}',E\right) Y_l^m(\mathbf{k}) \tag{3.3.14}$$

$$G_l\left(\mathbf{r},\mathbf{r}',E\right) = -i\sqrt{E} j_l\left(\sqrt{E}r_<\right) h_l\left(\sqrt{E}r_>\right) \tag{3.3.15}$$

with h_l being pherical Hankel functions and n_l are the spherical Neumann functions. The radii $r_<$ and $r_>$ are defined as $r_< = min\{r,r'\}$ and $r_> = max\{r,r'\}$. As in the previous section the potential for simplicity is considered to be given by a Muffin-Tin construction for the potential shape. In principle the method is valid for different treatments for the construction of the potential, Atomic Sphere Approximation (ASA), Wigner-Seitz construction or full potential implementations [85, 87–89].

The eigenfunctions, $R_l(\mathbf{r},E)$, of the radial Schrödinger equation for $r > R_{\mathrm{MT}}$, can be expressed as a function of the single site scattering matrix, $t_l(E)$, as shown in Eq. 3.3.16. Thus, one can write the relation between the t-matrix, which represents the scattering of the wavefunction from the potential, $V^n(r)$, centred at site $\mathbf{R}_n$, with the phase shifts $\delta_l(E)$ resulting from the scattered waves from the potential (Eq. 3.3.17).

$$R_l(\mathbf{r},E) = j_l\left(\sqrt{E}r\right) - i\sqrt{E} t_l(E) h_l\left(\sqrt{E}r\right) \tag{3.3.16}$$

$$t_l(E) = \sin\delta_l(E)\, e^{i\delta_l(E)} \tag{3.3.17}$$

The inhomogeneity in Eq. 3.3.16 means that the regular solutions $R_l(r,E)$ cannot completely represent the Green function for the scattering problem. Therefore, one needs to introduce a set of irregular solutions (i.e. diverging at $r \to 0$) $H_l^n(\mathbf{r},E) = H_l^n(\mathbf{r},E) Y_l^m(\mathbf{r})$. The irregular solutions must coincide with the spherical Hankel functions h_l when $r < R_{\mathrm{MT}}$. Using this information

one can expand the Green function for the scattering problem as the product of the regular and irregular solutions (Eq. 3.3.18).

$$G\left(\mathbf{r},\mathbf{r}',E\right)=-i\sqrt{E}\sum_{l,m}R_l\left(r_<,E\right)H_l\left(r_>,E\right)Y_l^m\left(\mathbf{r}\right)Y_l^m\left(\mathbf{r}'\right) \tag{3.3.18}$$

This expansion allows one to deal with a single scatterer, but in a solid there are multiple scattering sites. Each scattering site has its own potential which can be considered as a perturbation of the unperturbed Hamiltonian, i.e. the i-th site has a perturbation ΔV_i. Hence, one can define the total perturbation $\Delta\mathscr{V}=\sum_j \Delta V_j$. In the same way as one defines the total perturbation one can define a total $\mathbb{T}$-matrix that contains all the scatterers in the lattice

$$\begin{aligned}\mathbb{T}\left(E\right)=&\sum_i t_i\left(E\right)+\sum_{\substack{i,j\\ i\neq j}} t_i\left(E\right)G_0\left(E\right)t_j\left(E\right)+\\ &\sum_{\substack{i,j,k\\ i\neq j\\ j\neq k}} t_i\left(E\right)G_0\left(E\right)t_j\left(E\right)G_0\left(E\right)t_k\left(E\right)+\cdots\end{aligned} \tag{3.3.19}$$

The total scattering matrix $\mathbb{T}$ can be interpreted such that the first term deals with all the single site scattering processes, i.e. where an electron is scattered by a single scatterer which then leaves the area of interest. The second term deals with two successive scattering events with a propagation between them determined by the crystal Hamiltonian and following terms describe multiple scattering events. In this approach there can be only one scattering event at the same site.

As in the single scatterer case one needs to be able to find a relation between the free space Green function G_0 and the crystal green function G. For this purpose, when considering the MT potential construction, the free space Green function in the cell-centred representation can be written as

$$G_0\left(\mathbf{r}+\mathbf{R}_m,\mathbf{r}+\mathbf{R}_n,E\right)=G_0\left(\mathbf{r},\mathbf{r}+\mathbf{R}_n-\mathbf{R}_m,E\right) \tag{3.3.20}$$

$$G_0\left(\mathbf{r},\mathbf{r}+\mathbf{R}_n-\mathbf{R}_m,E\right)=-\sqrt{E}\sum_L j_L\left(\mathbf{r},\mathbf{E}\right)h_L\left(\mathbf{r}+\mathbf{R}_n-\mathbf{R}_m,E\right) \tag{3.3.21}$$

with $\mathbf{R}_n$ and $\mathbf{R}_m$ referring to the center of n-th and m-th cell respectively, thus implying that $m\neq n$ and introducing the combined symbol $L=l,m$. Using one of the identities of the Hankel functions

$$h\left(\mathbf{x}+\mathbf{x}'\right)=4\pi\sum_{L,L'} i^{l-l'+l''}C_{LL'L''}j_{L'}\left(\mathbf{x}_<\right)h_{l''}\left(\mathbf{x}_>\right) \tag{3.3.22}$$

where $C_{LL'L''}$ are the Gaunt coefficients

$$C_{LL'L''}=\int d\mathbf{r}Y_L\left(\mathbf{r}\right)Y_{L'}\left(\mathbf{r}\right)Y_{L''}\left(\mathbf{r}\right) \tag{3.3.23}$$

Thus, one can write free space Green function as

$$G_0\left(\mathbf{r}+\mathbf{R}_m,\mathbf{r}'+\mathbf{R}_n,E\right)=\sum_{L,L'} j_L\left(\mathbf{r},E\right)S^{m,n}_{0LL'}\left(E\right)j_{L'}\left(\mathbf{r}',E\right) \tag{3.3.24}$$

where one defines the KKR structure constants $S^{m,n}_{0LL'}\left(E\right)$ and the

$$S^{m,n}_{0LL'}\left(E\right)=4\pi i\sqrt{E}\sum_{L''} i^{l-l'+l''}C_{LL'L''}h_{L''}\left(\mathbf{R}_m-\mathbf{R}_n,E\right) \tag{3.3.25}$$

As the indexes m and n refer to different scattering sites the entries $S^{mm}_{0LL'}=0$. Henceforth, the free space Green function is expressed as

$$G_0\left(\mathbf{r}+\mathbf{R}_m,\mathbf{r}+\mathbf{R}_n,E\right)=\delta_{mn}G_0\left(\mathbf{r},\mathbf{r}',E\right)+\sum_{LL'} j_L\left(\mathbf{r},E\right)S^{m,n}_{0LL'}\left(E\right)j_{L'}\left(\mathbf{r}',E\right) \tag{3.3.26}$$

Henceforth, it is possible to rewrite Eq. 3.3.19 and the crystal Green function using the Dyson equation, obtaining $\mathbb{T}\left(E\right)=\left[t^{-1}\left(E\right)-G_0\left(E\right)\right]^{-1}$ and $G\left(E\right)=\left[G_0^{-1}\left(E\right)-t\left(E\right)\right]^{-1}$. Using the Dyson equation and Eq. 3.3.26 one can write the secular KKR equations in real space

$$\det\left[t_l^{-1}\left(E,\mathbf{r}\right)\delta\left(\mathbf{r}-\mathbf{r}'\right)\delta_{L,L'}-S_{LL'}\left(E,\mathbf{r}-\mathbf{r}'\right)\right]=0 \tag{3.3.27}$$

and in reciprocal space

$$\det\left[t_l^{-1}\left(E\right)\delta_{L,L'}-S_{LL'}\left(E,\mathbf{k}\right)\right]=0 \tag{3.3.28}$$

which allows the calculation of the eigenvalues and the band structure of the system. Also one can see that in both equations there is a separation between the terms that depend on the structure $S_{LL'}$ and terms that depend on the potential t. This is one of the main advantages of the KKR implementation, since the $S_{LL'}$ need to be calculated only once for each structure.

Another relevant quantity in the MST is the decomposition of the $\mathbb{T}$-matrix in the scattering path operator τ^{nm} (Eq. 3.3.29) which transfer the incoming electronic wave on site m to an outgoing wave from site n with all possible scattering events that may take place in between. This allows one to write the scattering path operator as a function of the single site scattering matrix and the free space Green function G_0 (Eq. 3.3.30)

$$\mathbb{T}\left(E\right)=\sum_{nm}\tau^{nm}\left(E\right) \tag{3.3.29}$$

$$\tau^{nm}\left(E\right)=t^n\left(E\right)\delta_{nm}+t^n\left(E\right)\sum_{k\neq n}G_0^{nk}\left(E\right)\tau^{km}\left(E\right) \tag{3.3.30}$$

3.3.3 Coherent Potential Approximation

The treatment of alloys presents a large challenge from the perspective of density functional theory since introducing a random alloy leads to the translational symmetry being lost. Many techniques have been proposed to overcome this difficulty such as the supercell technique, in which large computational cells are used so that they reproduce the concentration of the alloy components. However, this implies that in order to obtain representative quantities, a large number of atomic configurations must be taken into account and averaged over. An alternative approach is the special quasirandom structures (SQS) [90] which need a much smaller set of configurations to obtain representative quantities. Another proposed approach is the Virtual Crystal Approximation (VCA) which treats the alloy by proposing a fictitious element with atomic number Z' resulting from the average of the atomic numbers of the components [91], however, this approach makes it impossible to obtain reliable information from the components of the alloy. It is also a very crude approximation for elements that are not neighbours in the periodic table. For example, VCA would model $Fe_0.5Ni_0.5$ as Co.

Some of the previously discussed difficulties, can be partially solved by the introduction of the Coherent Potential Approximation (CPA) [92, 93]. The basic idea behind it is the creation of an effective potential that is able to reproduce the properties of the alloy. This potential is constructed by neglecting short range order and only taking into account the concentration of the atomic species. However, the CPA technique is the best single site average that can be performed [94]. This is a consequence of the fact that the coherent potential is derived by averaging the scattering properties of the different atoms in an effective potential. That infers that the average should not cause additional scattering with respect to the CPA medium as exemplified in Fig. 3.3. Then one can write the single site path operator matrices, for a random alloy $A_{x_A}B_{x_B}$ as

$$\tau^{nn}_{\mathrm{CPA}} = x_A \tau^{nn}_A + x_B \tau^{nn}_B \tag{3.3.31}$$

where τ^{nn}_{CPA}, τ^{nn}_A and τ^{nn}_B are the scattering path operator of the CPA medium and A and B components of the alloy respectively, x_A and x_B are correspondingly the concentrations of the A and B species. Thus reducing the problem to a single site impurity scattering problem.

The CPA method also allows for the calculation of the total Green's function of the system by taking into consideration the concentration weighted component projected Green's function G^{α} . On this way it is possible to obtain an averaged but component-specific information.

$$G\left(\mathbf{r},\mathbf{r}',E\right) = \sum_{\alpha} x_{\alpha} G^{\alpha}\left(\mathbf{r},\mathbf{r}',E\right) \tag{3.3.32}$$

The recovery of translational symmetry in the CPA technique allows the calculation of the dispersion relation of the material obtained from the Bloch

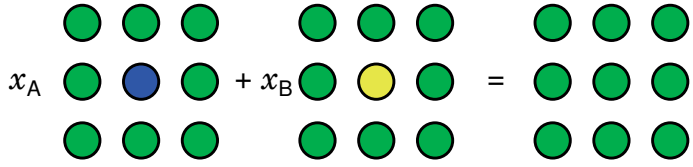

Figure 3.3. Schematic illustrating the CPA scheme, impurities are introduced in a host which represents the alloy, the average over impurities is constructed in such a way as to not introduce aditional scattering with respect to the medium.

spectral function, $A_B(\mathbf{k}, E)$. In **paper X**, permalloy ($Ni_{0.80}Fe_{0.20}$) doped with transition metals was studied by means of first-principles calculations using the KKR method. One of the studied quantities was the Bloch spectral function, and what effect impurities have when comparing it with pure permalloy. This comparison allows one to observe which bands are the most affected by the disorder and whether this can influence the magnetodynamic variables of the material.

One of the advantages of the CPA method in the Green function formalism is the fact that it can be used to treat low dimensional systems. The formalism developed for the CPA can also be applied to ferromagnetic systems at high temperatures, this by considering instead of chemical disorder disorder magnetic moments leading to a paramagnetic state, this is the so called Disordered Local Moments scheme (DLM) [95, 96]. Also recently a CPA analogy has been developed by Ebert *et al.* [97, 98] and Mankovsky *et. al* [99] to treat temperature effects for the calculation of the Gilbert damping parameter, this approach will be discussed in detail in Chapter 6.

As shown in this chapter, the KKR approach based on Green's functions has the advantage of presenting a formalism which is not restricted to systems with translational symmetry [85], and in which linear response theory can be easily introduced, thus allowing the calculation of susceptibilities [100, 101], transport properties [102], and as will be discussed in Chapter 6 the Gilbert damping parameter.

4. Calculation of exchange interactions

Magnetic ordering between magnetic moments, $\mathbf{m}_i$'s, is often described making use of the Heisenberg Hamiltonian

$$\mathscr{H}_{\text{Heis}} = -\sum_{i \neq j} J_{ij} \hat{m}_i \cdot \hat{m}_j \tag{4.0.1}$$

which was previously introduced in Chapter 2. The sign and magnitude of the exchange coupling constants, J_{ij}, determines the magnetic configuration, and dynamics of the system. Hence, a method to calculate the Heisenberg exchange interactions, J_{ij}'s, from first principles is of great importance to describe both static and dynamic properties of magnetic materials. In this chapter different methods for calculating these exchange interactions, J_{ij}, will be introduced. Some of the most used methods to calculate the exchange interactions are what will be called *direct calculation*, the *frozen magnon* method and the LKAG method.

The method that is dubbed here as the *direct calculation*, can be understood if one considers a magnetic material with two magnetic moments per unit cell (see Fig. 4.1). A simple approach to calculate the exchange interactions is to take the difference between a ferromagnetic configuration and an antiferromagnetic one, which results from "flipping"one of the spins in the cell. However, in order for such approach to be able to obtain relevant exchange interactions several configurations must be considered. In metals, exchange interactions are known to be long ranged [39–41] and can furthermore depend on the configuration [103], implying that the direct calculation method give only approximate results [104] unless more a detailed treatment is used.

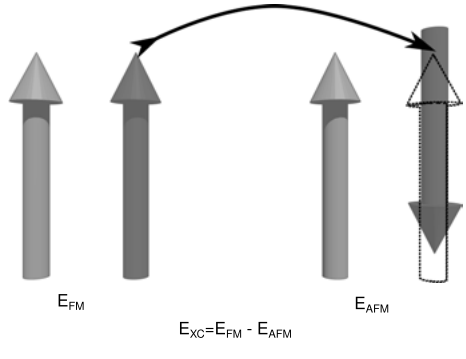

Figure 4.1. Schematic of a simple approach to calculate the Heisenberg exchange energy.

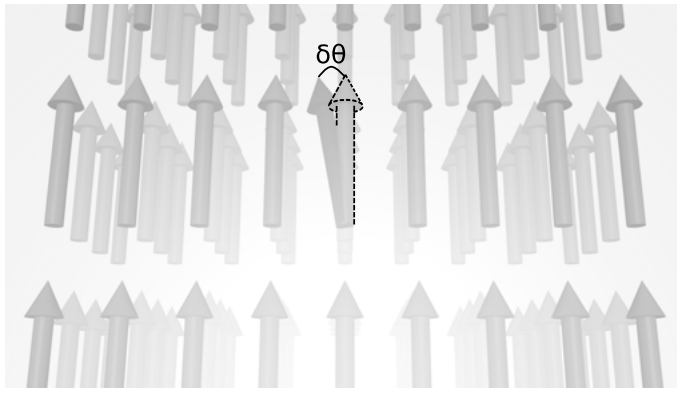

Figure 4.2. Deviation of one of the magnetic moments from the ferromagnetic background by an angle $\delta\theta$. Notice that the length of the magnetic moment is conserved during the rotation.

Another approach, is to calculate the exchange interactions via the so called *frozen magnon method*. This is a reciprocal space method, which is based on the calculation of total energies of different spin spiral configurations [105]. The use of the generalized Bloch theorem [106], which makes use of the periodicity of spin spirals, allows this kind of calculation to be performed without the need of large supercells. This approach can be generalized to materials with more than one atoms per unit cell, as used in Ref. [107].

4.1 LKAG Formalism

One of the most used methods to calculate the Heisenberg exchange interaction parameters, is the real space method developed by Liechtenstein, Katsnelsson, Antropov and Gubanov (LKAG) [31, 32]. It is based on Andersen's force theorem [108], determining the Heisenberg coupling constants by considering small deviations from a reference state.

Hence, by considering a small variation, $\delta\theta$, in one of the magnetic moments in a spin polarized host (see Fig. 4.2), the variation on the total energy δE can be calculated as

$$\delta E = -\int_{-\infty}^{E_F} d\varepsilon \delta N(\varepsilon) \tag{4.1.1}$$

where $\delta N(\varepsilon)$ is the variation of the integrated density of states. It is important to notice, that a variation of the magnetic moment does not change the total number of electrons, only the density itself is changed.

In the scattering matrix formalism the density of states can be expressed via Lloyd's formula [109], that is the density of states can be expressed as a function of the scattering path operator. This allows one to write the variation

of the energy as

$$\delta E = \frac{1}{\pi}\int_{-\infty}^{E_F} d\varepsilon \mathrm{Im}\left[\mathrm{Tr}\left(\ln\left[1+\delta t_i^{-1}\cdot\tau_{ii}\right]\right)\right] \tag{4.1.2}$$

where $\delta t_i^{-1} = \frac{1}{2}\left(t_{i\uparrow}^{-1} - t_{i\downarrow}^{-1}\right)\times\delta\hat{m}_i\cdot\sigma$, τ_{ii} is the scattering path operator, $t_i^{\uparrow(\downarrow)}$ is the single site scattering matrix for spin up(down) , $\delta\hat{m}_i$ is the variation of the orientation of the i-th magnetic moment, and σ the vector composed of Pauli matrices.

From the energy variation described in Eq. 4.1.2, it is possible to write the exchange coupling, related to the single site rotation, $J_i = \sum_{j\neq i} J_{ij}$, when only terms on the order $\delta\theta^2$ are kept, as

$$\begin{aligned} J_i = -\frac{1}{4\pi}\int_{-\infty}^{E_F} d\varepsilon \mathrm{Im}\Big\{\mathrm{Tr}\Big[\left(t_{i\uparrow}^{-1} - t_{i\downarrow}^{-1}\right)\left(\tau_{ii}^{\uparrow} - \tau_{ii}^{\downarrow}\right) + \\ \left(t_{i\uparrow}^{-1} - t_{i\downarrow}^{-1}\right)\tau_{ii}^{\uparrow}\left(t_{i\uparrow}^{-1} - t_{i\downarrow}^{-1}\right)\tau_{ii}^{\downarrow}\Big]\Big\} \end{aligned} \tag{4.1.3}$$

In a similar way, the interatomic exchange interactions can be calculated by considering a two-site rotation. That is two magnetic moments at sites i and j rotated by angles $\delta\theta_i$ and $\delta\theta_j$ respectively. Yielding the following expression for the J_{ij}'s

$$J_{ij} = \frac{1}{4\pi}\int_{-\infty}^{E_F} d\varepsilon \mathrm{Im}\left\{\mathrm{Tr}\left[\left(t_{i\uparrow}^{-1} - t_{i\downarrow}^{-1}\right)\tau_{ij}^{\uparrow}\left(t_{j\uparrow}^{-1} - t_{j\downarrow}^{-1}\right)\tau_{ji}^{\downarrow}\right]\right\} \tag{4.1.4}$$

An important fact about equation 4.1.4 is that is makes no assumption of which kind of exchange is being considered, i.e. which mechanism, allowing for a more complete description of the exchange interaction even at arbitrary distances. However, this makes a direct determination of which physical mechanism influence the exchange interactions quite difficult.

4.1.1 Exchange interactions for magnetic heterostructures

The LKAG formalism can be used to treat a diverse set of systems. In **paper VII** it was used to study the Co/Ni/Co heterostructures deposited on heavy metals with different crystallographic orientations. This study was done with the objective of characterizing their magnetic properties due to the unexpected domain wall dynamics that was previously observed in these systems [23, 24].

The studied underlayers, were Cu, Rh, Pd, Ag, Ir, Pt and Au in the fcc stacking, while Tc, Ru and Re were treated considering an hcp stacking. The lattice constants were taken to correspond to the bulk values of the underlayer elements. Structural optimization was considered in the out of plane direction.

In Fig. 4.3 the Heisenberg exchange interactions for the fcc(001) Co/Ni/Co on Pt heterostructure, when structural optimization was considered, are shown.

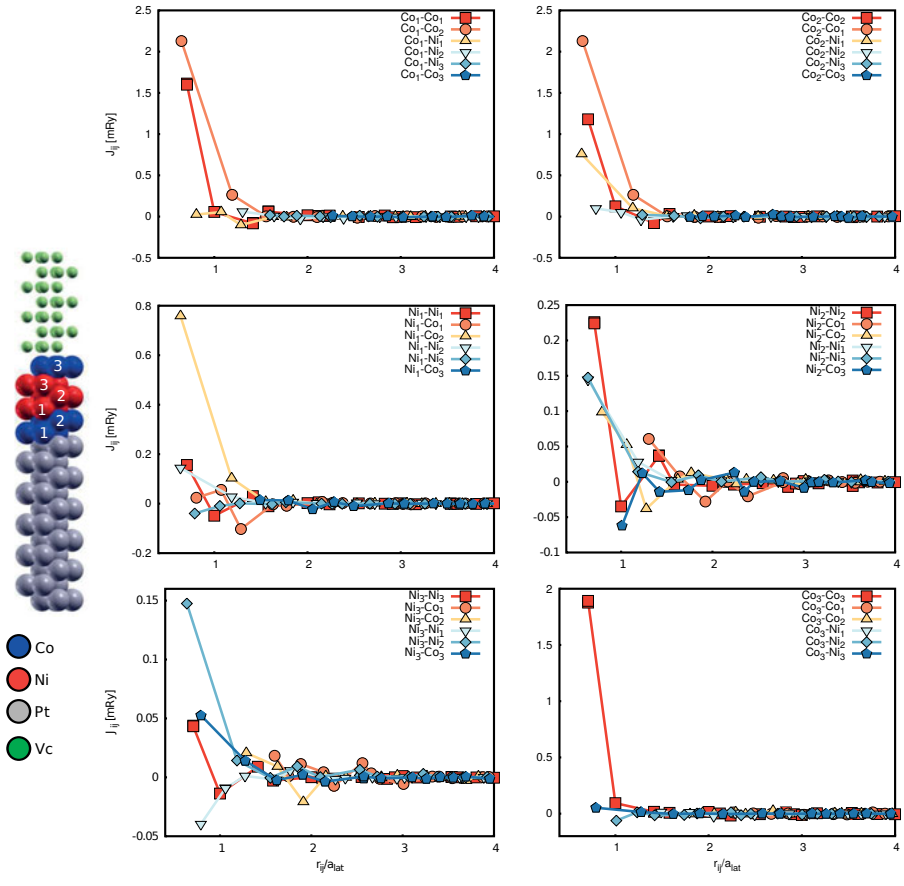

Figure 4.3. Exchange interactions for Co/Ni/Co on Pt heterostructure. A schematic view of the system is seen on the left hand side of the figure.

As can be seen their magnitude decreases rapidly as a function of distance, with nearest neighbour interactions dominating. However, the long-range behaviour of the interactions is much more apparent for the Ni-Ni exchange interactions. Also the atomic species of the magnetic ions has a clear influence on the magnitude of the exchange with the Co-Co being much larger than the Ni-Ni and Co-Ni interactions. Such behaviour is expected, the metallic nature of the system implies that long-ranged RKKY interactions will be present in it, as evidenced by the oscillations observed in Fig. 4.3. Also, the observation that Co has larger exchange interactions than Ni, is expected, since such behaviour corresponds with that is observed in the bulk systems, where Co has a larger Curie temperature than Ni.

It was also found, that even though the chemical composition of the non magnetic underlayer has an influence on the obtained exchange interactions, this influence is smaller than for other quantities as the magnetocrystalline anisotropy energy (MAE) and Dzyaloshinskii-Moriya interaction (DMI). As

both the MAE and the DMI strongly depend of the spin-orbit coupling, which varies greatly with the substrate. For the case of the Dzyaloshinskii-Moriya interaction, the hybridization between the $d-$states of the non-magnetic substrate and the $d-$states of the magnetic atoms, play a fundamental role in determining its strength, as will be discussed in the next section.

4.1.2 From first principles to micromagnetism

A direct measurement of the microscopic exchange interactions is no easy task. However, they can be used to express readily measurable experimental quantities such as the *spin-wave stiffness*, D, and as a consequence the *exchange stiffness*, A_{xc}. The spin-wave stiffness is a measurement of the curvature of magnetic excitation spectra in the limits of long wave-length magnons, i.e. when $\mathbf{q} \to 0\ E(\mathbf{q}) \sim Dq^2$ (see Chapter 7 for more details).

The spin wave stiffness, for a system with one atom per unit cell, can be defined for a cubic system as [110]

$$D = \frac{2}{3} \sum_{i,j} \frac{J_{ij}}{\sqrt{m_i m_j}} \left| r_{ij} \right|^2 \tag{4.1.5}$$

where r_{ij} is the distance between the i-th and j-th magnetic atoms m_i is the magnitude of the i-th magnetic moment. As Eq. 4.1.5 is a conditionally convergent summation, a factor, $\exp\left(-\eta \frac{r_{ij}}{a_{\mathrm{lat}}}\right)$, is included to ensure its convergence, with a_{lat} being the lattice constant of the material and η the convergence factor. The value of the stiffness can then be obtained by extrapolating $\eta \to 0$. The expression for the spin-wave stiffness can then be generalized for multi-sublattice systems [111]. This quantity is readily accessible in experiments, by techniques such as spin-polarized electron energy loss spectroscopy (SPEELS) [112], inelastic neutron diffraction [113] and Brillouin Light Scattering (BLS) [111].

The spin-wave stiffness can then be used to calculate the classic micromagnetic exchange stiffness, A_{xc} as

$$A_{\mathrm{xc}} = \frac{D M_{\mathrm{sat}}}{2 g \mu_{\mathrm{B}}}, \tag{4.1.6}$$

where M_{sat} is the saturation magnetization, g is the Landé g-factor and μ_{B} is the Bohr magneton. The exchange stiffness can be calculated making use of experimental techniques, such as the FMR approach [114]. This expression can then be generalized for systems in which the stiffness is not isotropic in space [115]. Hence, by determining the pair-wise interactions it is then possible not only to compare the spin-wave stiffness with experimental measurements, if not also to provide parameters to characterize micromagnetic simulations.

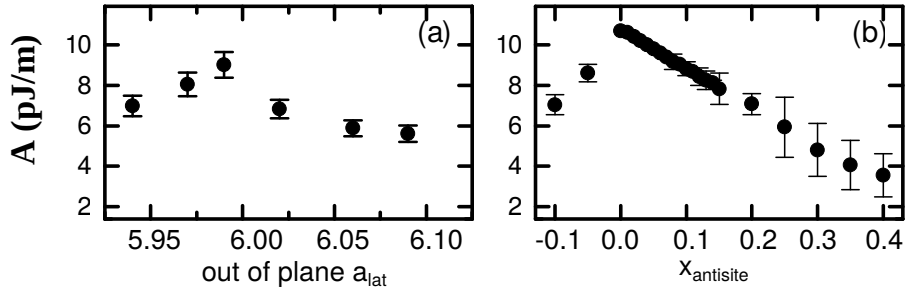

Figure 4.4. Exchange stiffness A_{xc} for $Ni_{1-x}Mn_{1+x}Sb$ from **a** experimental measurements and **b** theoretical calculations. Negative values for x imply the introduction of Ni Mn antisites and positive values are related to Mn Ni antisite defects

Exchange stiffness for NiMnSb

This approach was used in **paper IV** where the magnetodynamic variables of the $Ni_{1-x}Mn_{1+x}Sb$ half-Heusler alloy were studied using both theoretical and experimental approaches. Heusler alloys have been extensively studied as they are ideal candidates for many technological applications, resulting from properties, such as low Gilbert damping, and large Curie temperatures exhibited by materials such as Co_2MnSi. Which make them ideal candidates for spintronic applications. Controlling these important materials properties by alloying could pose one way to tailor the promising behaviour of these materials further.

The $Ni_{1-x}Mn_{1+x}Sb$ system was studied from the experimental point of view, making use of the FMR technique and considering both field dependent and frequency dependent sweeps, allowing the measurement of both the Gilbert damping and the exchange stiffness.

The chemically disordered alloys were treated via the CPA scheme [92, 93], and the pair-wise exchange interactions were calculated using the LKAG formalism discussed above. However, the calculation of the exchange stiffness depends on the distance between magnetic moments, as shown in Eqn. 4.1.5. As an effect, the real-space distribution of the defects in the sample affects the calculated exchange stiffness. Therefore it becomes necessary to generate a large number of supercells with different distributions of atoms representing the same chemical configuration. Then an average over the stiffness over the different configurations can be taken, which allows for a comparison with the experimental measurements. The theoretical values of the stiffness are larger than the experimental ones (see Fig. 4.4), which is in agreement with what was observed in previous studies [116]. The stiffness was found to decrease with defect concentration, due to the anti-ferromagnetic alignment, between the Mn antisites in the Ni sublattice and the Mn moments in the Mn sublattice.

Exchange stiffness for doped Permalloy

Another example of the capacity of tuning the exchange stiffness via alloying was studied in **paper X**. In this paper the effect that non-magnetic transition metal defects have over the exchange stiffness of the alloy permalloy (Py) was studied. Permalloy is an intensively studied Fe and Ni alloy from both theoretical and experimental point of view, partly due to its large T_c and relatively small Gilbert damping.

In general, it was found that the addition of defects decreases the stiffness significantly, the most pronounced effects were observed for elements with less than half-filled d-shell. This is consistent with the small value of the saturation magnetization obtained when these impurities are considered. However, the same behaviour is also observed in the spin wave stiffness, highlighting the fact that the change in the exchange stiffness not only results from the change in the magnetization, if not also changes in the pairwise exchange interactions.

4.1.3 Dzyaloshinskii-Moriya interactions

The Heisenberg Hamiltonian has been successfully used to describe many aspects of strong ferromagnetic materials. However, it cannot properly explain certain cases of non-collinear magnetic order, as the ones observed in non-centrosymmetric B20 structures, such as in the case of MnSi [117], and in low dimensional magnets as in a monolayer of Fe on Ir(111) [118].

To describe situations such as this, additional interactions must be introduced in the Heisenberg Hamiltonian. This was first phenomenologically proposed by Dzyaloshinskii [42] to describe "weak" ferromagnetism. Latter Moriya [43] proposed a model in which identified the spin orbit coupling, and the symmetry of the lattice as the microscopic causes behind the interaction. This Dzyaloshinskii-Moriya interaction (DMI), is then added to the Hamiltonian in the following way

$$\mathscr{H}_{\mathrm{DM}} = \sum_{i,j} \mathbf{D}_{ij} \cdot \hat{m}_i \times \hat{m}_j, \tag{4.1.7}$$

where the $\mathbf{D}_{ij}$ are the Dzyaloshinskii-Moriya vectors, it is important to notice that these vectors are anti-symmetric, i.e $\mathbf{D}_{ij} = -\mathbf{D}_{ji}$. Due to the relation between the spin and the lattice via the spin orbit coupling, the directions of the DM vectors are dictated by the structure of the lattice itself. This set of constraints was first proposed by Moriya for insulators, by studying the symmetries between two atoms i and j joined by a bonding vector $\mathbf{r}_{ij}$. They can be summarized as

- If there is an inversion center on the midpoint of $\mathbf{r}_{ij}$ then $\mathbf{D}_{ij} = 0$ (Fig. 4.5**a**).
- If there is a mirror plane perpendicular to $\mathbf{r}_{ij}$ and it passes through its midpoint, $\mathbf{D}_{ij}$ will be parallel to the mirror plane (Fig. 4.5**b**).

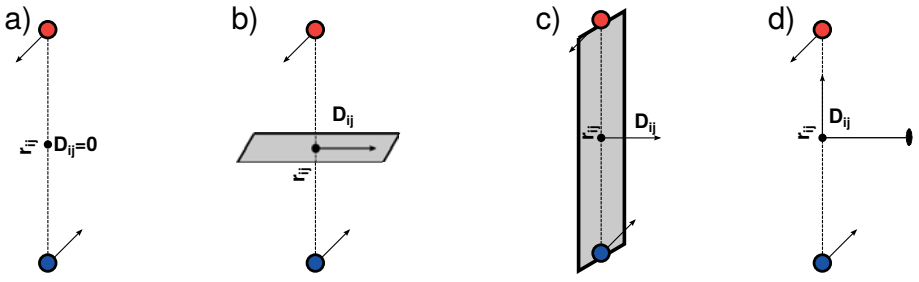

Figure 4.5. Schematic representation of the symmetry rules for the Dzyaloshinskii-Moriya vector.

- If the mirror plane includes the position of the $i-$th atom, $\mathbf{r}_i$ and the position of the $j-$th atom, $\mathbf{r}_j$, $\mathbf{D}_{ij}$ will be perpendicular to the mirror plane (Fig. 4.5**c**).
- If there is a two-fold rotation axis perpendicular to $\mathbf{r}_{ij}$ and passes through its midpoint, $\mathbf{D}_{ij}$ will be perpendicular to this axis (Fig. 4.5**d**).
- If there is an n-fold rotational axis along $\mathbf{r}_{ij}$, with $n > 2$, D_{ij} will be parallel $\mathbf{r}_{ij}$.

The original work by Dzyaloshinskii, treated insulating systems in which d-states are more localized that in metallic systems. For itinerant magnets, Fert and Levy [119] proposed a three site model, in which the DMI between two magnetic atoms, is mediated through a third non magnetic atom with a high spin orbit coupling, as schematically shown in Fig. 4.6. The Fert-Levy model is based on the $s-d$ Heisenberg Hamiltonian (not to be mistaken with Eq. 2.2.2) which describes the interaction between a localized magnetic moment $\mathbf{m}_i$ and an itinerant electron s. This treatment, considers the RKKY model when spin orbit coupling is present, which then allows one to write the energy resulting from the DM interaction

$$\mathscr{H}_{\mathrm{DM}} = -V(\xi)\frac{\sin\left[k_F\left(r_i+r_j+r_{ij}\right)+\eta\right]\hat{r}_i\times\hat{r}_j}{r_i r_j r_{ij}}\left(\hat{r}_i\times\hat{r}_j\right)\left(\hat{m}_i\times\hat{m}_j\right) \quad (4.1.8)$$

where $V(\xi)$ is a term which depends on the spin orbit coupling, r_i and r_j is the position of the i-th and j-th magnetic atoms taking as the origin the non-magnetic atom, r_{ij} is the distance between the i-th and j-th atom, η is a phase shift induced by the non-magnetic impurity and k_F is the Fermi momentum. As can be seen the DM interaction as presented here is long ranged and oscillatory, meaning that to describe metallic systems, more than nearest neighbour interactions must be considered.

The Moriya rules used for insulating bulk systems, can also be applied to systems with broken symmetry. This was first proposed by Crépieux and Lacroix [120] that demonstrated that symmetry breaking at the surface of magnetic materials can give rise to finite DM vectors. These DM vectors, induced due to symmetry breaking at the surface, have been recently demonstrated to

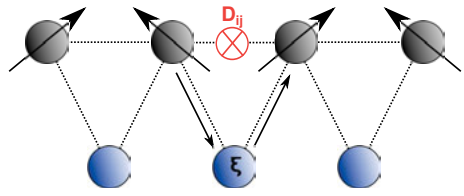

Figure 4.6. Schematic picture of the Fert-Levy model. The DM interaction between two magnetic atoms is meadiated through a non-magnetic atom with spin orbit coupling ξ, leading to a finite $\mathbf{D}_{ij}$.

be instrumental in the modelling of magnetic states at low dimensional systems. For example as in the formation of chiral magnetic ordering in Fe on W(110) [121].

The relativistic origin of the DM interaction, implies that if one wishes to calculate them from first principles a fully relativistic approach must be used, and a generalization of the LKAG in which spin orbit coupling is considered must be introduced. Two of these approaches are the one proposed by Uvardi *et al.* [122] and an alternative method devised by Ebert and Mankovsky [123]. Throughout this thesis the latter approach is used in the numerical simulations here within. In it, the Heisenberg Hamiltonian is considered in a general form

$$\mathscr{H} = -\sum_{i,j} \hat{m} \underline{\underline{J}}_{ij} \hat{m}_j \tag{4.1.9}$$

where $\underline{\underline{J}}_{ij}$ is the exchange tensor. Where its trace is related to the scalar, Heisenberg exchange, and the antisymmetric part of the J tensor is the Dzyaloshinskii-Moriya interaction.

Hence, one can write the components of the exchange matrix as

$$J_{ij}^{\alpha_i \alpha_j} = -\frac{1}{\pi} \mathrm{Im} \int_{-\infty}^{E_F} d\varepsilon \mathrm{Tr} \Delta \underline{V}^{(Z)\alpha_i} \tau_{ij} \Delta \underline{V}^{(Z)\alpha_j} \tau_{ji} \tag{4.1.10}$$

where $\Delta \underline{V}^{(Z)\alpha_i}$ is the change in the full relativistic spin dependent potential and $\alpha = (x, y, z)$ is the spin direction.

DM interactions in Co/Ni/Co heterostructures

As discussed above, the Dzyaloshinskii-Moriya interaction can have profound effects in the magnetic configuration of the system. In **paper VII** the DM vectors in Co/Ni/Co fcc heterostructures deposited on heavy metal substrates were calculated, since they are speculated to have a profound effect in the type of domain walls which can be stabilized in them [23, 24].

When considering the case of Co/Ni/Co deposited on Pt, the DM vectors for the nearest Co layer to the Pt substrate follow, as expected, the Moriya rules as presented in Fig. 4.7. In the fcc(001) stacking the DM vectors are shown to be perpendicular to the bonding vector between the magnetic atoms. Another

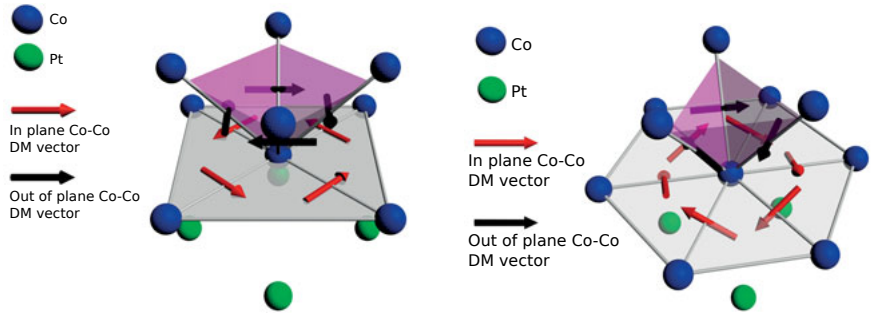

Figure 4.7. Direction of the DM vectors for the nearest Co layer to the Pt layer as described in **paper VII**.(left panel) In the fcc (001) stacking the DM vectors are perpendiular to the bonding vectors. (right pannel) On the other hand in the fcc(111) structure the direction of the DM are not completely determined by the Moriya rules.

observation is that the out of plane component of the DM vector is zero as expected from the Moriya rules. In contrast the DM vectors in the fcc(111) structure have a clear out of plane component, this is once again in agreement with the Moriya rules, where the DM vectors are predicted to be in a plane perpendicular to the bonding vector between the magnetic atoms. However, its direction in this plane cannot be completely determined by symmetry arguments [120].

It was also seen, that both the magnitude and out-of plane component of the DM vectors, intrinsically depend on the material of the underlayer. Interestingly enough, despite the need of spin orbit coupling (SOC) to obtain a finite DM, a high SOC does not necessarily yield a strong anti-symmetric interaction, which is seen in the case of Au underlayers. This is consistent with the work of Kashid *et al.* [124], in which it was shown that the hybridization of the magnetic 3*d* states with the non-magnetic 5*d* states, are also a determinant factor in both the strength and magnitude of the DM vectors. It is also important to mention that relaxation effects can have a profound influence in both the magnitude and direction of the DM vectors, which is consistent to what has been observed in .

The results obtained here correspond quite well with a recent work by Yang *et al.* [125], in which Co layers are deposited on heavy metal substrates.

Helical spin spirals on FeGe

Another set of systems which are known to exhibit a finite DMI, are those that crystallize in the non-centrosymmetric B20 structure. In **paper V** the B20 FeGe system was studied via both theoretical and experimental techniques. FeGe is a system that has gathered a great deal of attention due to the fact that skyrmions, topologically protected magnetic textures in the continuum limit, can be stabilized in this material and in other B20-structured materials. [126].

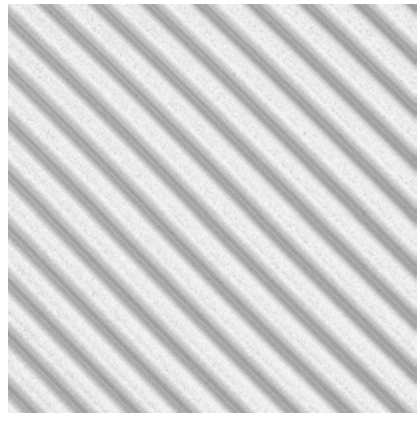

Figure 4.8. Spin spiral ground state at low temperature for FeGe from coarse grained first principles parameters.

Hence, an understanding of the helical structures, and their dynamics, are of great interest.

Experimentally, the system was studied using a combination of magnetic force microscopy and Nitrogen-vacancy (NV) center based magnetometry [127, 128]. The NV technique, is a novel measurement approach which allows for the detection of weak magnetic fields in atomic scale, allowing for the detection of domain wall profiles in systems with perpendicular magnetic anisotropy [129].

By using these techniques, the system was found to be a non-collinear helical spin spiral with a wavelength of $\lambda = 70 \pm 5$ nm, which is consistent with previous measurements [130]. By using the generalized LKAG formalism described above, both the Heisenberg exchange and Dzyaloshinskii-Moriya vectors were calculated. The pair-wise interactions were then coarse grained as to form an effective micromagnetic model, which is done in a similar approach, as the one previously used for the spin-wave stiffness. By using Monte Carlo techniques (for details see Chapter 7.1) the magnetic ground state was found to be a helical spin spiral, as seen in Fig. 4.8, with a wavelength of $\lambda \sim 100$ nm, which is also in reasonably good agreement with the experimental results.

The critical temperature of the spiral state was found to be $T_N = 240$ K, which is in quite good agreement with the experimental measurement of 276 K [131]. The good agreement observed in the spiral wavelength and the critical temperature, indicate that the used method can be used to describe the magnetic properties of this exotic non-collinear system. However, it is important to notice that the LKAG formalism as shown here is derived from a collinear reference frame, and the non-collinear ground state might influence the exchange parameters. Recent efforts have been done to improve the description as to include these effects [132].

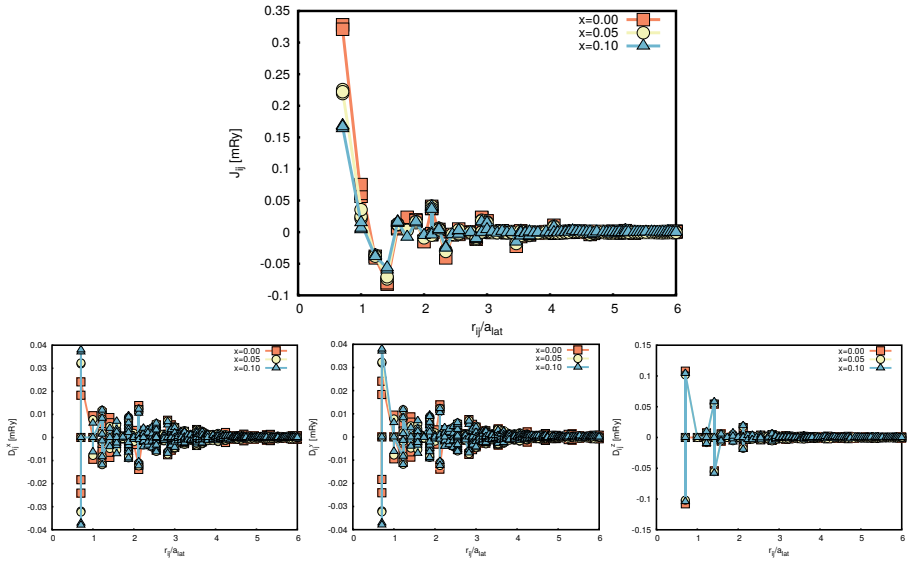

Figure 4.9. (top panel) Heisenberg exchange interactions for $MnPt_{1-x}Ir_xSn$. As the concentration of Ir is increased the nearest neighbour Mn-Mn interaction decreases.(lower panels) Dzyaloshinskii-Moriya interaction between Mn atoms for different concentration of Ir defects, from left to right D^x_{ij}, D^y_{ij} and D^z_{ij} respectively.

DM in the $MnPt_{1-x}Ir_xSn$ half-Heuslers

Another important effect, is how alloying can affect the magnitude of the DM interaction. This is the topic studied in **paper VII**, where the half-Heuslers $MnPt_{1-x}Ir_xSn$ are studied. The half-Heusler family of Mn_2YSn with Y=(Rh, Pt, Ir) alloys have been shown to have a helical ground state [133]. By using the CPA, the effect that the inclusion of Ir defects have over the interatomic exchange interactions and DM vectors was studied. Thus, opening the possibility of tuning the spiral wavelength via alloying. This is of great interest, as controlling the spiral wavelength would be of great importance for any possible skyrmioninc state present in them.

By increasing the concentration of Ir the alloy was found to become magnetically softer, as demonstrated in Fig. 4.9. The magnitude of the nearest neighbour exchange interaction decreases, which in turn has profound effects on the spin spiral wavelength of the system, due to the fact that the helimagnetic phase comes from a competition between the Heisenberg exchange and the Dzyaloshinskii-Moriya interaction.

The magnitude of the DM vectors is also affected by the concentration of Ir. With the nearest neighbour D^x_{ij} and D^y_{ij} components increasing with increasing concentration of Ir, while, any change to the D^z_{ij} is very minor. Such observation indicates that it is possible to tune the wavelength of a helical spin spiral by increasing the concentration of dopants.

5. Magnetocrystalline anisotropy

5.1 Origins of the magnetic anisotropy

Magnetic moments in magnetic materials tend to align towards a certain orientations, with respect to its structural axes. This *magnetocrystalline anisotropy* (MCA), cannot be explained alone by the Heisenberg Hamiltonian, since for exchange interactions only relative orientation between the moments are considered. Therefore, if one wishes to consider this effect, additional interactions must be included. One can start by considering, that there exist certain magnetic axes which minimize the energy of the system. Hence, the energy of the magnetic anisotropy depends on the direction cosines α_1, α_2, α_3 of the magnetic moments with respect to the magnetic easy axes. Thus, one can write the total energy as

$$E = E_0 + f(\alpha_1\alpha_2\alpha_3) \tag{5.1.1}$$

where E_0 contains all the isotropic energy contributions, and f is a function that must be determined. Brooks [134] demonstrated that the function f can be determined by the symmetry of the crystalline system. For a cubic system this results in

$$E = E_0 + K_1\left(\alpha_1^2\alpha_2^2 + \alpha_2^2\alpha_3^2 + \alpha_1^2\alpha_3^2\right) + K_2\left(\alpha_1^2\alpha_2^2\alpha_3^2\right) \tag{5.1.2}$$

where K_1 and K_2 are coefficients denoting the strength of the magnetic anisotropy and are usually referred as the *magnetic anisotropy constants*. The simplest case that can be described by Eq. 5.1.2 is the *uniaxial anisotropy*, in which there is only one magnetic axis which minimizes the magnetic anisotropy energy. For this case, and considering polar coordinates, Eq. 5.1.2 can be written as [135]

$$E = E_0 + K_1\sin^2\theta + K_2\sin^4\theta + \cdots \tag{5.1.3}$$

5.1.1 Shape anisotropy

The treatment presented above only deals with how one can express the energy related to the MCA. However, the determination of the magnitude anisotropy energy, requires that one understands the microscopic mechanisms behind it. For this purpose an interaction in which the positions of the moments in the lattice becomes necessary. The first proposed contribution was the dipole-dipole interaction

$$\mathscr{H}_{\text{dip}} = -\sum_{ij}\frac{\mu_0}{4\pi\left|\mathbf{r}_{ij}\right|^3}\left[3\left(\mathbf{m}_i\cdot\hat{r}_{ij}\right)\left(\mathbf{m}_j\cdot\hat{r}_{ij}\right) - \mathbf{m}_i\cdot\mathbf{m}_j\right] \tag{5.1.4}$$

with μ_0 being the permeability of free space, $\mathbf{m}_i$ being the i-th magnetic moment and $\mathbf{r}_{ij}$ being the distance vector between the i-th and j-th magnetic moments.

As can be seen in Eq. 5.1.4, the dipolar interaction has a clear dependence on the geometrical distribution of the magnetic moments. The geometrical shape of the sample itself can lead to the so-called *shape anisotropy*. The dipolar interaction predicts that for certain geometries, such as cubic systems, then $E_{\mathrm{MAE}} = 0$. However, cubic systems such as bcc Fe [136] and fcc Co [137], have finite magnetic anisotropy energy. Also, only taking into account the dipolar interactions is not sufficient to explain the magnetic easy axis observed in some ultra-thin films, which showcase an out-of plane magnetic easy axis in contrast to the in-plane axis predicted by the dipolar interactions [138]. Thus, despite of the importance of the dipolar interaction in stabilizing magnetic textures such as domain wall (for details see Chapter 7.3) and as mentioned before in the description of the shape anisotropy, it is not the only microscopic mechanism behind the the MAE.

5.1.2 Spin-orbit coupling and MAE

It was Van Vleck [139] that identified the spin-orbit coupling (SOC) as the mechanism behind the MAE, which, as mentioned in Chapter 3 is a relativistic effect. Therefore, to understand what are the determining factors for the MAE, one can look at the spin-orbit coupling Hamiltonian

$$\mathscr{H}_{\mathrm{SOC}} = \xi \mathbb{L} \cdot \mathbb{S} \tag{5.1.5}$$

where ξ is the spin-orbit coupling parameter and $\mathbb{L}$ and $\mathbb{S}$ are the angular momentum and spin operator respectively. By considering states $|\psi\rangle$ then is possible to calculate the expectation value of the SOC Hamiltonian. However, when calculating the expectation value of the angular momentum, $\langle\psi|\,\mathbb{L}\,|\psi\rangle$, if the state $|\psi\rangle$ is non-degenerate, a purely imaginary value is obtained [71], which is a contradiction since the angular momentum is an observable, implying that $\langle\psi|\,\mathbb{L}\,|\psi\rangle = 0$, that is the angular momentum is quenched [140].

Henceforth, to consider the effects of the spin-orbit coupling one must treat it via perturbation theory. In an uniaxial magnet, the first non-zero contribution is found when considering second order perturbation theory

$$\mathscr{H}_{\mathrm{SOC}} = \xi^2 \sum_{n \neq k} \frac{|\langle\psi_n|\,\mathbb{L}\cdot\mathbb{S}\,|\psi_k\rangle|^2}{E_n - E_k} \tag{5.1.6}$$

where $|\psi_n\rangle$ and $|\psi_k\rangle$ are states of the unperturbed Hamiltonian, and E_n and E_k are the eigenvalues of the Hamiltonian for the states $|\psi_n\rangle$ and $|\psi_k\rangle$ respectively. For cubic system the first non-zero contribution comes from the fourth-order of the spin orbit coupling.

However, not all states contribute to the energy arising from the SOC term, since if $|\psi_n\rangle$ and $|\psi_k\rangle$ are both occupied or unoccupied, their terms in the summation will cancel out, resulting in only states that cross the Fermi energy contributing to the energy [141, 142]

$$\mathscr{H}_{\mathrm{SOC}} = \xi^2 \sum_{n\in \mathrm{occ.}} \sum_{k\in \mathrm{unocc.}} \frac{|\langle\psi_n|\,\mathbb{L}\cdot\mathbb{S}\,|\psi_k\rangle|^2}{E_n - E_k} \tag{5.1.7}$$

as can be seen, this implies that not only the SOC parameter, ξ, is determinant in obtaining a large *magnetocrystalline anisotropy* (MCA), if not also details of the band structure are of great importance, which can lead to high MCA's in systems with low spin-orbit coupling [143].

It is important to notice, that even if the spin orbit coupling, is responsible for the magnetocrystalline anisotropy, the dipolar interaction is still present, and it does yields an important contribution to the total *magnetic anisotropy energy* (MAE). However, throughout the rest of this thesis, the term MAE will be used to refer only to the magnetocrystalline contribution to the energy.

Large magnetocrystalline anisotropy is of profound importance for potential technological applications. The large magnetocrystalline anisotropy can lead to thin films with an out of plane magnetic easy axis, which are very promising candidates for the development of magnetic memory devices with high information density [144].

5.2 Calculating MAE from first principles

5.2.1 Total energy calculations

From Eq. 5.1.7, is possible to see, that in order to calculate the MAE one would need to consider the total energy of the system for two different magnetization directions, $\hat{m}$ and $\hat{m}'$. With $\hat{m}$ being the easy axis orientation and $\hat{m}'$ being a perpendicular direction to the easy axis. Hence, the magnetocrystalline energy can be written as

$$E_{\mathrm{MAE}} = E\left(\hat{m}'\right) - E\left(\hat{m}\right) \tag{5.2.1}$$

The sign convention usually used is for the MAE, states that $E_{\mathrm{MAE}} > 0$ indicates an out of plane magnetocrystalline anisotropy axis and $E_{\mathrm{MAE}} < 0$ indicates an in-plane easy axis. This convention is followed through this thesis.

From a computational standpoint, this would require two self-consistent calculations, one for each magnetization direction. However, the magnetocrystalline energy is generally very small in comparison with the total energy of the system. Hence, usually a very accurate method and large number of points in the reciprocal space is needed to ensure numerical convergence and the desired energy resolution.

5.2.2 Force theorem method

Performing two self-consistent calculations with a large number of k-points can be very expensive from the computational standpoint. Also there is the difficulty that one might not know a priory the direction of the magnetic easy axis, making the search process even more prohibitive. However, by making use of the *force theorem* the computational effort needed to perform the calculations is significantly lowered.

A force theorem based approach, reduces the computational time by approximating the E_{MAE}, as the difference of the single particle Kohn-Sham energies (band energies) of the two magnetic orientations from a frozen spin potential

$$E_{\mathrm{MAE}} = \sum_{i,\mathbf{k}}^{\mathrm{occ}} \varepsilon_i \left(\hat{m}', \mathbf{k}\right) - \sum_{i,\mathbf{k}}^{\mathrm{occ}} \varepsilon_i \left(\hat{m}, \mathbf{k}\right) \tag{5.2.2}$$

where the ε_i are the Kohn-Sham eigenvalues and $\mathbf{k}$ are the reciprocal vectors. Hence, only one self-consistent calculation is required. All that would be required afterwards, would be a single iteration of using the already converged potential but for a different orientation of the magnetization.

The force theorem has been demonstrated to be applicable to monolayers and low dimensional systems [145].

5.2.3 Torque method

Another alternative for the calculation of the MAE is the *torque method*. This approach, first proposed by Wang *et al.* [146], can be understood by looking at Eq. 5.1.3, which describes the magnetic energy of system as a function of the deviation of the magnetization from the magnetic easy axis. For an uniaxial magnet the torque, $T(\theta)$, can be defined in the following way

$$T(\theta) = \frac{dE(\theta)}{d\theta} = K_1 \sin(2\theta) + 2K_2 \sin^4(\theta) \tag{5.2.3}$$

where θ is the angle between the magnetization and the normal axis. Using the Hellman-Feynman theorem, the torque can then be written as

$$T(\theta) = \sum_{n \in \mathrm{occ}} \langle \psi_n | \frac{\partial \mathscr{H}_{\mathrm{SOC}}}{\partial \theta} | \psi_n \rangle . \tag{5.2.4}$$

Lastly, noting that the E_{MAE} can be defined from the torque as

$$E_{\mathrm{MAE}} = E(\theta = 90) - E(\theta = 0) \tag{5.2.5}$$

$$E_{\mathrm{MAE}} = K_1 + K_2 = T(\theta = 45) \tag{5.2.6}$$

thus, the calculation of the MAE is reduced to the calculation of the torque for $\theta = 45$. This approach can be used in conjunction with the magnetic force

theorem, again simplifying the determination of the MAE as only one self-consistent calculation needs to be performed.

The torque, can also be expressed in the MST formalism, by considering the rotation along of the magnetization with respect to an axis $\hat{u}$, in the following way [85]

$$T_{\theta^{\hat{u}}}^{\hat{m}} = -\frac{1}{\pi}\mathrm{Im}\int^{E_F} dE \frac{\partial}{\partial \theta^{\hat{u}}}\left[\ln\left\{\det\left(t^{-1}\left(\hat{m}\right) - G_0\right)\right\}\right] \tag{5.2.7}$$

hence, by integrating in the path between the directions $\hat{m}$ and $\hat{m}'$ it is possible to calculate the E_{MAE}.

As has been shown, no matter which method one uses to calculate the MAE, it is imperative to consider relativistic effects. This can either be done by a Pauli-Schrödinger equation with the inclusion of spin-orbit coupling or via the fully relativistic Dirac equation.

MAE for $L1_0$ binary alloys

As previously mentioned, not only a strong SOC but also the details of the band structure determines if a considered system has a large MAE. This subclass of materials with large MAE but low SOC, have attracted large amount of attention, not only due to their possible applications, if not also due to the fact that they do not contain neither heavy elements nor rare-earths. This is of profound importance for technological applications due to the difficulties to obtain such elements.

Hence, in **paper II**, the torque approach was used to calculate the MAE for a series of tetragonally distorted systems with low SOC but with high magnetic anisotropy. The studied systems were FeNi, CoNi, MnAl and MnGa, all of them crystallizing in the $L1_0$ crystalline structure, where the lattice parameters a and c were optimized by minimizing the total energy using the WIEN2K package [147]. The MAE found for these compounds was to be in relative good agreement with the previous experimental measurements, with the first principles calculations in general yielding larger values than experiments. Such behaviour can be understood when considering that in experiments chemical disorder and finite temperature effects can affect the measured MAE values [148, 149]. It is important to notice, that the obtained MAE values are quite large (see Table 5.1), with the Mn based systems being comparable to the MAE of FePt in the $L1_0$ structure [149].

Another important factor, was that for the Mn based systems, chemical disorder was found to be necessary for the stabilization of a ferromagnetic solution. The Mn antisites in either the Al of Ga sublattice present antiferromagnetic exchange interaction with respect to the Mn sublattice, helping to stabilize not only the ferromagnetic solution if not also, increasing the Curie temperature of the system.

Quantity	FeNi	CoNi	MnAl	MnGa
a (Å)	3.56	3.49	3.89	3.83
c (Å)	3.58	3.60	3.49	3.69
$E_{\mathrm{MAE}}^{\mathrm{W2k}}$ (μeV/f.u.)	68.7	135.1	275.1	378.2
$E_{\mathrm{MAE}}^{\mathrm{kkr}}$ (μeV/f.u.)	110.3	184.7	320.8	385.7
$E_{\mathrm{MAE}}^{\mathrm{W2k}}$ (MJ/m^3)	0.48	0.99	1.67	2.24
$E_{\mathrm{MAE}}^{\mathrm{kkr}}$ (MJ/m^3)	0.77	1.35	1.95	2.28
$E_{\mathrm{MAE}}^{\mathrm{exp}}$ (MJ/m^3)	0.58(Ref. [150])	0.54(Ref. [151])	1.37(Ref. [152])	-

Table 5.1. *Lattice parameters calculated using WIEN2k,magnetic anisotropies calculated using WIEN2k and SPR-KKR for $L1_0$ binary alloys FeNi, CoNi, MnAl and MnGa.*

MAE in magnetic heterostructures

The torque method was also used in **paper VII**, where Co/Ni/Co heterostructures deposited on heavy metals were studied. Due to the low dimensionality of these systems, and the strong spin-orbit coupling that is present in some of the underlayer materials, they are expected to show an out of plane or perpendicular magnetocrystalline anisotropy (PMA). That means that the magnetrocrystalline anisotropy that these heterostructures have is large enough to overcome the in-plane shape anisotropy of the system. The advantage of PMA materials, is that they can present very narrow domain wall widths, which as previously mentioned can lead to higher bit densities in magnetic memory devices. As in Chapter 4.1.3, where the anisotropic Dzyaloshinskii-Moriya interactions for these systems were presented, different crystallographic orientations for the stacking of the systems were also considered for the calculations of the MAE.

In Fig. 5.1 the effect that the underlayer has over the MAE can be observed. In general, the fcc(111) structure has a larger MAE than the fcc(001) structure for systems with the same underlayer. It is also worth noticing, that the the magnitude of the MAE is not only related to the SOC, since if that would be the case the MAE would increase with increasing atomic number, as heavier atoms have larger spin-orbit coupling parameter ξ. Further evidence of this can be also seen when studying the hcp(001) stacking, where for the three different studied underlayers large variations were found.

The kind of oscillatory behaviour seen here, has been previously studied via first principles calculations, were the magnitude and sign of the MAE could be related to how filled is the $d-$band of the studied material [153, 154]. Also, the hybridization of the Co $d-$states with the $d-$states of the underlayer will have a profound effect on the MAE, as shown in previous calculations, in which the effect of the overlayer for a Co monolayer on Cu(001) was studied via the force theorem [155].

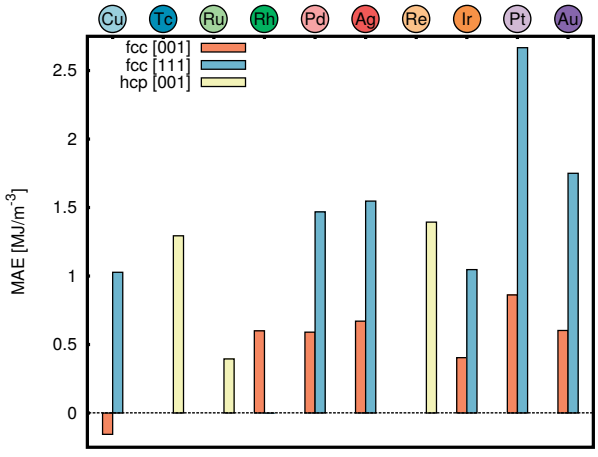

Figure 5.1. Magnetocrystalline energy for Co/Ni/Co heterostructures deposited over different substrates and different crystallographic orientations.

6. The Gilbert damping parameter

When magnetic moments in a material are driven out of their equilibrium position they will precess around the effective magnetic field acting over them, however, this precession does not last for an infinite time. After a finite time the magnetization will reach an equilibrium state. The reason is that the magnetic system dissipates energy, and this process is modelled by the second term of the Landau-Lifshitz-Gilbert equation (Eq. 2.3.5), which was previously presented. The rate of energy dissipation from the magnetic sub-system is determined by the Gilbert damping. From a magnetization dynamics standpoint the damping is usually treated as a free parameter or taken from experimental measurements. In experiments the damping can be determined from the peak linewidth obtained from ferromagnetic resonance (FMR) techniques. In these techniques the obtained damping contains both *intrinsic* and *extrinsic* contributions, some of which can be separated in experiments [26], although with some difficulty.

Intrinsic contributions to the damping refer to the microscopic mechanisms that give rise to the damping, whilst *extrinsic* contributions to the damping refer to effects such as eddy-currents, sample defects, magnon-magnon scattering, among others. In experiments it is possible to separate extrinsic and intrinsic contributions to the damping by performing measurements with both angular dependent and frequency dependent measurements.

However, from the theoretical standpoint the determination of the damping parameter from first principle calculations has been the focus point of intense development in the past decades [27, 28, 97–99, 156–159]. A fundamental aspect from the microscopic point of view is the fact that the damping parameter is a consequence of the spin-orbit coupling [156], which couples the magnetic moment to the lattice, and allows for the dissipation of energy and angular momentum from the spin system to the lattice. In the following a brief overview of theoretical treatments to determine the damping parameter from first principles will be presented.

6.1 Overview of theoretical methods

As it was previously discussed the time evolution of the magnetization, $\mathbf{M}$, of a system is described via the phenomenological Landau-Lifshiftz-Gilbert equation, Eq. 2.3.5, which can be rewritten in an alternative way as

$$\frac{d\mathbf{M}}{dt} = -\gamma \mathbf{M} \times \mathbf{B}_{\text{eff}} + \gamma \mathbf{M} \times \left[\frac{\tilde{G}(\mathbf{M})}{\gamma^2 |\mathbf{M}|^2} \frac{d\mathbf{M}}{dt} \right] \tag{6.1.1}$$

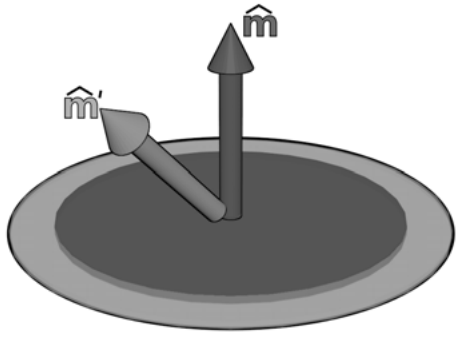

Figure 6.1. Schematic of the change of the Fermi surface for two different magnetization directions $\hat{m}$ and $\hat{m}'$. As can be seen the Fermi surface changes with the spin orientation.

where $\mathbf{B}_{\text{eff}}$ is the effective magnetic field acting over the magnetization, γ is the gyromagnetic ratio and $\tilde{G}$ is the relaxation tensor which is related to the damping parameter. Usually the Gilbert damping is assumed to be a scalar, however, in principle it is a tensor that depends on the spin orientation. There are two methods that have been developed to treat the damping from first principle methods, the **Breathing Fermi Surface** (BFS) method developed by Kamberský [27] and the **Torque-Correlation Model** (TCM) [28].

6.1.1 Breathing Fermi surface model

The model proposed by Kamberský [27] for the description of the Gilbert damping in metallic systems is based on the observation that if one considers an effective single electron theory in the presence of spin-orbit coupling, the energy of the electronic states, $\varepsilon_{j,\mathbf{k}}$, depends not only on the band number, j, and the wavevector, $\mathbf{k}$, but also on the direction of the magnetic moment $\hat{m}$. In this treatment the electrons transfer energy and angular momentum from the electrons to the lattice via scattering events. In the absence of dipolar interactions the spin-orbit coupling is necessary for this effect [158].

Under these considerations, one can study the same electronic system with two different magnetic orientations $\hat{m}$ and $\hat{m}'$, resulting in different energies for the magnetic states, therefore modifying the population number of states around the Fermi energy, due to the change of the shape of the Fermi surface as schematically shown in Fig. 6.1.

The process of redistribution of the occupation numbers, $n_{j,\mathbf{k}}$, occurs due to scattering processes between the different electronic states around the Fermi energy. Assuming a relaxation ansatz it is possible to write the time evolution of the non-equilibrium populations as

$$\frac{dn_{j,\mathbf{k}}(t)}{dt} = -\frac{1}{\tau_{j,\mathbf{k}}}\left[n_{j,\mathbf{k}}(t) - f_{j,\mathbf{k}}(t)\right] \tag{6.1.2}$$

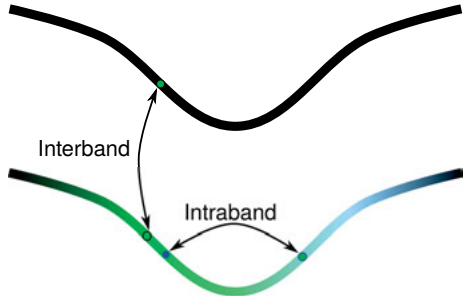

Figure 6.2. Schematic representation of intraband scattering events and interband scattering events, which can contribute to the Gilbert damping.

where $f_{j,\mathbf{k}}(t)$ are the equilibrium population give by the Fermi function and $\tau_{j,\mathbf{k}}$ is the relaxation time parameter, which codifies all the information about the scattering processes in the system. This relaxation ansatz is only valid for intraband scattering processes [157], meaning that no interband scattering processes are considered (see Fig. 6.2). As previously mentioned only states close to the Fermi energy are considered in this treatment.

If one considers the characteristic time of the motion of the magnetic moments as being much larger than the relaxation time $\tau_{j,\mathbf{k}}$ one can approximate the solution of Eq. 6.1.2 as

$$n_{j,\mathbf{k}}(t) = f_{j,\mathbf{k}}(t) - \tau_{j,\mathbf{k}} \frac{df_{j,\mathbf{k}}(t)}{dt}. \tag{6.1.3}$$

Considering that the total electron energy density is given by

$$E = \frac{1}{\Omega} \sum_{j,\mathbf{k}} \varepsilon_{j,\mathbf{k}} n_{j,\mathbf{k}} \tag{6.1.4}$$

where Ω is the volume of the Brillouin-Zone, it is then possible to define an effective field which mimics the action of the damping as

$$\mathbf{B} = -\frac{1}{|M|\,\Omega} \sum_{j,\mathbf{k}} n_{j,\mathbf{k}} \frac{\partial \varepsilon_{j,\mathbf{k}}}{\partial \delta \hat{m}} \tag{6.1.5}$$

where $\delta \hat{m}$ is the variation of the magnetic moment direction $\hat{m}$. This then allows one to write the Gilbert damping tensor as

$$\alpha_{\mu,\nu} = -\frac{\gamma}{|\mathbf{M}|} \sum_{j,\mathbf{k}} \tau_{j,\mathbf{k}} \frac{\partial f_{j,\mathbf{k}}}{\partial \varepsilon_{j,\mathbf{k}}} \frac{\partial \varepsilon_{j,\mathbf{k}}}{\partial \delta \hat{m}_\mu} \Big|_M \frac{\partial \varepsilon_{j,\mathbf{k}}}{\partial \delta \hat{m}_\nu} \Big|_M \tag{6.1.6}$$

with $\mu, \nu = x, y, z$. In the adiabatic limit the relaxation time is taken to be uniform $\tau_{j,\mathbf{k}} = \tau$. It is important to notice that the relaxation time τ depends on the mean free path of the electrons between scattering events. The temperature dependence of the relaxation time is usually taken to be given in the same way as for the Drude model for the itinerant electron [156, 157]. Another relevant factor is that in theoretical approaches based on the BFS τ is a parameter.

6.1.2 Torque correlation model

The torque correlation model (TCM) proposed by Kamberský [28], in principle depends on the same relaxation time, τ, as the BFS method, but the TCM allows for interband transitions. However, such restriction was lifted by Brataas *et al.* [159]. The damping can be described if one considers the dissipation of magnetic energy, E_{mag}, to be determined by the expectation value of the time evolution of the non-equilibrium many body Hamiltonian $\mathscr{H}$

$$\frac{dE_{\text{mag}}}{dt} = \langle \frac{d\mathscr{H}}{dt} \rangle . \tag{6.1.7}$$

It is also possible to write the loss of magnetic energy from the LLG equation (Eq. 6.1.1) by considering

$$\frac{dE_{\text{mag}}}{dt} = \mathbf{B}_{\text{eff}} \cdot \frac{d\mathbf{M}}{dt} = \frac{1}{\gamma^2} \frac{d\mathbf{M}}{dt} \left[\tilde{G}(\mathbf{M}) \frac{d\mathbf{M}}{dt} \right] \tag{6.1.8}$$

The Hamiltonian, $\hat{H}$, depends on the direction of the magnetization, $\hat{m}$. As the Hamiltonian considers the spin-orbit coupling it does not commute with the spin operator. Considering that one can take the time evolution of the magnetic moment $\hat{m}$ to be given by $\hat{m}(t) = \hat{m}_0 + \delta\hat{m}(t)$, with $\hat{m}_0$ the equilibrium state magnetization and $\delta\hat{m}(t)$ a small perturbation around the equilibrium state. Performing an expansion of the Hamiltonian up to the first order on $\delta\Updownarrow(t)$

$$\mathscr{H}(t) = \mathscr{H}(\hat{m}_0) + \delta\hat{m}(t) \cdot \frac{\partial\mathscr{H}}{\partial\delta\hat{m}}\Big|_{m_0} \tag{6.1.9}$$

and combining Eq. 6.1.8, Eq. 6.1.7 and Eq. 6.1.9 one can write the Gilbert damping tensor $\tilde{\alpha} = \frac{\tilde{G}}{|\mathbf{M}|\gamma}$ as

$$\begin{aligned} \alpha^{\mu\nu} = -\pi\hbar \sum_{\mu,\nu} \sum_{i,j} \frac{d\delta m^{\mu}}{dt} \frac{d\delta m^{\nu}}{dt} \langle \psi_i | \frac{\partial\mathscr{H}}{\partial\delta m^{\mu}} | \psi_j \rangle \times \\ \langle \psi_j | \frac{\partial\mathscr{H}}{\partial\delta m^{\nu}} | \psi_i \rangle \delta(\varepsilon_F - \varepsilon_i) \delta(\varepsilon_F - \varepsilon_j) \end{aligned} \tag{6.1.10}$$

with $\mu, \nu = x, y, z$. This expression can be re-written using the definition of the retarded single-particle Green's function

$$\text{Im}G^{+}(E_F) = -\pi \sum_i = |\psi_i\rangle \langle \psi_i| \delta(E_F - E_i) \tag{6.1.11}$$

$$\alpha^{\mu\nu} = -\frac{\hbar\gamma}{\pi|\mathbf{M}|} \text{Tr} \left(\frac{\partial\mathscr{H}}{\partial\delta m_{\mu}} \text{Im}G^{+}(E_F) \frac{\partial\mathscr{H}}{\partial\delta m_{\nu}} \text{Im}G^{+}(E_F) \right). \tag{6.1.12}$$

Considering the Hamiltonian, $\mathscr{H}$, to be given by the fully relativistic Dirac Hamiltonian in the local spin density approximation

$$\mathscr{H} = c\alpha \cdot \mathbf{p} + \beta mc^2 + V(\mathbf{r}) + \beta\sigma \cdot \hat{m}B(\mathbf{r}) \tag{6.1.13}$$

with α and β being the Dirac matrices, $\mathbf{p}$ is the relativistic momentum operator, $V\mathbf{r}$ is the spin averaged part of the LSDA potential and $B(\mathbf{r})$ is the spin dependent part of the LSDA potential. Then it is possible to define the magnetic torque operator as

$$T^{\mu} \equiv \frac{\partial \mathscr{H}}{\partial \delta m_{\mu}} = \beta B(\mathbf{r})\, \sigma_{\mu}. \tag{6.1.14}$$

The Green's function based expression for the damping parameter can be rewritten in the language of multiple scattering theory, which yields an expression for $\tilde{\alpha}$ which depends on the torque operator and the scattering path operator, $\tilde{\tau}^{nm}_{\Lambda\Lambda'}$, which in matrix notation yields

$$\alpha^{\mu\nu} = \frac{g}{\pi \mu_{\text{tot}}} \sum_{n} \text{Tr}\left(\underline{T}^{0\mu}\, \underline{\tilde{\tau}}^{0n}\, \underline{T}^{n\mu}\, \underline{\tilde{\tau}}^{n0}\right) \tag{6.1.15}$$

with $g = 2\left(1 + \frac{\mu_{\text{orb}}}{\mu_{\text{spin}}}\right)$, $\mu_{\text{tot}} = \mu_{\text{spin}} + \mu_{\text{orb}}$ is here the total magnetic moment while μ_{spin} and μ_{orb} the spin and orbital magnetic moments respectively.

For chemically disordered systems an average over configurations must be performed, this can be taken into account thanks to the coherent potential approximation (CPA), which implies than in Eq. 6.1.15 and average $\langle \cdots \rangle_c$ is necessary. It also has been shown [85, 102] that vertex corrections such as $\langle T^{\mu} \text{Im} G^{+} \rangle_c - \langle T^{\mu} \text{Im} G^{+} \rangle_c \langle T^{\nu} \text{Im} G^{+} \rangle_c$ are of great importance to ensure that "scattering-in"processes are properly taken into account.

Substitutional disorder in Heusler alloys

Since chemical disorder affects the scattering processes in a material it can have profound effects on the Gilbert damping. As previously mentioned, Heusler alloys have been extensively studied due to their favourable properties for possible spintronic applications.

In **paper IV** the effect of chemical disorder over the damping parameter for the half-Heusler $Ni_{1+x}Mn_{1-x}Sb$ was studied using both experimental measurements and first principle calculations based on the TCM as implemented in the SPR-KKR package [85, 97]. In Fig. 6.3 a comparison between experimental measurements and theoretical calculations can be observed.

It can be seen that as the concentration of antisites increases, the damping decreases. This can be understood when one considers that the chemical disorder leads to an increase of the scattering of electrons. The calculated behaviour matches quite well with the experimental trends, obtained via FMR measurements. The theoretical values are smaller than the measurements, this can be explained in part due to the difficulties of separating intrinsic and extrinsic damping effects in experiments [26]. Also one cannot neglect that other types of defects may be present in the samples, something that in not captured in the calculations.

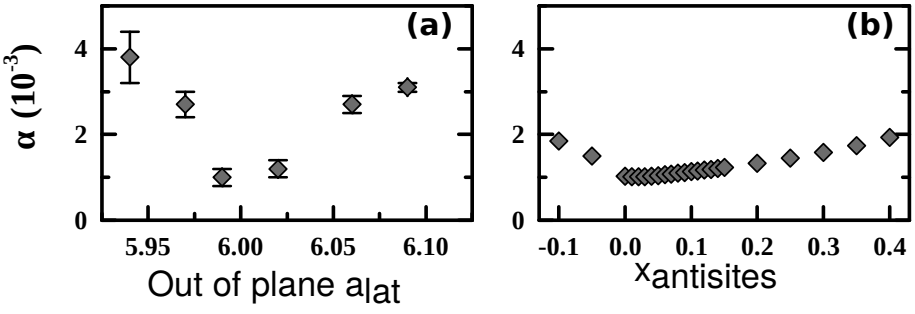

Figure 6.3. Dependence of the damping with increased concentration of Ni, a) experimentally and b) from first principle calculations. Negative values for x imply the introduction of Ni_{Mn} antisites and positive values are related to Mn_{Ni} antisite defects.

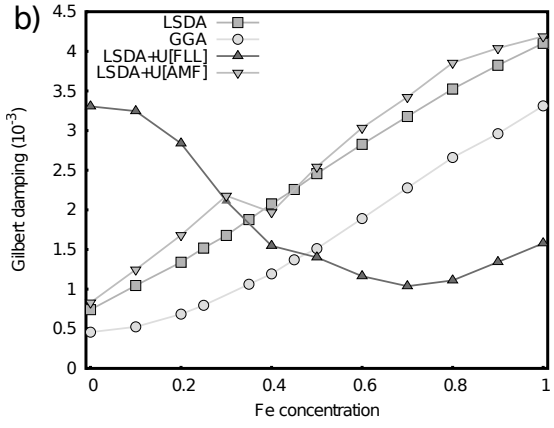

Figure 6.4. Dependence of the Gilbert damping for $Co_2Mn_{1-x}Fe_xSi$ as a function of the Fe concentration, for different treatments of the exchange correlation potential.

Another example of the influence of chemical disorder in the Gilbert damping, is the case of the alloy $Co_2Mn_{1-x}Fe_xSi$, which was studied in detail in **paper VI**. Both Co_2MnSi and Co_2FeSi are full Heusler alloys which crystallize in the $L2_1$ structure. As for the previous case the damping was calculated using the TCM approach, considering the geometry of the potential to be given by ASA. In Fig. 6.4 the dependence of the damping with Fe concentration is presented. One can see that considering the exchange correlation potential to be given by LSDA, GGA or LSDA+U[AMF] the obtained trend is quite similar. However, when considering the double counting term to be given by the FLL treatment the observed trend is quite different than for the other cases. This can be explained due to the fact that the FLL treatment may not be good approximation to describe this set of materials.

The observed behaviour of the damping is not only a consequence of the increased scattering due to defects. It is also heavily influenced by the loss of

half-metallicity of the system as the concentration of Fe increases. In the considered approximations Co_2MnSi is a half-metallic material, whilst Co_2FeSi is not. This has a profound influence on the damping of the material, as numerous studies suggest that there is a correlation between the density of states at the Fermi level and the damping parameter [160–162]. Hence, for materials with a small density of states at the Fermi energy the damping parameter is expected to be small when compared to the values of metallic systems.

For both $Ni_{1+x}Mn_{1-x}Sb$ and $Co_2Mn_{1-x}Fe_xSi$ the damping parameter was calculated for a finite temperature $T = 300$ K. How temperature effects can be included in the calculation of the Gilbert damping will be discussed in the next section.

Temperature effects

Temperature effects can be taken into account by considering the electron-phonon self energy $\Sigma_{\text{el-ph}}$ in the calculation of the Green's function [97]. An alternative is to consider a quasi-static approximation for thermal displacements of atoms from their equilibrium positions. This approach has been developed by Ebert *et al.* [97, 98]. Here an alloy analogy was used to average over atomic displacements, and the discrete set of displacements is chosen such that the root mean square of the displacement is given by the Debye model for a system with one atom per unit cell

$$\langle \sigma^2 \rangle = \frac{1}{4} \frac{3h^2}{\pi^2 m k_{\text{B}} \Theta_D} \left[\frac{\Phi\left(\frac{\Theta_D}{T}\right)}{\frac{\Theta_D}{T}} + \frac{1}{4} \right] \tag{6.1.16}$$

where Θ_D is the Debye temperature, Φ is the Debye function, k_{B} is the Boltzmann constant and h is Planck's constant.

In a similar way as for atomic displacements, Ebert *et al.* [98] also developed an alloy analogue model to treat spin fluctuations. Here several configurations of spin orientations are averaged over using the CPA approach, whilst considering a rigid spin approximation in the spin dependent part of the exchange correlation potential.

In **paper VI** the Gilbert damping for the full Heusler families Co_2MnZ, Co_2FeZ and Mn_2VZ with Z = (Al, Si, Ga, Ge) was calculated when both lattice displacements and spin fluctuations are considered. The effect that different exchange correlation potentials can have in the Gilbert damping can be seen in Fig. 6.5 for the full Heusler Co_2MnSi. When the exchange correlation potential is considered to be given by LSDA, GGA or LSDA+U[AMF], the damping first decreases with temperature, in what is dubbed a conductivity like behaviour, after that the damping increases with temperature, in a resistivity like behaviour. Whilst when the exchange correlation potential is considered via the LSDA+U[FLL] the damping is observed to decrease with temperature. Such profound difference can be explained by looking at the density of

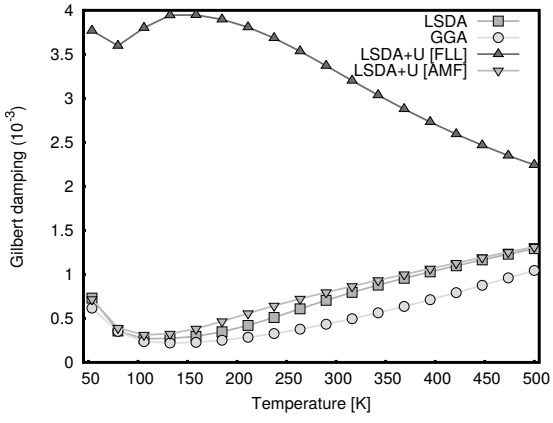

Figure 6.5. Temperature dempence for Co_2MnSi for different exchange correlation potentials. The dependence on temperature is greatly affected by the way when correlation effects are taken into account via the LSDA+U spproach.

states at the Fermi energy for the different exchange correlation potential as previously mentioned. As the LSDA+U[FLL] treatment destroys the half-metallic state, hence increasing the damping of the material, with respect to the half-metallic state.

The obtained values for the damping for all the studied Heusler alloys, are in general smaller than the experimental values. As previously mentioned this could be partly due to the consequence of the difficulties in separating intrinsic and extrinsic contributions to the damping. Also, for the particular case of Co_2MnSi the damping parameter can be profoundly affected by the loss of half-metallicity due to surface states, which can occur in specific terminations [163]. If the termination is chosen as to keep the half-metallicity ultralow damping can be obtained [162].

The effect that thermal and spin fluctuations have on the Gilbert damping for permalloy (Py) with composition $Fe_{0.19}Ni_{0.81}$, when it is dopped with transition metals was studied in **paper X**. In this work it was shown that spin fluctuations can have a profound effect on the magnitude of the damping, depending on which heavy metal that is used as a dopant for Py. In particular one can see that with increasing temperature, the spin fluctuations start to play a larger role. This is expected since the fluctuations of the magnetic moments will be larger the closer it is to the Curie temperature of the material.

7. Atomistic spin dynamics

The LLG equation (Eq. 2.3.5) has been used to study the magnetization at microscopic scale and *ab initio* methods can be used to parametrize the Heisenberg Hamiltonian, as described in previous chapters. As the magnetic moments are a quantum mechanical property it is natural to think that their behaviour can be described from first principle methods. Therefore, the question is whether there is a robust framework that allows one to combine the LLG equation and *ab-inito* methods to describe the magnetization dynamics.

Recent works such as the one from Antropov *et al.* [164] try to answer this question. In Chapter 3 the spin dependent Kohn-Sham equations were presented and how information about magnetic systems could be obtained from them was discussed. However, the formalism was developed for time independent systems, and to fully understand the dynamics one must consider the time dependent Schrödinger or Dirac equation. In the following, the derivation will be based on the Schrödinger equation as in the work by Antropov *et al.* [164]

$$i\frac{\partial \psi_{i\alpha}(\mathbf{r},t)}{\partial t} = \sum_{\beta=1}^{2}\left[-\nabla^2\delta_{\alpha\beta} + V_0(\mathbf{r},t)\,\delta_{\alpha\beta} + (\sigma\cdot\mathbf{B}_{\text{eff}}(\mathbf{r},t))_{\alpha\beta}\right]\psi_{i\beta}(\mathbf{r},t)\,. \tag{7.0.1}$$

where the first term on the right hand side is the kinetic term, $V_0(\mathbf{r},t)$ is a scalar potential and $\sigma\cdot\mathbf{B}(\mathbf{r},t)$ is the magnetic potential.

Hence, a solution of the time dependent Kohn-Sham equations would require a time dependent parametrization of the exchange-correlation potential.

Since a parametrization of the time independent problem is already difficult, the introduction of time-dependent effects complicate the situation even more. Therefore, for most applications the *adiabatic approximation* is made, where the fast degree of freedoms are separated from the slow ones. The slow variables are considered to be frozen while the fast ones are allowed to evolve freely. An example of an adiabatic approximation is the Born-Oppenheimer approximation where the ions would be the slow variables and the electrons the fast ones. This approximation was used in Chapter 3 to formulate the Kohn-Sham equations.

In the case of magnetism, the separation between fast and slow variables is not as intuitive. The slow variables are the local directions of the magnetization while the fast variables are the electron densities. The magnetization density also fluctuates rapidly due to the scattering of itinerant electrons which are prevalent in $3d-$transition metals, henceforth an average over the typical

electron scattering time is of relevance to ensure that the localized atomic moment treatment is valid [164, 165]. The separation between the electronic and magnetic subsystem is possible due to the fact that the transversal excitations of the magnetization are orders of magnitude smaller than the electronic structure energies. The approximation is also justified by looking at the different energy scales present in the system, the exchange interactions, J_{ij}, are usually small (< 100 meV) when compared to the electronic energies, i.e. the band formation energy, bandwidth, etc. [164].

The separation of degrees of freedoms allows the transformation of the time dependent Kohn-Sham equations to its time independent counterpart for a fixed direction of the magnetization, which is Eq. 3.1.13 for a set of instantaneous eigenstates. The electronic density, $n(\mathbf{r})$, is then used as a potential for the effective magnetic field that will exert a torque on the magnetization. As the magnetization is dictated by spin of the electrons, it is useful to define the spin density as $\mathbf{S}(\mathbf{r},t) = \psi^{\dagger}(\mathbf{r},t)\,\mathbb{S}\,\psi(\mathbf{r},t)$, where $\mathbb{S}$ is the spin operator. Therefore, one can then find the equation of motion for the slow variables i.e. the directions of the atomic magnetic moments, by taking the Schrödinger equation

$$i\frac{\partial \psi(\mathbf{r},t)}{\partial t} = \mathscr{H}_{\mathrm{KS}}\psi(\mathbf{r},t) \tag{7.0.2}$$

$$-i\frac{\partial \psi^{\dagger}(\mathbf{r},t)}{\partial t} = [\mathscr{H}_{\mathrm{KS}}\psi(\mathbf{r},t)]^{\dagger} \tag{7.0.3}$$

where $\mathscr{H}_{\mathrm{KS}}$ is the spin dependent Kohn-Sham Hamiltonian (see Eq. 7.0.1). Then considering the time evolution of the spin density one can write

$$\frac{\partial \mathbf{S}(\mathbf{r},t)}{\partial t} = \psi^{\dagger}(\mathbf{r},t)\,\mathbb{S}\frac{\partial \psi(\mathbf{r},t)}{\partial t} + \frac{\partial \psi^{\dagger}(\mathbf{r},t)}{\partial t}\mathbb{S}\psi(\mathbf{r},t) \tag{7.0.4a}$$

$$\frac{\partial \mathbf{S}(\mathbf{r},t)}{\partial t} = \frac{1}{i}\left[\psi^{\dagger}(\mathbf{r},t)\,\mathbb{S}\mathscr{H}_{\mathrm{KS}}\psi(\mathbf{r},t) - [\mathscr{H}_{\mathrm{KS}}\psi(\mathbf{r},t)]^{\dagger}\,\mathbb{S}\psi(\mathbf{r},t)\right] \tag{7.0.4b}$$

neglecting any possible relativistic effects, the spin operator commutes with the effective scalar potential $V_0(\mathbf{r})_{\alpha\beta}$. Hence, only terms containing the kinetic term or the magnetic field will determine the time evolution of the spin density. Thus, one can write

$$\frac{\partial \mathbf{S}(\mathbf{r},t)}{\partial t} = -\nabla\cdot\mathbf{Q}_{\mathrm{KS}}(\mathbf{r},t) - \gamma\mathbf{S}(\mathbf{r},t)\times\mathbf{B}_{\mathrm{eff}} \tag{7.0.5}$$

where the last term of the right hand side is a consequence of the commutation relation of the spin operator, and $\mathbf{Q}_{\mathrm{KS}}(\mathbf{r},t)$ is defined as

$$\mathbf{Q}_{\mathrm{KS}}(\mathbf{r},t) = \frac{1}{2i}\left[\left(\mathbb{S}\nabla\psi^{\dagger}(\mathbf{r},t)\right)\psi(\mathbf{r},t) - \psi^{\dagger}(\mathbf{r},t)\,\mathbb{S}\nabla\psi(\mathbf{r},t)\right] \tag{7.0.6}$$

where the term $\nabla\cdot\mathbf{Q}^{\mathrm{KS}}(\mathbf{r},t)$ describes the action of the spin currents in the system. For insulators, or in general, materials in which the spin current is

negligible one can neglect this term, nevertheless this term is of great importance when one describes the spin transfer torque (STT) effect [9–11, 17, 166], which will be explained in detail in section 7.3.2. Neglecting the current term and integrating over the atomic cells, one can obtain the equation of motion for the atomic magnetic moments from Eq. 7.0.5

$$\frac{\mathrm{d}\mathbf{m}_i}{\mathrm{d}t} = -\gamma \mathbf{m}_i \times \mathbf{B}^i_{\mathrm{eff}}(\mathbf{r},t)\,, \tag{7.0.7}$$

as can be seen the equation of motion obtained here corresponds to the precession term of the LLG equation 2.3.5.

As shown here, the precession term of the LLG equation can be obtained from first principles and the description of the damping term can also in principle be obtained from *ab initio* considerations. If the magnetic system would be completely isolated the angular momentum and the energy would be conserved, but in reality the system is connected to a lattice and the magnetic moments do interact with the electrons. Damping mechanisms extend from the spin-orbit coupling, to damping trough radiation when considering the Maxwell equations. A Gilbert like term can be obtained from a single electron picture when considering a non-relativistic expansion of the Dirac equation [167]. Henceforth, an atomistic analogous to Eq. 2.3.5, can be written for each atomic moment, $\mathbf{m}_i$, subjected to an effective field, $\mathbf{B}^i_{\mathrm{eff}}$, with a Gilbert damping α_i

$$\frac{\mathrm{d}\mathbf{m}_i}{\mathrm{d}t} = -\frac{\gamma}{1+\alpha_i^2}\left(\mathbf{m}_i \times \mathbf{B}^i_{\mathrm{eff}} + \alpha_i \mathbf{m}_i \times \left[\mathbf{m}_i \times \mathbf{B}^i_{\mathrm{eff}}\right]\right) \tag{7.0.8}$$

In Chapter 6, some of the theoretical approached used to obtain the damping from first principles were presented, allowing a more complete parametrization of the atomistic LLG equation. Theoretical models treating the damping as a tensorial quantity have also been proposed as well as generalizations of the LLG equation including an inertial tensor contribution which can be relevant for ultrafast processes [168]. Calculations of the Gilbert damping (scalar) term from DFT methods have been performed with a reasonable good agreement with the parameters extracted from FMR experiments [97–99], as previously presented in Chapter 6. For these reasons it becomes clear that the use of the LLG equation for atomistic level systems is justified as long as one keeps in mind the fact that the atomistic LLG equation is only valid in the adiabatic approximation, i.e. one must be able to separate the electronic and the magnetic subsystems. Therefore, one can use the LLG equation in conjunction with *ab initio* approaches to describe and model systems which one would not be able to with the conventional micromagnetic formalism.

However, there are several limitations that any approach based in the LLG equation presents. One that is very relevant, due to the recent developments in the area of *ultrafast dynamics*, is that the adiabatic approximation limits the phenomena which can be studied using the LLG equation. Excitations in

which the magnetization and electronic processes are in the same time scales, such as ultrafast demagnetization processes, cannot in principle be properly treated with the LLG equation. Nevertheless, several models have been proposed to try to solve these shortcomings [169, 170].

For atomistic models, another problem from the computational point of view is the treatment of the dipolar interaction. Due to the long range nature of the dipolar interaction its treatment becomes very expensive computationally, as situations in which the dipolar interactions become relevant would require billions of atoms to be considered. Therefore parallelization schemes and methods such as the Fast Multipole Method (FMM) have to be considered.

7.1 Temperature effects

As previously discussed in Chapter 2 the magnetic order of a system can vary due to temperature effects. Several techniques are generally used to describe such effects, for static properties Monte Carlo methods are usually the method of choice, whilst for dynamic properties a reformulation of the LLG equation (Eq. 2.3.5) on the spirit of Langevin dynamics must be performed.

7.1.1 Monte Carlo methods

Monte Carlo (MC) methods, refers to a series of importance sampling algorithms which search through the possible configurations of a system, with the objective of finding the most probable one at a given set of conditions. One of the most used algorithms, in the context of magnetism, is the Metropolis algorithm, which is used to describe the static properties of a magnetic system, described by a certain Hamiltonian, usually the Heisenberg Hamiltonian.

For a system of N magnetic moments, the Metropolis algorithm can be summarized in the following way

1. Randomly select a magnetic moment i in the computational cell.
2. Perform a trial rotation of the $i-$th moment, any rotation on the unit sphere is permitted.
3. Calculate the energy difference, ΔE, between the initial configuration and the trial configuration.
   - If $\Delta E < 0$ the trial move is accepted.
   - If $\Delta E > 0$ the trail move is accepted with a probability given by $e^{-\frac{\Delta E}{k_B T}}$
4. Select a new trial moment and repeat from step 2 until the number of visited moments is equal to the number of moments in the system.
5. When a number of trials equal to N one MC step has been done, repeat from step 1.

The Metropolis algorithm can be used to obtain properties of the system such as the Curie temperature. This can be obtained by looking at the Binder

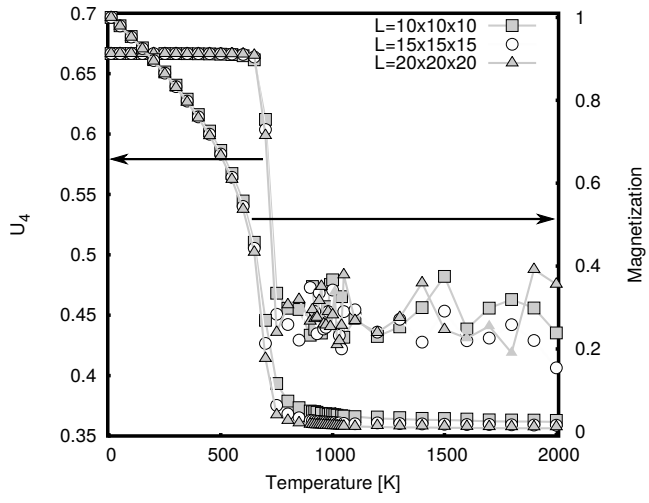

Figure 7.1. Binder cumulant as a function of temperature for Co_2FeSi for different simulation box sizes. The intercept of the curves indicates the transition temperature of the system.

cumulant, which for a ferromagnet can be written as

$$U_4 = 1 - \frac{\langle m^4 \rangle}{3\langle m^2 \rangle^2} \tag{7.1.1}$$

where m is the magnetization of the system. The intersect of U_4 for different simulation cell sizes can be then used to determine the critical temperature [171].

This approach was used in **paper VI** where the critical temperature of several Heusler alloys was determined, using exchange interactions determined from first principles calculations. In Fig. 7.1 the Binder cumulant as a function of temperature for Co_2FeSi is presented. The exchange interactions were obtained with the LKAG formalism presented in Chapter 4, considering the exchange correlation potential to be given by LSDA and the geometry of the potential to be described by ASA. The calculated T_c for this combination of exchange correlation potential and geometrical shape of the potential, is smaller than the experimental results. This could be due to the loss of half-metallicity in this approximation. Which results in smaller exchange interactions, than the ones that would occur in the half-metallic state. This also corresponds to the calculations performed using a full-potential scheme. In them the pseudogap present in one of the spin channels is better described than in the ASA case, resulting in larger exchange interactions, and as a consequence, a larger Curie temperature. The Binder cumulant is constant until the effects of thermal disorder become more relevant close to T_c. At this point large oscillations can be seen due to the fact that the system has reached the paramagnetic state.

Despite of the usefulness of the Metropolis algorithm in describing static properties of a material, it is not suited to treat dynamical processes since Monte Carlo time, i.e. number of MC steps performed in a simulation, is not necessarily linked to a physical time. Kinetic Monte Carlo (KMC) approaches [172], overcome this difficulty by calculating the time between unlikely events separated by an energy barrier.

7.1.2 Langevin Dynamics

In the Langevin picture, thermal effects are included by redefining the effective field $\mathbf{B}_{\text{eff}}$ to include a stochastic field $\mathbf{b}(t)$, such that $\mathbf{B}_{\text{eff}} = \mathbf{B}_{\text{eff}} + \mathbf{b}(t)$. The stochastic field is modelled as a Gaussian white noise, to make all possible excitations equally preferred. The constraint to a Gaussian distribution is not necessary and several other alternatives can in principle be considered to describe certain physical processes, such as ultrafast dynamics in which the noise might be correlated [173, 174]. Nevertheless, most applications model the fluctuation term as a Gaussian with certain restrictions being applied to it to better reproduce the experimental observations. This term must fulfil certain criteria which can be resumed as follows

$$\langle \mathbf{b}(t) \rangle = 0 \tag{7.1.2a}$$

$$\langle b_i(t)\, b_j(t') \rangle = 2D\delta_{ij}\delta(t-t') \tag{7.1.2b}$$

$$D = \frac{\alpha}{(1+\alpha^2)} \frac{k_{\text{B}}T}{\mu_B m}, \tag{7.1.2c}$$

where $\langle \cdots \rangle$ denotes time average. The later set of equations show that the time average of the stochastic field is zero (Eq. 7.1.2a), that the field is uncorrelated in time ($\delta(t-t')$) and in each of the directions (δ_{ij} where $i = \{x, y, z\}$) (Eq. 7.1.2b). The strength of this field, D ,depends on the temperature T and can be obtained from the stationary solution of the Fokker-Planck equation [175].

Therefore by introducing the stochastic field the LLG equation becomes

$$\frac{\mathrm{d}\mathbf{m}_i}{\mathrm{d}t} = -\frac{\gamma}{1+\alpha^2}\left(\mathbf{m}_i \times \left(\mathbf{B}^i_{\text{eff}} + \mathbf{b}^i(t)\right) + \frac{\alpha}{m_i}\mathbf{m}_i \times \left[\mathbf{m}_i \times \left(\mathbf{B}^i_{\text{eff}} + \mathbf{b}^i(t)\right)\right]\right), \tag{7.1.3}$$

allowing one to describe dynamical magnetization processes at finite temperature. The stochastic LLG is used throughout this thesis when spin dynamics simulations at finite temperatures are performed. Such capability has been demonstrated to be of great interest with the discovery of phenomena as the spin Seebeck effect [176] among others.

7.1.3 Thermally driven dynamics in FeGe

Thermally driven dynamics of magnetic structures have also garnered a large amount of attention from experiments. This in combination with techniques such as diamond nano-vacancy magnetometry, allows the study of magnetic structures not usually available with other techniques.

In **paper V** thermally driven dynamics for helical magnetic structures have been studied both via experimental and theoretical techniques. The studied system was the non-centrosymmetric FeGe, which is known to have a large DM interaction, giving rise to helical spin spiral configurations as reported in section 4.1.3.

By using a combination of Magnetic Force Microscopy (MFM) [177] and diamond nanovancy (NV) magnetometry [127, 128], it was possible to experimentally measure the spin spiral period for FeGe at temperature close to the Neel temperature of the system, thus allowing the observation of thermally driven dynamics. As previously discussed in Chapter 4, NV magnetometry is a novel technique that allows the study of magnetic textures with very high spatial resolution [129, 178].

More importantly, the present techniques allows one to obtain information on the time domain, allowing one to track the thermal dynamics of helical systems. In Fig 7.2**a** a snapshot of the magnetic structure of the system at $T = 255$ K is shown, the alternating dark and bright regions represent the alternating orientation of the magnetic structure. One can also see that there is an edge dislocation present in the sample, which is highlighted in panel **b**, this kind of defects are known to have a non-trivial topology [126, 179–181], i.e. they have a non-zero topological number (for details on topological numbers see section 7.4). In panel **c**, one can see an schematic representation of the defects, where it is shown how the magnetization alternate between orientations in the spiral state, and how the defect introduces a change in this pattern. However, the most relevant aspect comes when examining panel **e**, in which the time dependence of the spiral period is measured. It can be seen that at ~ 110 s an abrupt jump in the spiral period is observed.

The abrupt change in the period can be understood by looking at the thermal dynamics of the defects. For this the exchange interactions and DM vectors for FeGe were calculated using the LKAG formalism, as previously described in Chapter 4. These were coarse grained such as to obtain an effective micromagnetic model, which captures the same spin spiral wavelength than the atomistic description. In Fig. 7.2 panels **f**, **g** and **h** snapshots of the thermal dynamics obtained from the LLG are presented, in this one can see that due to temperature fluctuations it is possible to stabilize the edge dislocations observed in experiments. Even more, stochastic fluctuations can cause the defects to move, either perpendicular to the spiral wave vector, trying to reach the edge of the sample to obtain a perfectly ordered spiral configuration (panel **f**). Or along the spiral wave vector, resulting in multiple defects with different topological

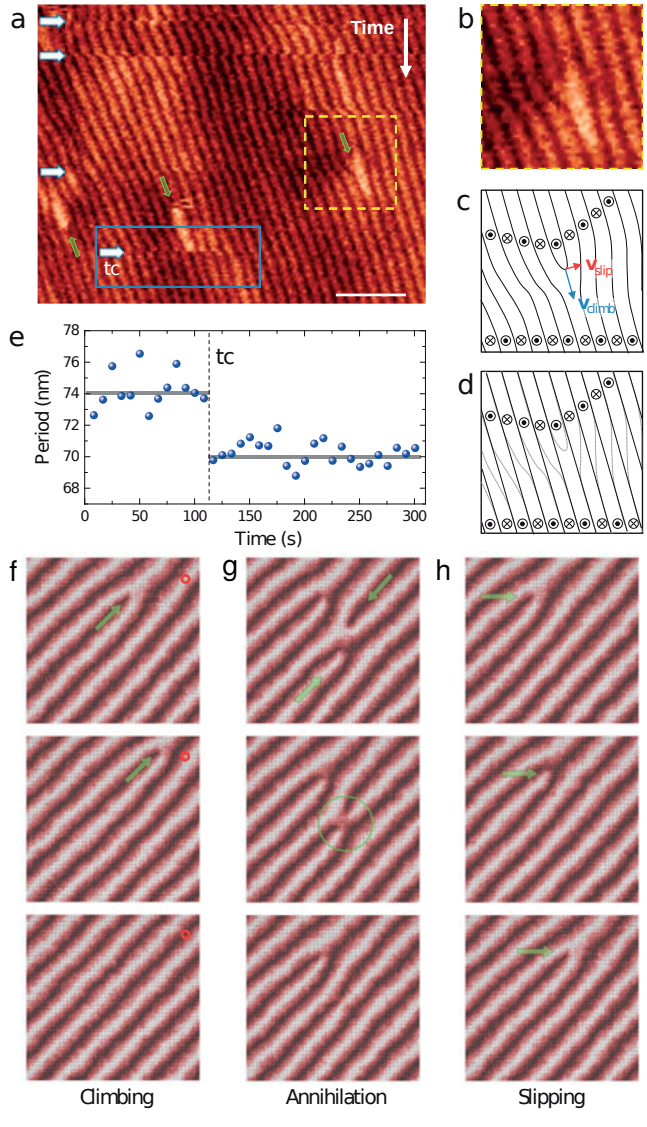

Figure 7.2. **a** MFM image of the helical magnetic structure displaying topological defects, as identified by green arrows. The white arrows represent stochastic jumps of the magnetization. **b** Zoom-in of the area highlighted with the yellow box in **a** which showcases one of the mentioned defects. **c** Schematic representation of the edge dislocations, the arrows indicate the directions of the possible motion of the defect. **d** Schematic illustration of the magnetic structure after the defect has moved. **e** Evolution of the local spin spiral period as a function of time evaluated in the blue box in **a**. The lower panels **f**, **g** and **h** showcase the results from spin dynamic simulations where different mechanisms for the motion of the defect can be seen.

number being annihilated (panel **g**) or the defect "jumping", between different magnetic orientations.

This stochastic motion of the defects can be one the factors responsible behind the abrupt change of the spiral period, since if the measurement is performed in an area of the sample where this defects are present the obtained wavelength is not the one of a perfectly ordered system. Temperature fluctuations could then lead this defect to move out of the measurement region, leading to a measurement of the fully ordered magnetic structure. Understanding the behaviour of the edge dislocations is valuable for the description of the formation and stabilization of skyrmionic textures, since the key role that they play in the nucleation of these textures.

7.2 Spin Waves

The atomistic LLG equation describes the motion of the magnetic moments of the atoms dictated by a certain effective field. The effective field for the i-th atom, $\mathbf{B}_{\text{eff}}^{i}$, contains interactions terms which depend on other magnetic moments in the sample as exemplified by the extended Heisenberg Hamiltonian (Eq. 2.2.2), meaning that the equations of motion for different moments are coupled. Hence, an excitation of any kind of one of the moments will propagate trough the sample.

To understand the propagation of these interactions, one can consider a 1D ferromagnetic spin chain with only nearest neighbour Heisenberg exchange interactions J.

$$\mathscr{H} = -\sum_{\langle i,j \rangle} J\hat{m}_i \cdot \hat{m}_j \tag{7.2.1}$$

then, the field acting over the j-th magnetic moment is written as

$$\mathbf{B}_{\text{eff}}^{j} = 2J\left(\hat{m}_{j+1} + \hat{m}_{j-1}\right), \tag{7.2.2}$$

considering that the temperature is set to zero and that there is no damping term the equation of motion is written as

$$\frac{\mathrm{d}\hat{m}_j}{\mathrm{d}t} = -\gamma\hat{m}_j \times \left[2J\left(\hat{m}_{j+1} + \hat{m}_{j-1}\right)\right]. \tag{7.2.3}$$

If the moments are considered to be aligned towards the z-axis, one can write the LLG in Cartesian coordinates in the following way

$$\frac{\mathrm{d}m_j^x}{\mathrm{d}t} = -\gamma 2J\left[m_j^y\left(m_{j-1}^z + m_{j+1}^z\right) - m_j^z\left(m_{j-1}^y + m_{j+1}^y\right)\right] \tag{7.2.4}$$

plus cyclic permutation terms. In the limit of small deviations $m_j^z = m_j$, which means that the quadratic terms on the transversal components i.e. x and y can

be neglected, leading to

$$\frac{\mathrm{d}m_j^x}{\mathrm{d}t} = -\gamma 2J\left[2m_j^y - m_{j-1}^y - m_{j+1}^y\right] \tag{7.2.5}$$

$$\frac{\mathrm{d}m_j^y}{\mathrm{d}t} = \gamma 2J\left[2m_j^x - m_{j-1}^x - m_{j+1}^x\right] \tag{7.2.6}$$

$$\frac{\mathrm{d}m_j^z}{\mathrm{d}t} = 0. \tag{7.2.7}$$

Now it becomes a matter of finding the solution to Eq. 7.2.5 and Eq. 7.2.6. Considering that there is a spacing a between each spin and that the chain is infinite the solutions can be written as

$$m_j^x = A\exp\left(i\left[jqa - \omega_q t\right]\right) \tag{7.2.8}$$

$$m_j^y = B\exp\left(i\left[jqa - \omega_q t\right]\right), \tag{7.2.9}$$

where q is the wave vector and ω_q is the frequency. If one introduces these solutions in the equation of motion and remembers that $\gamma = \frac{g_e\mu_B}{\hbar}$ it is possible to write

$$\hbar\omega_q = 4J\mu_B g_e\left[1 - \cos\left(qa\right)\right]. \tag{7.2.10}$$

This equation is the dispersion relation of a ferromagnet which in the limit of small wave vectors reduces to

$$\varepsilon_q \approx Dq^2, \tag{7.2.11}$$

where $D = 2J\mu_B g_e a^2$ is the spin-wave stiffness.

Due to the coupled nature of the LLG equation an excitation will not be localized but will propagate. These excitations are known as *spin waves* in the semi-classical Heisenberg model, while the particle like equivalent excitation is known as a *magnon*. The characteristics of these excitations in the sample will be dictated by the dispersion relation of the system, which as shown in the example of the 1D Heisenberg chain is completely determined by the Hamiltonian of the system (which is related to the crystalline structure of the system).

The calculation of the magnon dispersion relation is of great importance as it give us information about which kind of excitations are allowed in the system. In a real system the situation is more complex, hence numerical methods must be used to obtain the dispersion relation.

7.2.1 Adiabatic magnon spectra

One of the used methods to calculate the spin wave dispersion relation is the adiabatic magnon spectra (AMS) [182]. In this approach, one can obtain the dispersion relation by performing a Fourier transform of the interatomic exchange interactions J_{ij}'s. In the case of a single atom per unit cell, this implies

that for a ferromagnetic ground state, the energy as a function of the reciprocal vectors can be written as

$$E(\mathbf{q}) = \sum_{j\neq 0} J_{0j}\left[\exp\left(i\mathbf{q}\cdot\mathbf{r}_{0j}\right) - 1\right] \tag{7.2.12}$$

where the $\mathbf{r}_{ij}$ is the relative position vector between the $i-$th and $j-th$ site. Hence, one can then generalize this approach for a system with N_A atoms for unit cell, by constructing a $2N_A \times 2N_A$ matrix

$$\begin{bmatrix} \sum_j^{\mathrm{NA}} J_0^{ij} - J^{ii}(\mathbf{q}) & -J^{ij}(\mathbf{q}) \\ -J^{ij}(\mathbf{q})^* & \sum_j^{\mathrm{NA}} J_0^{ij} - J^{jj}(\mathbf{q}) \end{bmatrix} \tag{7.2.13}$$

The calculation of the eigenvalues of this matrix would then yield the adiabatic magnon spectra for a system with N_A atoms per unit cell.

It is important to notice that in the present approach, neither temperature effects nor broadening due to the finite lifetime of the magnons are taken into account. Also, until recently the calculation of spin wave dispersion relation for non-collinear systems with this approach was not possible, however, recent works such as the one by Toth and Lake [183],has allowed for a linear spin wave theory approach for incommensurate magnetic structures.

7.2.2 Dynamical structure factor

Atomistic spin dynamics is an excellent tool to obtain the magnon dispersion relation of complex materials. If one introduces temperature to a system, it will be excited and spin waves will propagate through it. One way to calculate the spin waves is to make use of the space and time displaced correlation function $C^k(\mathbf{r}-\mathbf{r}',t)$. This quantity gives information on how alike are two different magnetic moments, where $\mathbf{r}$ and $\mathbf{r}'$ are their positions, t it the time and k is the Cartesian coordinate of the moments. The correlation function is written as

$$C^k\left(\mathbf{r}-\mathbf{r}',t\right) = \langle m_{\mathbf{r}}^k(t)\, m_{\mathbf{r}'}^k(0)\rangle - \langle m_{\mathbf{r}}(0)\rangle\langle m_{\mathbf{r}'}(0)\rangle, \tag{7.2.14}$$

the brackets signify an average over ensembles. Performing a Fourier transform in space and time results in the *dynamical structure factor*

$$S^k(\mathbf{q},\omega) = \frac{1}{\sqrt{2\pi}N}\sum_{\mathbf{r},\mathbf{r}'} e^{i\mathbf{q}\cdot\left(\mathbf{r}-\mathbf{r}'\right)} \int_{-\infty}^{\infty} e^{i\omega t} C^k\left(\mathbf{r}-\mathbf{r}',t\right)\mathrm{d}t, \tag{7.2.15}$$

where $\mathbf{q}$ and ω are the momentum and energy transfer. The dynamical structure factor gives information about the excitations that are present in the system, in a similar way as the data obtained via neutron scattering experiments. If one plots the peaks of $S(\mathbf{q},\omega)$ along a particular path in the reciprocal space, the dispersion relation of the system can be obtained. An aspect worth noticing is that one needs temperature to have spin waves. These excitations need

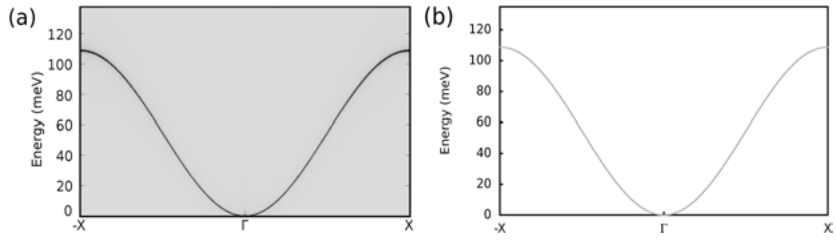

Figure 7.3. Magnon dispersion relation for a 1D Heisenberg chain obtained from the dynamical structure factor $\mathbf{S}(\mathbf{q},\omega)$ (Eq. 7.2.15) and Eq. 7.2.10. Both methods correspond quite well showing that the correlation function can be used to calculate the dispersion relation of complex magnetic systems.

a certain energy to exist, a system in its ground state at $T = 0$ K has no spin waves as there would be no energy to displace the moments from the equilibrium position.

Using this method, the dispersion relation for the ferromagnetic Heisenberg chain previously presented can be calculated. In Fig 7.3 it is possible to see that the dispersion relation obtained from the correlation function and the analytical expression correspond quite well. The height and width of the $\mathbf{S}(\mathbf{q},\omega)$ from the LLG equation depends on the choice of damping parameter α and temperature at which the calculations are made. It is also relevant to notice that the obtained dispersion relation only considers exchange interactions, if one would consider the excitations that result from dipolar interactions they would present much lower energies (i.e. lower frequencies $\omega_{exc} \sim$ THz $\omega_{dip} \sim$ GHz) and correspond to small $\mathbf{q}$-values.

It is important to notice that under the LLG equation the magnitude of the moments has to be kept constant. At high enough temperatures Stoner excitations will be present, in which an electron is excited from an occupied state of the majority spin channel to an empty state of the spin channel, causing the local atomic moment to change size, this is expected to play a big role in itinerant magnets such as nickel. Also, this affects the intensity of the magnon dispersion relation, as Stoner excitations will damp the intensity of the optical branch, such effects cannot be captured with the present approach, and methods as TD-DFT are needed to capture some of them [184].

Comparison between AMS and $S(\mathbf{q},\omega)$

The adiabatic magnon spectra and the dynamical structure factor can be then used to study materials with parameters from first principles. In **paper VI** the half-metallic Heusler families Co_2MnZ, Co_2FeZ and Mn_2VAl with Z=(Al, Si, Ga, Ge) were studied. In Fig. 7.4 a comparison between the adiabatic magnon spectra and the dynamical structure factor at $T = 300$ K for Co_2FeSi is presented, with the exchange interactions obtained from the LKAG formalism

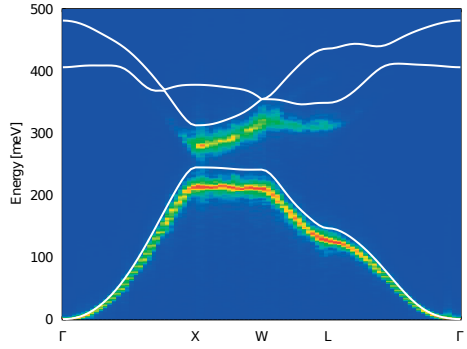

Figure 7.4. As presented in **paper VI**, a comparison of the adiabatic magnon spectra (solid lines) with the dynamical structure factor $S(\mathbf{q},\omega)$ for Co_2FeSi at $T = 300$ K, when the shape of the potential is considered to be given by the atomic sphere approximation and the exchange correlation potential to be given by LSDA, some softening can be observed due to temperature effects specially observed at higher q-points.

introduced in Chapter 4. The Gilbert damping was calculated with the method described in Chapter 6, which yield a value of $\alpha = 0.004$ for $T = 300$ K.

The main differences between the AMS and dynamical structure factor, arise from the temperature effects included in the atomistic spin dynamics, but are not taken into account in the AMS treatment which is observed in the softening of the spectra. Due to the fact that the critical temperature of the system is much larger than $T = 300$ K ($T_c = 655$K in LSDA), temperature effects are quite small. The high energy optical branches are also softened and in general are much less visible. This is expected since the correlation was studied using only vectors in the first Brillouin zone and as has been shown in previous works [185], a phase shift is sometimes necessary to properly reproduce the optical branches, implying the need of vectors outside the first Brillouin zone. Stoner excitations dealing with electron-hole excitations result in the Landau damping which affects the intensity of the optical branches. Such effects are not captured by the present approach, but can be studied by other methods such as time dependent DFT [184]. The shape of the dispersion relation along the path $\Gamma - X$ also corresponds quite well with previous theoretical calculations performed by Kübler [34].

It is important to notice, that as the damping increases the broadening of the bands increases, and the overall intensity of the bands is also affected. In the limit of small damping and vanishing temperatures, the AMS and $S(\mathbf{q},\omega)$ would match with each other. Also, the present scheme can be used to treat systems in which Dzyaloshinskii-Moriya interaction is present, which can lead to anti-symmetric dispersion relations, as in the case of two monolayers of Fe on W(110), which was found to exhibit a large antisymmetric dispersion relation from experiments [186] and theoretically described [187] by making use of the methodology described above.

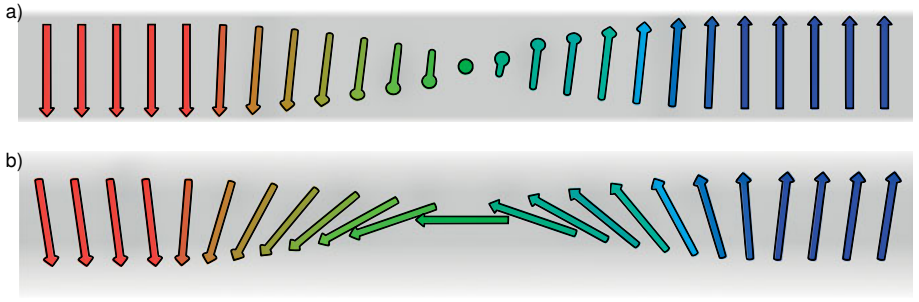

Figure 7.5. Difference between the Bloch wall **a** and the Néel wall **b**. The Bloch wall rotates out of the plane of the magnetization while the Néel wall has the moments rotating in plane.

7.3 Domain wall dynamics

The region between two magnetic domains is known as a *domain wall* (DW) and it is characterized by a given width and magnetic configuration. The size and shape of such region depends on the strength of the interactions present in the system as well as the geometry of the sample.

For instance the exact size of the domain wall is the result of the competition between the exchange interaction and the uniaxial anisotropy. The exchange interaction in a ferromagnetic material tends to align all the magnetic moments parallel to each other, hence an abrupt transition between two domains is energetically unfavourable for the exchange term, since this would be minimized if the transition is as smooth as possible. On the other hand, the anisotropy term will prefer the domain wall to be as sharp as possible as any deviation from the easy axis leads to a gain in the anisotropy energy.

In Fig. 7.5 one can see two of the most common types of domain walls, the Bloch wall (Fig. 7.5**a**) and the Néel wall (Fig. 7.5**b**). In the Bloch wall the magnetization rotates trough the plane of the wall, while in the Néel wall the moments rotate within the plane of the wall.

The difference between the Bloch and Néel wall comes from the magnetostatic term. In a thin film the Bloch wall generates a larger demagnetizing field than the Néel wall, as the demagnetizing field of the Bloch wall would occur at the surface of the wall, while the one for the Néel wall occurs in the volume. On the contrary, in a bulk material Bloch walls will be preferred [188, 189].

As previously mentioned the competition between the exchange interaction and the anisotropy determine how wide the domain wall is. This can be easily seen for a Bloch wall if one writes the Heisenberg Hamiltonian in the continuous form

$$E_{\text{tot}} = E_{\text{ex}} + E_{\text{ani}} = \int \left(A \left(\frac{\partial \theta}{\partial x} \right)^2 + K \sin^2 \theta \right) \mathrm{d}x, \qquad (7.3.1)$$

where A is the exchange stiffness, i.e. the continuous approximation for the exchange term, θ is the angle with respect to the plane of the wall and x is the position. For simplicity no external magnetic field is considered and the magnetostatic term is neglected, although some of its effects can be considered by redefining K as an effective anisotropy term which takes into account the microscopic effects as well as the shape anisotropy contribution $K_{\text{eff}} = K + K_{\text{shape}}$.

As shown in Ref. [33] the domain wall width can be easily obtained by minimizing the micromagnetic energy. That can be done by using the Euler-Lagrange equations for a given functional $F\left(x, \theta(x), \theta'(x)\right)$, which in this case is the micromagnetic energy

$$\int F\left(x, \theta(x), \theta'(x)\right) dx \rightarrow \frac{\partial F}{\partial \theta} - \frac{\mathrm{d}}{\mathrm{d}x}\frac{\partial F}{\partial \theta'} = 0, \tag{7.3.2}$$

with $\theta' = \frac{\partial \theta}{\partial x}$. Allowing one to write the following relation

$$2A\left(\frac{\partial^2 \theta}{\partial x^2}\right) - K\sin(2\theta) = 0, \tag{7.3.3}$$

which leads to the expression for the angle $\theta(x)$

$$\theta(x) = \pm 2\arctan\left[\exp\left(\frac{x}{\Delta_{\text{DW}}}\right)\right], \tag{7.3.4}$$

where the sign depends on whether the domain wall rotates clockwise or counterclockwise, Δ_{DW} is the domain wall width in the continuum model, and is given by

$$\Delta_{\text{DW}} = \sqrt{\frac{A}{K}}. \tag{7.3.5}$$

From here it is clear that a domain wall cannot exist without an anisotropy term, regardless of its origin, i.e. shape anisotropy alone could give rise to domain walls. By studying two extreme cases of magnetic anisotropy it is possible to obtain the two limits of the domain wall width. If $K \rightarrow 0$ the domain wall width $\Delta_{\text{DW}} \rightarrow \infty$ which means that the magnetic moments are all parallel to each other. On the other hand, if $K \rightarrow \infty$ the domain wall width $\Delta_{\text{DW}} \rightarrow 0$ i.e. there is a sharp transition between the domains.

However, the creation of the domain wall requires energy, depending on how large are the exchange stiffness A and the anisotropy constant K. Therefore, it is useful to define the energy density for the domain wall γ_{DW}

$$\gamma_{\text{DW}} = 4\sqrt{AK}. \tag{7.3.6}$$

Hence the energy density is a way to see if the creation of a domain would minimize the total energy.

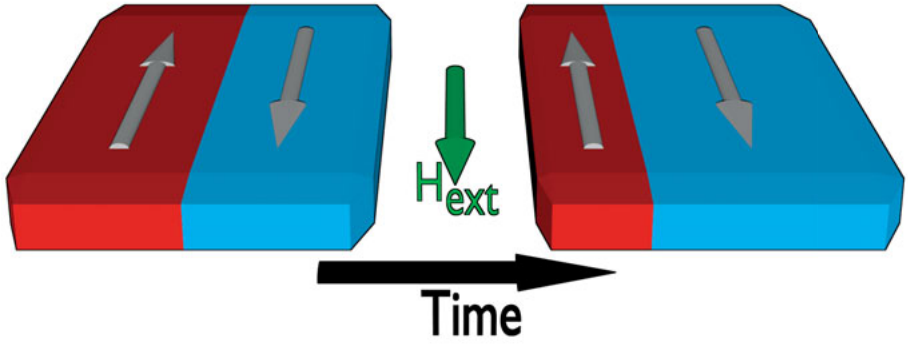

Figure 7.6. When a field is applied in the direction of the magnetization of a domain the moments tend to align towards it minimizing the energy of the system, this makes one of the domains grow.

The interaction of the domain with an external magnetic field will depend on the strength of the field and its orientation. Thus, it is known that if one applies a sufficiently large external magnetic field to a ferromagnetic material in the direction of one of the domains, its magnetization will reach saturation (the moments reorient themselves along the direction of the field). This implies that the domain aligned with the field has grown.

The growth of a magnetic domain can be understood if one considers a situation like the one presented in Fig. 7.6. If one applies a magnetic field in the "up"direction, the moments aligned anti-parallel to the magnetic field increase the energy of the system. As previously mentioned the magnetic moments are related to the spin, which has the same structure as the angular momentum. From a classical perspective, the change of angular momentum implies that the system is being subjected to a torque which means that in a case such as the previously described, the external magnetic field is exerting a torque over the magnetic moments of the sample. Therefore, if the moments are perfectly anti-parallel to the field there is no torque being exerted by the external field over them, but the field will exert a torque over the moments belonging to the wall. These moments will rotate to try to align themselves toward the field, thus minimizing the total energy of the material. This reorientation of the moments towards the field is known as *domain wall motion*.

At low fields the domain wall behaves as a solid object, i.e. its shape is preserved as it moves through the sample [190]. When the field is increased, the torque acting over the moments belonging to the wall also increases, therefore the domain wall moves with a speed proportional to the strength of the field. Intuitively, one considers the domain wall as a solid object, the wall is an elastic membrane and the field pushes it with a force proportional to its strength.

The pressure over the domain wall increases along with the increasing field until a critical field H_{Walker} is reached. Above this value the domain wall starts to be deformed, resulting in a sharp drop in the domain wall speed. This is known as the *Walker breakdown limit* [190]. An expression for the domain wall speed above and below this limit were obtained by Walker [33, 190]

$$v_{\text{DW}} = \frac{\gamma}{\alpha}\Delta_{\text{DW}}H, \quad H \ll H_{\text{Walker}} \tag{7.3.7a}$$

$$v_{\text{DW}} = \frac{\gamma\alpha}{1+\alpha^2}\Delta_{\text{DW}}H, \quad H \gg H_{\text{Walker}}, \tag{7.3.7b}$$

where γ is the gyromagnetic ratio and α is the Gilbert damping which will be discussed in detail later.

Domain wall dynamics have been extensively studied both from the theoretical and experimental point of view. Besides magnetic fields, several external stimuli can also be used to move domain walls, which will be described in the following sections. Usually, the 1D Walker model is used to describe and predict domain wall motion, however, recently the work by Yoshimura *et al.* [191] has cast some doubt on the validity of the 1D model when Dzyaloshinskii-Moriya interaction is considered.

7.3.1 Thermally driven domain wall motion on Fe/W(110)

In recent experiments [176, 192, 193] it has been shown that when a magnetic material is subjected to a thermal gradient, a spin voltage is created, i.e. spins of one character are accumulated on an edge of the sample while spins of the opposite character are accumulated on the other. This is what is known as the Spin Seebeck Effect (SSE). The microscopic origins of such phenomenon are widely disputed due the large variety of materials in which it has been observed, magnonic [194] and phononic [195] mechanisms have been proposed to explain its origin.

The interest in the SSE has lead to a wide variety of studies on the behaviour of magnetic systems under the influence of thermal gradients, from the development of thermo-magnonic devices [5, 6] to domain wall motion via thermal gradients [22, 196–199].

It has been claimed that the reason behind such motion is due to the excitation of spin waves by the thermal gradient. In an effort to understand the factors that determine the dynamics of such systems, stochastic atomistic spin dynamics simulations of both material specific and model systems were performed in **paper I**.

The system chosen to study this phenomena is a monolayer of Fe on W(110), the reason behind this is that due to its soft exchange and large anisotropy the domain wall width, δ_{DW}, is expected to be very narrow [200]. Which makes it an excellent case for atomistic spin dynamics simulations, which provides great spatial resolution. The crystalline structure of the system can be seen

in Fig. 7.7. It contains a long axis in the (1-10) which corresponds to the magnetic easy axis, the magneto crystalline anisotropy for such a system is $2SK_{eff} = 4.6$ meV as reported in an experimental study [201]. The exchange interactions for this system were calculated in a previous study [202], which result in an exchange stiffness of 160 meVÅ^2. To take into consideration the long range nature of the exchange term 40 interaction shells were considered.

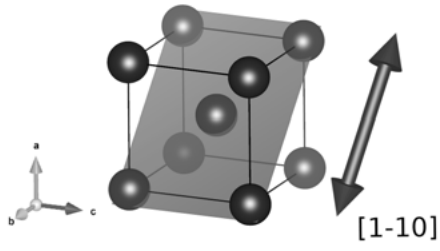

Figure 7.7. Unit cell structure and easy axis of Fe on W(110) [203], with a lattice parameter of 3.16 Å. The direction (1 -1 0) denotes the magnetization easy axis.

Two different sample geometries were studied, which would correspond to two different types of domain wall configurations. The first system was constructed by 100 repetitions along the (1 -1 0) direction (this axis will be referred to as the x axis from now on) and 40 repetitions in the (0 0 1) (y axis), which would result in a head to head domain wall configuration. The second configuration was obtained by taking 100 repetitions in the (0 0 1) direction and 40 in the (1 -1 0) resulting a in a Bloch domain wall.

The small system size sets the exchange interactions as the dominant energy term, therefore the dipolar interactions are neglected in this study. However, to test which effect their inclusion would have in the dynamics, several test simulations were performed, in general the dynamics were mostly unaffected with only about a $\sim 3\%$ of difference observed between both cases. Such an observation coupled with the great computational burden that the calculation of dipolar interaction brings justifies their neglect. Nonetheless, for larger system sizes the magnetostatic effects will be relevant and should be included.

Due to the lack of dipolar interactions domain walls are metastable states and no observable difference was observed between the two studied geometries, hence in the following the rest of the discussion will deal with the head to head domain wall structure. Such configuration is achieved, by setting half of the moments aligned in the +x direction while the other half is set in the -x direction. The system is then allowed to relax at a finite temperature T_{ave} to obtain the domain wall shape and width expected from the interactions present, this is achieved by using the stochastic atomistic LLG equation (Eq. 7.1.3).

The metastable nature of the domain walls in the system, make it necessary to consider several ensembles when studying finite temperature cases, in order

to neglect any possible Brownian motion. Such an effect becomes noticeable when one studies the position of the domain wall in the different ensembles, as there is a clear distribution of domain wall positions (Fig. 7.8) which increases with temperature. Nevertheless, it is important to notice that in average the domain wall is located in the middle of the sample.

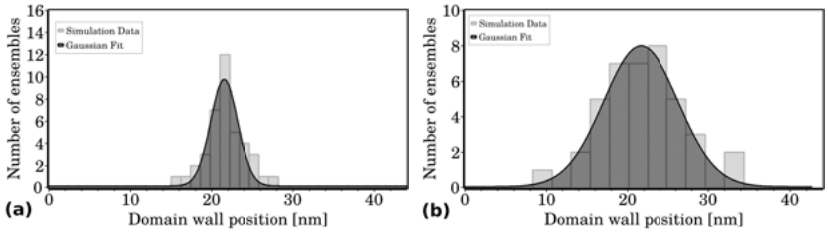

Figure 7.8. Domain wall position distribution for different temperatures as studied in **paper I**. In **a** and **b** the distributions for $T_{\text{ave}} = 20\,\text{K}$ and $T_{\text{ave}} = 60\,\text{K}$ are shown respectively. As the equilibration temperature increases the spread of the distribution also increases which is consistent with Brownian motion.

After the thermalization of the system, a thermal gradient is imposed in the sample, transient effects are ignored and the material is assumed to have reached the steady state, i.e. no time evolution of the temperature. The shape of the gradient is set to be linear, and the temperature difference ΔT is created in such a way as to maintain the local temperature of the domain wall constant, as to avoid any sudden changes in the local temperature of the domain wall which could influence our results, also on such a way the "average temperature", T_{ave}, of the sample is maintained.

When a thermal gradient is applied to the system the domain wall moves towards the hotter edge of the sample as seen in previous works [22, 197]. The domain wall speed is shown to increase linearly with the gradient strength as seen in Fig. 7.9 (notice the log-log scale). Such behaviour is observed for up to three orders of magnitude of ΔT, it is also relevant to observe that the dynamics seems unaffected by the average temperature T_{ave}. The large error bars at low gradients are due to the logarithmic scale of the plot, and the fact that finite temperature effects, introduce fluctuations which are un-biased and they will compete with the ones produced by the gradient.

However, the models presented in the theory [196, 197] predict a much smaller speed than the one that is obtained in the present work. One of the main differences between the theoretical model and the studied system is the domain wall width. In Fe on W(110) the domain wall width is ~ 2 nm which is smaller than the wavelength of the thermally excited magnons interacting with it λ_{therm}. Such aspect is key when comparing with the previously proposed models, since the departure point for them is the adiabatic approximation in which the domain wall width is assumed to be much larger than the thermal magnon wavelength. Yan and Bauer [204] showed that the transmis-

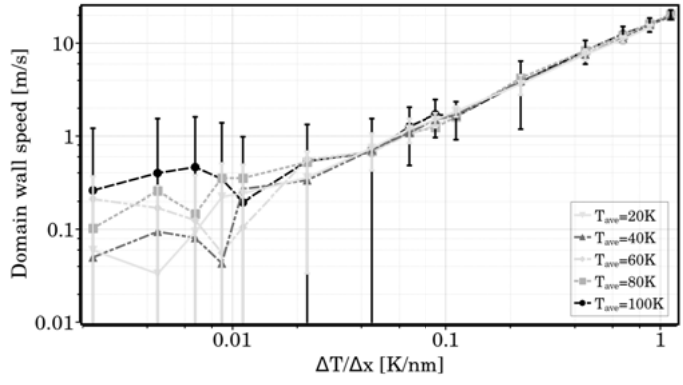

Figure 7.9. Log-Log plot of the DW speed as a function of the temperature change per nm $\frac{\Delta T}{\Delta x}$ for the ML of Fe on W(110) presented in **paper I**. As $\frac{\Delta T}{\Delta x}$ increases, the speed increases linearly with it. At low gradients the spread in the measurements due to the stochastic fluctuations hides any possible global behavior. Note: the error bars respect the log scale of the axis.

sion coefficient for spin waves of ultranarrow domain walls changes with their width, i.e. some spin waves are reflected from the domain wall, a fact that is not taken into account in the continuum model.

The change of the transmission coefficient with the domain wall width should affect the interaction of the spin waves with the domain wall, hence affecting the magnonic spin transfer torque which in turns controls the speed of the wall. To test this hypothesis, model simulations were performed in which the anisotropy constant, K, and the exchange interaction, J, were varied, which would result in a change in the domain wall width. It was observed that as the domain wall width increases the speed that is obtained for a given gradient also increases (Fig. 7.10). Thus, the domain wall width for ultranarrow domain walls becomes of great importance when considering motion via spin wave interactions. Such observation is conflicting with previous models in which the domain wall width does not explicitly affect the domain wall speed. This discrepancy could be a result from the fact that such models were obtained by considering the continuum model, which seems ill equipped to deal with ultranarrow domain walls.

When the thermal gradient is applied to the system, magnons are produced at the hotter edge and they diffuse towards the colder region [22], these magnons interact with the domain wall resulting in a magnonic spin transfer torque [21, 204], i.e. the spin waves interact with the moments that belong to the DW making the precess, changing their orientation and eventually causing the DW to move. From our simulations we see that the interaction between the magnons and the atomically sharp DW changes as the DW becomes broader as evidenced in the change of the DW speed. This is consistent with the work previously done by Yan and Bauer [204] in which the interaction between spin

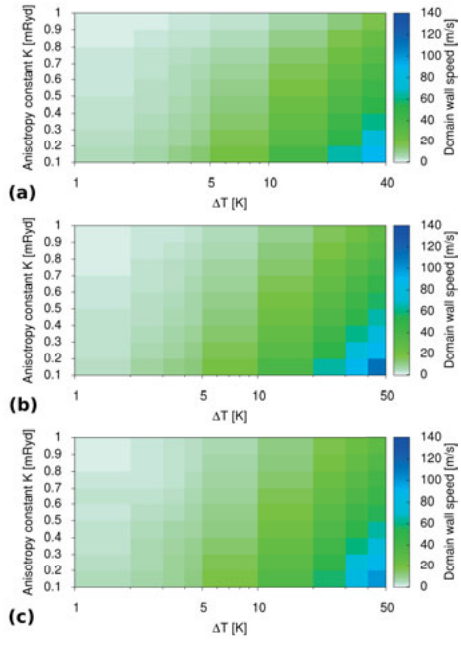

Figure 7.10. Dependence of the domain wall speed on the anisotropy constant K and the temperature difference ΔT (notice the logarithmic x-axis) for the model systems treated in **paper I**. The dependence of the speed is presented for $T_{\text{ave}} = 20\,\text{K}$ **a** , $T_{\text{ave}} = 60\,\text{K}$ **b** and $T_{\text{ave}} = 100\,\text{K}$ **c**. For all cases, as the anisotropy constant diminishes the DW speed that can be achieved with a given gradient for a given T_{ave} increases.

waves and ultra-narrow DW was studied. In that study it was found that for narrow DW ($\frac{K}{J} \ll \frac{2}{3}$) the transmission coefficient of the DW with respect to spin waves changes as the $\frac{K}{J}$ ratio changes. In contrast to what is expected for broad domain walls in the 1D continuum model, where the DW do not reflect spin waves, ultra-narrow DW have a transmission coefficient that is less than one, i.e. some spin waves are reflected from the DW, as schematically shown in Fig. 7.11. As the anisotropy is reduced, i.e. the DW becomes broader the system becomes closer to the one described in the continuum model.

Several alternative models, have been recently proposed [205–208] to describe the underlying mechanisms behind the thermally driven motion domain wall motion. However, most of the work has been realized for systems in the micromagnetic limit in which domain walls are much larger than the wavelength of the spin waves interacting with them.

7.3.2 Current driven domain wall motion

Magnetic textures, such as domain walls, can be moved when a spin polarized current is applied to them. This was first proposed by Berger [9–11] and later

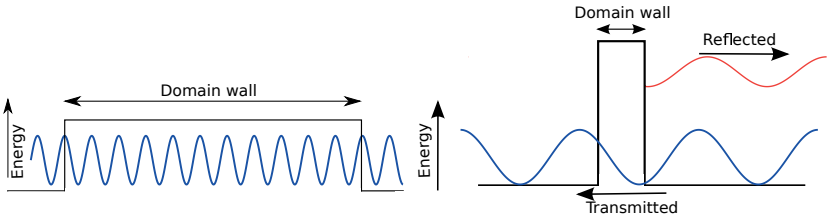

Figure 7.11. Schematic representation of the interaction between spin waves and domain walls, for wide walls (left panel) the spin wave is completely transmitted, whilst for narrow walls (right panel) part of the spin wave is reflected.

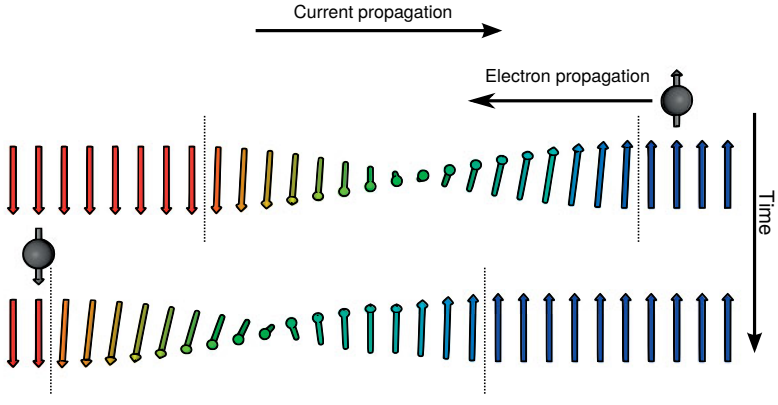

Figure 7.12. Schematic representation of the transfer of angular momentum between the conduction electrons and the magnetic texture. The transfer of momentum causes the magnetic texture to move as to conserve the agnular momentum of the system. The dotted region is a guide to the eyes denoting the domain wall region.

Slonczewski [166] provided a mathematical formalism to couple this contribution to the LLG equation (Eq. 2.3.5). This phenomena is named the spin transfer torque (STT), as it describes the transfer of angular momentum from the spin polarized electrons circulating through the sample to the magnetic texture.

A spin polarized electronic current flowing through a magnetic material will be undisturbed if its polarization matches the magnetic field of the sample. However, if there is a magnetic texture, such as a domain wall, the electrons will interact with this spatially dependent magnetic field, trying to align themselves with it, as a consequence of the angular momentum conservation, angular momentum will be transferred from the spin polarized current to the magnetic texture, causing it to move, as exemplified in Fig. 7.12. This phenomena has been experimentally observed [23, 24, 209–212] and modelled in numerical simulations [17–19, 213].

In the numerical simulations here within, the STT terms are included in the stochastic LLG equation (Eq. 7.1.3) following the approach proposed in

Ref. [19]. Leading to the following expression

$$\frac{\mathrm{d}\mathbf{m}_i}{\mathrm{d}t} = -\frac{\gamma}{1+\alpha^2}\left[\mathbf{m}_i \times \left(\mathbf{B}^i_{\mathrm{eff}} + \mathbf{b}^i(t)\right) + \frac{\alpha}{m_i}\mathbf{m}_i \times \left(\mathbf{m}_i \times \left[\mathbf{B}^i_{\mathrm{eff}} + \mathbf{b}^i(t)\right]\right)\right] + \frac{1+\beta\alpha}{1+\alpha^2}\frac{\mathbf{u}}{m_i^2}\cdot\left(\mathbf{m}_i \times \left[\mathbf{m}_i \times \nabla\mathbf{m}_i\right]\right) - \frac{\alpha-\beta}{1+\alpha^2}\frac{\mathbf{u}}{m_i}\cdot\left[\mathbf{m}_i \times \nabla\mathbf{m}_i\right] \quad (7.3.8)$$

where β is the non-adiabatic parameter, which describes situations in which the spin transport length is much smaller than the domain wall width [18], $\mathbf{u}$ is a parameter with units of velocity which is related to the current density $\mathbf{j}_e$ as

$$\mathbf{u} = \frac{\mathbf{j_e} P g \mu_B}{2eM_s} \quad (7.3.9)$$

where P is the polarization, M_s is the saturation magnetization of the system, g is the Landé g-factor, e is the electronic charge and μ_B is the Bohr magneton.

Spin-Hall effect driven torques

Recent experiments [24, 211], have also highlighted that an extra torque can arise in a magnetic material in contact with a non-magnet, when the non-magnet it has a strong spin orbit coupling. It has been proposed, that one of the mechanism behind such torques is the Spin Hall Effect (SHE), since as an electronic current flows through a non-magnetic material with large SOC, a spin current perpendicular to both the electronic current propagation and the quantization axis is generated. This pure spin current can interact with magnetic textures, leading to dynamics that cannot be described with the traditional STT treatment.

The torque generated by the SHE can be included in the LLG equation (Eq. 2.3.4) as in previous theoretical works [214–218] for a 1D system, by considering

$$\frac{\partial\mathbf{M}}{\partial t} = \underbrace{-\gamma\mathbf{M}\times\mathbf{B}_{\mathrm{eff}}}_{\text{precesion}} + \underbrace{\frac{\alpha}{M}\mathbf{M}\times\frac{\partial\mathbf{M}}{\partial t}}_{\text{damping}} \underbrace{- b_i^j\mathbf{M}\times\mathbf{M}\times\frac{\partial\mathbf{M}}{\partial x} - \beta b_i^j\mathbf{M}\times\frac{\partial\mathbf{M}}{\partial x}}_{\text{STT}} + \underbrace{\theta_i^{SH}c_i^j\mathbf{M}\times\mathbf{M}\times\hat{y}}_{\text{SHE STT}} \quad (7.3.10)$$

where b_i^j is the STT coefficient, $\theta_i^{SH}c_i^j$ is the magnitude of the spin hall current. In the present model the direction of the current is assumed to be along the +x direction. In general the direction of the SHE-STT can be obtained by considering that the SHE torque, τ_{SHE}, is obtained by

$$\tau_{\mathrm{SHE}} = -\gamma\frac{\hbar\theta^{SH}|j_e|}{2eM_s t_f}\left(\hat{M}\times\left(\hat{j}\times\hat{z}\right)\times\hat{M}\right) \quad (7.3.11)$$

with θ^{SH} being the spin hall angle, j_e the current density, $\hbar$ the reduced Planck constant, γ the gyromagnetic ratio, M_s the saturation magnetization and t_f the thickness of the ferromagnetic layer over which the torque is acting on.

By making use of the properties of vectorial algebra (for details see Appendix A), it is then possible to write the LLG equation including the Slonczewski STT terms and the SHE STT terms as

$$\begin{aligned}\frac{\partial \mathbf{M}}{\partial t} = -\frac{\gamma}{1+\alpha^2}\mathbf{M}\times\Bigg[&\mathbf{B}_{\text{eff}} + \alpha\hat{M}\times\mathbf{B}_{\text{eff}} - (1+\alpha\beta)\,\mathbf{u}'\cdot\hat{M}\times\nabla\hat{M} \\ &+(\alpha-\beta)\left(\mathbf{u}'\cdot\nabla\right)\hat{M} + \frac{\theta_i^{SH}u'}{Pt_f}\left[\left(\hat{u}'\times\hat{z}\right)\times\hat{M} - \alpha M\left(\hat{u}'\times\hat{z}\right)\right]\Bigg]\end{aligned} \tag{7.3.12}$$

where $\mathbf{u}' = \frac{\mathbf{u}}{\gamma}$, where $\mathbf{u}$ is the STT velocity parameter previously defined.

As can be seen in Eq. 7.3.8 the presence of the spin Hall effect leads to the inclusion of new terms to the equation of motion, which do not depend on the gradient of the magnetization, but on the orientation of the electronic current with respect to the quantization axis. These terms can act over magnetic textures of certain symmetries, and under certain conditions can be large enough to be the dominant term, as is in the case of domain walls on thin films deposited on non-magnetic materials with a large SOC. The interfacial DMI present in these materials can lead to the stabilization of a Neél wall, which has the correct symmetries to allow the SHE torque to act over it, such behaviour has been observed in both experiments [24, 211, 219] and in numerical simulations [214, 218].

In **paper IX** the effects that both STT and SHE have on the domain wall dynamics are studied. This is done by a combination of model systems and material specific calculations. The considered materials were Co/Ni/Co heterostructures deposited on heavy metal substrates previously characterized in **paper VII**, making use of the pairwise Heisenberg exchange interactions and the Dzyaloshinskii-Moriya vectors. The magnitude of the DM interaction is large enough such that Neél walls are stabilized as seen in Fig. 7.13, due to the fact that the magnetic moments rotate along the long edge of the sample.

It is important to notice that in the [001] stacking both Pt and Ir have the same chirality, while in the [111] stacking, Pt and Ir moments rotate in different orientations, this illustrates the influence that the different crystallographic orientations can have over the domain wall profile. A consequence of the different chirality between the stackings, is that the SHE torque will have a different sign profoundly affecting the dynamics.

7.4 Topology in magnetism

Topological effects in physics is a subject that has gathered a large amount of attention, some examples of these are topological insulators [220], the quan-

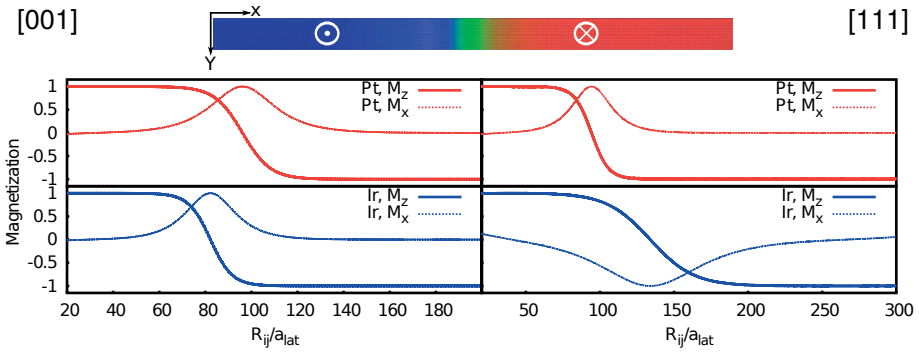

Figure 7.13. Domain wall profile for Co/Ci/Co deposited on Pt and Ir. The left panel shows the [001] stacking, while the right panel shows the [111].

tum Hall effect [221], the Aharonov–Bohm's effect [222], the Josephson junction [223], and skyrmions in magnetic materials [224–227].

Magnetic textures such as skyrmions, have gathered much attention due to their topological properties, namely they are topologically protected. Which means that they are very resistant to external perturbations, thus making ideal candidates for potential applications. Skyrmions were originally proposed by Tony Skyrme in the context of stability of baryons in particle physics [228, 229]. However, in magnetic materials they were proposed by Bogdanov, which demonstrated that solitonic solutions such as skyrmions, can appear in ferromagnetic materials without spatial inversion symmetry [230, 231]. The lack of inversion symmetry implies that a finite DMI will be present in these systems. This prediction, has been experimentally observed in materials such as the non-centrosymmetric MnSi in the so called A-phase [117], where skyrmionic states are stabilized by a competition of Heisenberg exchange and Dzyaloshinskii-Moriya interactions at certain considerations of external magnetic fields and temperature.

Topological effects can be described by the concept of Berry phase [232]. That is when considering the time evolution of an eigenstate of the system along a closed path, the eigenstate will obtain an overall complex phase factor, which depends on geometrical considerations of the Hamiltonian. As illustrated in Ref. [71], the Berry phase can be obtained by considering a Hamiltonian, $\mathscr{H}(\lambda)$, which depends on a parameter λ that belongs to a differentiable manifold $\mathscr{M}$. By taking that $\mathscr{M}$ can be separated into two zones P_1 and P_2 which fulfil $P_1 \cap P_2 \neq \varnothing$, it is possible to define two sets of eigenstates of $\mathscr{H}(\lambda)$, $|n\lambda\rangle$ and $|n\lambda\rangle'$, which differ only by a complex phase factor when $\lambda \in P_1 \cap P_2$

$$|n\lambda\rangle' = e^{i\chi_n(\lambda)} |n\lambda\rangle \tag{7.4.1}$$

By considering the time evolution of the eigenstates along a closed loop belonging to one of the zones of the manifold in the adiabatic limit, it becomes

possible to write the Berry phase as

$$\gamma_n(t) = \int_{\lambda(0)}^{\lambda(t)} i \langle n\lambda(\tau) | \nabla_{\lambda_i} | n\lambda(\tau) \rangle \, d\lambda_i \tag{7.4.2}$$

Making use of the Berry phase concept, it is possible then to define the Berry curvature Ω_{ij}^n and the Chern numbers C_n as

$$\Omega^n = i\nabla_\lambda \times \langle n\lambda | \nabla_\lambda | n\lambda \rangle \tag{7.4.3}$$

$$C_n = \frac{1}{2\pi} \int_S d\mathbf{S}\Omega^n(\lambda) \tag{7.4.4}$$

where the integration of the Berry curvature is performed over the surface S defined by the close path C.

These quantities allows one to characterize states which exhibit different topological properties. This is of special significance for the Chern numbers, since it is not possible to perform a smooth transformation such that one can go between states associated to different Chern numbers.

Another quantity of interesting when describing topological excitations in magnetic systems, is the *topological charge* $\mathscr{Q}$ which in two dimensions can be written as [118]

$$\mathscr{Q} = \frac{1}{4\pi} \int dxdy \left(\hat{m} \cdot \left[\frac{\partial \hat{m}}{\partial x} \times \frac{\partial \hat{m}}{\partial y} \right] \right) \tag{7.4.5}$$

where the integral is taken over the two dimensional unit cell.

The topological charge can be used to classify the different types of topological magnetic excitations, skyrmionic states are often characterized with the number +1, and anti-skyrmions, topological structures with opposite chirality with the number -1. This concept also allows one to differentiate non-trivial topology, i.e. topologically protected states, from trivial textures with topological charge $\mathscr{Q} = 0$.

7.4.1 Kagome lattice

Pyrocholore materials, such as $Lu_2V_2O_7$ along the [111] direction can be considered as alternating stack of magnetic atoms in a Kagome lattice. Recent experiments performed by Onose *et al.* [233] have measured the presence of a transversal spin current to an applied thermal gradient, this effect is dubbed the magnon Hall effect.

In **paper III** the topological properties of the 2D kagome lattice were studied via atomistic spin dynamics simulations. The system was modelled by considering nearest neighbour Heisenberg exchange interactions, J, and nearest neighbour DM vectors, D, such as to reproduce the ferromagnetic ground

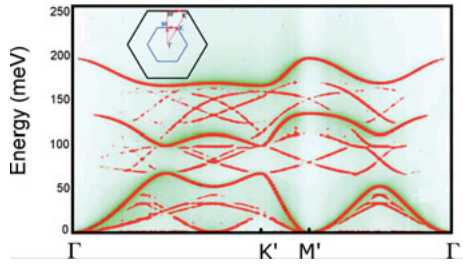

Figure 7.14. Dynamical structure factor for a Kagome lattice in a ferromagnetic states where a non-zero Berry phase is present due to the Dzyaloshinskii-Moriya interaction.

state of the system, whilst keeping a ratio between the interactions of $\frac{D}{J} = 0.4$ which is comparable to the experimental ratio of 0.32 [233]. The ferromagnetic groundstate obtained despite the large DMI, is a result of the relative orientation of the DM-vectors as given by the Kagome lattice.

In Fig. 7.14 the dynamical structure factor for the ferromagnetic Kagome lattice is presented, this was obtained by considering a simulation cell of 500x40 simulation cells. Due to the presence of Dzyaloshinskii-Moriya interactions, a band gap is open between the bands, which corresponds to what was previously obtained in Ref. [234] and Ref. [235]. The intense bands in the figure correspond to the bulk bands, where each of these bands can be characterized by a different Chern number. Even more, between the bulk bands topologically protected edge states can be seen crossing the band gap. These edge states have a given chirality. Excitations belonging to edge states can only be transmitted through them, as they belong to the band gap region of the bulk, similar to what happens in topological insulators. This opens up the possibility for the development of magnonic devices based on the protection of these topological states.

The edge states are also responsible for the magnon Hall effect. The transversal heat current is a consequence of the edge states where the non-zero Berry curvature contributes to the transversal thermal Hall conductivity as shown by Matsumoto and Murakami [236, 237] for a 2D model system. Later numerical work by Zhang *et al.* [235] and Mook *et al.* [238] showcased the importance that the edge states have over the heat current for the 2D Kagome lattice.

The properties of the kagome lattice also allow the excitation of topological structures, these can be nucleated by applying a localized external magnetic field or a local spin transfer torque. For simplicity the simulations were performed at 1 mK to minimize the stochastic fluctuations. The local torque causes the spins in the region to be reversed. Once the external excitation is removed the affected area will relax to a structure similar to a skyrmion-like or skyrmion-antiskyrmion pair, as seen in Fig. 7.15, which were found to be stable for times > 100 ps. These excitations can move through the sample until they reach the sample edge. At the edge, due to the chiral nature of

the edge states the skyrmion-antiskyrmion pair becomes decoupled and they move along the edge of the sample. Once decoupled, they can be described in terms of meron-antimeron pairs, that is topological excitations with topological charge $\frac{1}{2}$ or $-\frac{1}{2}$ respectively, which were first proposed in the framework of the Yang-Mills theory [239].

It is important to notice, that the nucleation process of the excitations has some stochasticity present in it, since when the external torque is removed spin waves are excited in the system, which can affect the excitations. However, they are found to move in a very predictable way at the edge of the sample. This property can be used to achieve meron-antimeron collisions and meron-meron collisions. In the case of meron-meron collisions, the collision is observed to be elastic, that is the linear momentum and kinetic energy are conserved. However, for the case of meron-antimeron collision, due to their opposite chiralities the excitations annihilate each other resulting in an emission of spin waves [240].

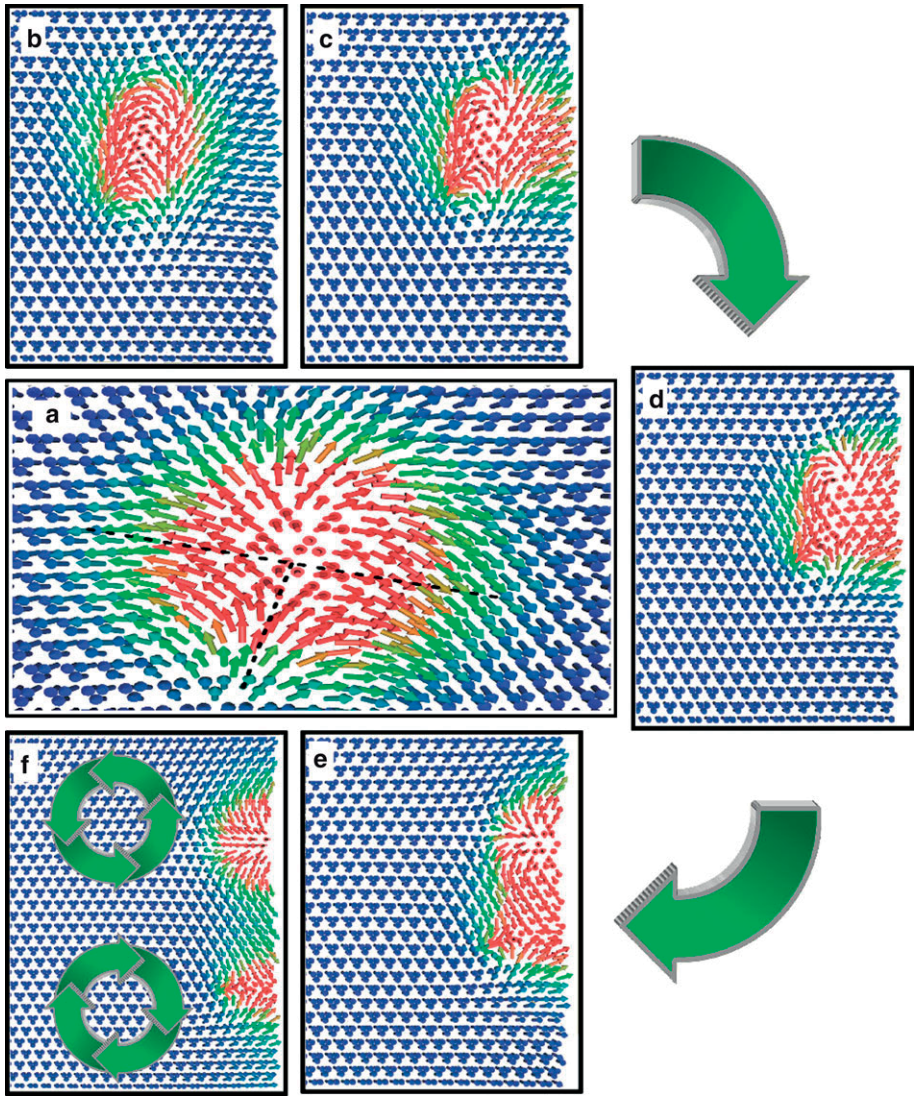

Figure 7.15. **a** Illustrations of the skyrmion-antiskyrmion pair in the kagome strip. Dashed lines are a guide to the eye to recognize the different magnetic structures of the skyrmion and anit-skyrmion half of the magnetic structure. Snapshots **b**-**f** show the collision of the excitation with the simluation edge and how they become decoupled at the edge due to the chiral nature of the edge states.

8. Conclusions and Outlook

The capacity to combine first principle calculations with atomistic spin dynamics simulations has been proven to be a valuable technique to study magnetization dynamics. The recent developments in *ab initio* methods allow the determination of magnetic parameters, such as the Dzyaloshinskii-Moriya vectors. This improves the description of non-collinear structures and their dynamics. Here the effect that DM interactions can have on the motion of magnetic textures such as domain walls have been studied. One considered system consisted of Co/Ni/Co heterostructures deposited on heavy metals. Here the material of the non-magnetic underlayer was found to be of profound importance for the magnitude and direction of the DM vectors, and thus for the magnetic textures which can be stabilized on them.

Atomistic spin dynamics has also been shown to be a very useful formalism, for describing the dynamics of systems with reduced dimensionality. One example is the case of ultranarrow domain walls driven by thermally excited spin waves. Here the thermally driven domain-wall motion was studied, both for material specific and model parameters using atomistic spin dynamics. When a domain wall is established in a ferromagnetic material, which is subjected to a thermal gradient, the domain wall is observed to move towards the hotter end of the sample. This phenomenon can be understood due to the creation of a spin wave current which interacts with the wall resulting in a magnonic spin transfer torque.

In contrast with what is expected from the continuum model for the electronic spin transfer torque, the domain wall speed is observed to depend on the domain wall width. Hence, wide domain walls move faster than their thinner counterparts. The dependence of the speed with respect to the domain wall width for ultranarrow domain walls can be understood in the basis of the work performed by Yan and Bauer [204]. They demonstrated that for ultranarrow domain walls, the width is a determinant factor in the spin wave wall interaction and the simulations presented in this thesis supports that observation.

The presented approaches has also been applied to the description of topological magnetic structures, such as the topological excitations stabilized in the Kagome lattice and the motion of topological defects on FeGe. These applications are of great importance as the topological protection present in them, could lead to the development of very robust information devices.

Also, the developments in first principle methods was used for the accurate determination of the Gilbert damping. Thus, giving a powerful tool, to understand the factors that influence the intrinsic damping in magnetic materials, as well as a reliable way to both predict and compare with experimental

measurements. In particular, these techniques allowed the calculation of the Gilbert damping for half-metallic full Heusler alloys. Here the calculations could highlight the profound effects that that the half-metallicity of the material has over the damping parameter.

The techniques presented here can be used to explore systems that are only now gathering attention, such as the dynamics of antiferromagnetic materials, where the high spatial resolution of atomistic spin dynamics is uniquely suited to deal with these kinds of systems. Another topic of interest, is the capacity of using topological properties of a material to drive the dynamics of a magnetic textures, such as domain walls, akin to what was done for the Kagome lattice. Also, the study of the dynamics of magnetic textures, under the influence of spin orbit torque, is a novel topic of profound interest.

9. Summary in Swedish

De magnetiska egenskaper hos material har använts av oss människor i hundratals år. Deras egenskaper har möjliggjort utvecklingen av många tekniska uppfinningar, till exempel den magnetiska kompassen, hårddiskar och magnetiska RAM-minnen. Det är dock först under det senaste århundradet som vi börjat förstå de mikroskopiska mekanismerna som ger upphov till magnetism. Magnetism är en kvantmekanisk effekt som är relaterad till elektronens spin. Följaktligen, om man önskar beskriva och förutsäga egenskaperna hos magnetiska material, är en kvantmekanisk beskrivning av fasta kroppar nödvändig.

På grund av det stora antalet partiklar i en fast kropp är en analytisk lösning av Schrödingerekvationen omöjlig. 1964 föreslog Hohenberg och Kohn [51] ett alternativ sätt, istället för att använda flerkroppselektronvågfunktionen kan elektrontäthet användas som ett objekts grundläggande enhet. Detta är grunden för täthetsfunktionalteorin (Eng: density functional theory, DFT).

För magnetiska material är några av de viktigaste egenskaperna relaterade till växelverkan mellan de magnetiska momenten. Dessa interaktioner bestämmer både de statiska egenskaperna hos materialet, samt eventuella dynamik egenskaper. En typ av interaktion mellan magnetiska moment som fått stor uppmärksamhet är Dzyaloshinskii-Moriya interaktionen [42, 43] (DMI). DMI kan leda till exotiska magnetiska tillstånd, så som spin-spiraler och magnetiska skyrmioner. Skyrmioniska tillstånd är av stort intresse för forskningen på grund av eventuella tekniska tillämpningar eftersom de har potential att ge upphov till mycket robust metoder för att koda information.

En annan egenskap med stor betydelse för beskrivningen av den magnetiserande dynamiken är Gilbert dämpningen. Denna dämpning beskriver överföringen av rörelsemängdsmoment och energi från ett magnetiskt subsystem till gittret. Detta har stor betydelse för olika tillämpningar eftersom det avgöra hur långt information kan propagera genom materialet på ett tillförlitligt sätt i den typ av enheter.

I denna avhandling använts täthetsfunktionalteori tillsammans med atomistiska spindynamika beräkningar för att erhålla en tillförlitlig beskrivning av de magnetiska egenskaperna hos ett system. I synnerhet studerades dynamiken i magnetiska domäner hos lågdimensionella system. Ett exempel är ett monoskikt av Fe på W(110) där domänväggens rörelse studerandes när den utsätts för en termisk gradient. Vidare studerades även domänväggarna i material ett lager av Co/Ni/Co heterostrukturer ovanpå bulk-material av tungmetaller. Denna typ av system möjliggör beräkningar från grundläggande principer, vilket tillåter oss att se vilka effekter DM interaktionen har på domänväggdynamiken.

En annan aspekt som noggrant undersöktes i denna avhandling är fastställandet av Gilbert dämpning från grundläggande principer. De tekniker som använts tillåter oss att beräkna den inneboende dämpningen så att resultaten kan jämföras med experimentella mätningar. I synnerhet har half-metalliska Heusler-familjer; Co_2MnZ, Co_2FeZ och Mn_2VZ med Z = (Al, Si, Ga, Ge), studerats. De funna trenderna överensstämmer relativt bra med de experimentella resultaten, även om de erhållna värdena är något mindre än de experimentella.

10. Acknowledgments

I would like to thank my supervisors Anders, Lars and Olle for all their help, for always having time to answering any questions and for always being there for anything I needed. Thank you very much for your guidance and patience, this thesis would not be possible without you.

Also special thanks to Manuel, for all his crazy ideas, to always being there to have a discussion. And for being the only other person here a Sunday at night making me me feel not quite so bad for being here.

I would also like to thank Pablo, thanks to his example I know where rock bottom is, and that cheers me up. To Iulia for the dancing Hamiltonians and for no matter what being happy, making everyone happy at the same time. To Vancho for ruling with an iron fist that makes us to always have something to do. To Igor for his capacity to be horrified with my jokes. To Ralph the dancing German, for demonstrating that a German person can dance much better than a Latino.

Thank you also astronomy people, for your board game nights, horrible jokes and interesting discussions.

To Kostas and Robert, for knowing what is good in life, for sharing my love of Arnold and bad movies. Without them nothing of this would be possible, you see guys I'm trying to be nice and breaking the 4th wall at the same time.

To Sara for her unlimited support and patience. For always helping me to fight whatever is thrown in my way and to help me always keep moving forward no matter what. None of this would be possible without you.

To everybody else that made this thesis possible, either for your direct help or just your presence that made the hard times possible. To Sumanta, Vancho, Corina, Soum, Nina, Leyla, Cactus, Sputnik, the BS solver, among many others. Thank you.

Last but not least thank you to my family no matter how far away you are you always help me and guide me. It is your example the one that has gotten me here. And to Bob for helping me.

A. SHE torques in the LLG equation

The LLG equation including the STT Slonczewski terms plus the torque generated from the Spin Hall Effect can be written as [214–217]:

$$\frac{\partial \mathbf{M}}{\partial t} = \underbrace{-\gamma \mathbf{M} \times \mathbf{B}_{\text{eff}}}_{\text{precesion}} + \underbrace{\frac{\alpha}{M}\mathbf{M} \times \frac{\partial \mathbf{M}}{\partial t}}_{\text{damping}} \underbrace{- b_i^j \mathbf{M} \times \mathbf{M} \times \frac{\partial \mathbf{M}}{\partial x} - \beta b_i^j \mathbf{M} \times \frac{\partial \mathbf{M}}{\partial x}}_{\text{STT}} + \underbrace{\theta_i^{SH} c_i^j \mathbf{M} \times \mathbf{M} \times \hat{y}}_{\text{SHE STT}} \tag{A.0.1}$$

where b_i^j is the STT coefficient, $\theta_i^{SH} c_i^j$ is the magnitude of the spin hall current. In the present the direction of the current is assumed to be along the +x direction, in general the direction of the SHE-STT can be obtained by considering that the SHE torque, τ_{SHE}, is obtained by

$$\tau_{\text{SHE}} = -\gamma \frac{\hbar \theta^{SH} |j_e|}{2eM_s t_f} \left(\hat{M} \times \left(\hat{j} \times \hat{z} \right) \times \hat{M} \right) \tag{A.0.2}$$

with θ^{SH} the spin hall angle, j_e the current density, $\hbar$ the reduced Plack constant, γ the gyromagnetic ratio, M_s the saturation magnetization and t_f the thickness of the ferromagnetic layer over which the torque is acting on.

Then one needs to transform the LLG to its LL form, for this one can mutiply both sides of Eq. A.0.1 by $\mathbf{M}\times$

$$\begin{aligned} \mathbf{M} \times \frac{\partial \mathbf{M}}{\partial t} = & -\gamma \mathbf{M} \times (\mathbf{M} \times \mathbf{B}_{\text{eff}}) + \frac{\alpha}{M}\mathbf{M} \times \mathbf{M} \times \frac{\partial \mathbf{M}}{\partial t} \\ & - b_i^j \mathbf{M} \times \mathbf{M} \times \mathbf{M} \times \frac{\partial \mathbf{M}}{\partial x} - \beta b_i^j \mathbf{M} \times \mathbf{M} \times \frac{\partial \mathbf{M}}{\partial x} + \theta_i^{SH} c_i^j \mathbf{M} \times \mathbf{M} \times \mathbf{M} \times \hat{y} \end{aligned} \tag{A.0.3}$$

Using the triple vector product identity $\mathbf{a} \times (\mathbf{b} \times \mathbf{c}) = \mathbf{b}(\mathbf{a} \cdot \mathbf{c}) - \mathbf{c}(\mathbf{a} \cdot \mathbf{b})$ one can rewrite Eq. A.0.3 as

$$\begin{aligned} \mathbf{M} \times \frac{\partial \mathbf{M}}{\partial t} = & -\gamma \mathbf{M} \times (\mathbf{M} \times \mathbf{B}_{\text{eff}}) - \alpha M \frac{\partial \mathbf{M}}{\partial t} + b_i^j M_i^2 \mathbf{M} \times \frac{\partial \mathbf{M}}{\partial x} \\ & - \beta b_i^j \mathbf{M} \times \mathbf{M} \times \frac{\partial M}{\partial x} - \theta_i^{SH} c_i^J M^2 \mathbf{M} \times \hat{y} \end{aligned} \tag{A.0.4}$$

Introducing Eq. A.0.4 in Eq. A.0.1

$$\frac{\partial \mathbf{M}}{\partial t} = -\gamma \mathbf{M} \times \mathbf{B}_{\text{eff}} + \frac{\alpha}{M}\left[-\gamma \mathbf{M} \times (\mathbf{M} \times \mathbf{B}_{\text{eff}}) - \alpha M \frac{\partial \mathbf{M}}{\partial t} + b_i^j M_i^2 \mathbf{M} \times \frac{\partial \mathbf{M}}{\partial x}\right] + \frac{\alpha}{M}\left[-\beta b_i^j \mathbf{M} \times \mathbf{M} \times \frac{\partial M}{\partial x} - \theta_i^{SH} c_i^j M^2 \mathbf{M} \times \hat{y}\right] - b_i^j \beta \mathbf{M} \times \frac{\partial \mathbf{M}}{\partial x} - b_i^j \mathbf{M} \times \mathbf{M} \times \frac{\partial \mathbf{M}}{\partial x} + \theta_i^{SH} c_i^j \mathbf{M} \times \mathbf{M} \times \hat{y} \tag{A.0.5}$$

doing some algebra one can write

$$\frac{\partial \mathbf{M}}{\partial t} = -\frac{\gamma}{1+\alpha^2}\left[\mathbf{M} \times \mathbf{B}_{\text{eff}} + \alpha \mathbf{M} \times \mathbf{M} \times \mathbf{B}_{\text{eff}}\right] - \frac{1+\alpha\beta}{1+\alpha^2}\frac{b_i^j}{M^2}\mathbf{M} \times \mathbf{M} \times \frac{\partial \mathbf{M}}{\partial x} + \frac{\alpha-\beta}{1+\alpha^2}\frac{b_i^j}{M}\mathbf{M} \times \frac{\partial \mathbf{M}}{\partial x} + \frac{\theta_i^{SH} c_i^j}{1+\alpha^2}\left(\mathbf{M} \times \mathbf{M} \times \hat{y} - \alpha M^2 \mathbf{M} \times \hat{y}\right) \tag{A.0.6}$$

For simplicity of implementation this equation can be easily re-writen to fit with the Depondt scheme

$$\frac{\partial \mathbf{M}}{\partial t} = -\frac{\gamma}{1+\alpha^2}\left[\mathbf{M} \times \mathbf{B}_{\text{eff}} + \alpha \hat{M} \times \mathbf{M} \times \mathbf{B}_{\text{eff}} + (1+\alpha\beta)\frac{b_i^j}{\gamma M^2}\mathbf{M} \times \mathbf{M} \times \frac{\partial \mathbf{M}}{\partial x}\right] - \frac{\gamma}{1+\alpha^2}\left[-(\alpha-\beta)\frac{b_i^j}{\gamma M}\mathbf{M} \times \frac{\partial \mathbf{M}}{\partial x}\right] - \frac{\gamma}{1+\alpha^2}\left[-\frac{\theta_i^{SH} c_i^j}{\gamma}\mathbf{M} \times \left(\hat{M} \times \hat{y} - \alpha M \hat{y}\right)\right] \tag{A.0.7}$$

Remembering that

$$b_i^j = -\frac{g \mu_B P j_e}{2|e| M_s} \tag{A.0.8}$$

$$\theta_i c_i^j = \frac{\theta_i^{SH} \hbar \gamma}{2|e| M_s t_f} \tag{A.0.9}$$

with g being the Landé g-factor, M_s the saturation magnetization, j_e the current density and P the polarization. One can define the quantity $u = -\frac{b_i^j}{\gamma}$ (for consistency with ASD implementation) and obtain

$$\frac{\partial \mathbf{M}}{\partial t} = -\frac{\gamma}{1+\alpha^2}\mathbf{M} \times \left[\mathbf{B}_{\text{eff}} + \alpha \hat{M} \times \mathbf{H} - (1+\alpha\beta)\, u \hat{M} \times \frac{\partial \hat{M}}{\partial x}\right] - \frac{\gamma}{1+\alpha^2}\mathbf{M} \times \left[(\alpha-\beta)\, u \frac{\partial \hat{M}}{\partial x} + \frac{\theta_i^{SH} j_{\text{vec}}}{P t_f}\left(\hat{M} \times \hat{y} - \alpha M \hat{y}\right)\right] \tag{A.0.10}$$

This can then generalized for a current **u** in any direction

$$\begin{aligned}\frac{\partial \mathbf{M}}{\partial t} =& -\frac{\gamma}{1+\alpha^2}\mathbf{M}\times\left[\mathbf{B}_{\text{eff}}+\alpha\hat{M}\times\mathbf{B}_{\text{eff}}-(1+\alpha\beta)\,\mathbf{u}\cdot\hat{M}\times\nabla\hat{M}\right] \\ & -\frac{\gamma}{1+\alpha^2}\mathbf{M}\times\left[(\alpha-\beta)\,(\mathbf{u}\cdot\nabla)\,\hat{M}+\frac{\theta_i^{SH}u}{Pt_f}\left[\left(\hat{j}\times\hat{z}\right)\times\hat{M}-\alpha M\left(\hat{j}\times\hat{z}\right)\right]\right]\end{aligned} \tag{A.0.11}$$

References

[1] Martin Hilbert and Priscila López. The world's technological capacity to store, communicate, and compute information. *Science*, 332(6025):60–65, 2011.

[2] SINTEF. *Big Data, for better or worse: 90% of world's data generated over last two years*. [Online]. Available from: `www.sciencedaily.com/releases/2013/05/130522085217.htm`. [Accessed December 15, 2014].

[3] M. N. Baibich, J. M. Broto, A. Fert, F. Nguyen Van Dau, F. Petroff, P. Etienne, G. Creuzet, A. Friederich, and J. Chazelas. Giant magnetoresistance of (001)fe/(001)cr magnetic superlattices. *Phys. Rev. Lett.*, 61:2472–2475, Nov 1988.

[4] G. Binasch, P. Grünberg, F. Saurenbach, and W. Zinn. Enhanced magnetoresistance in layered magnetic structures with antiferromagnetic interlayer exchange. *Phys. Rev. B*, 39:4828–4830, Mar 1989.

[5] Simone Borlenghi, Weiwei Wang, Hans Fangohr, Lars Bergqvist, and Anna Delin. Designing a spin-seebeck diode. *Phys. Rev. Lett.*, 112:047203, Jan 2014.

[6] Simone Borlenghi, Stefano Lepri, Lars Bergqvist, and Anna Delin. Thermomagnonic diode: Rectification of energy and magnetization currents. *Phys. Rev. B*, 89:054428, Feb 2014.

[7] Andrii V Chumak, Alexander A Serga, and Burkard Hillebrands. Magnon transistor for all-magnon data processing. *Nat. Commun.*, 5, 2014.

[8] Stuart S. P. Parkin, Masamitsu Hayashi, and Luc Thomas. Magnetic domain-wall racetrack memory. *Science*, 320(5873):190–194, 2008.

[9] L. Berger. Prediction of a domain-drag effect in uniaxial, non-compensated, ferromagnetic metals. *J. Phys. Chem. Solid*, 35(8):947 – 956, 1974.

[10] L. Berger. Exchange interaction between ferromagnetic domain wall and electric current in very thin metallic films. *J. Appl. Phys.*, 55(6):1954–1956, 1984.

[11] L. Berger. Possible existence of a josephson effect in ferromagnets. *Phys. Rev. B*, 33:1572–1578, Feb 1986.

[12] J. Slonczewski. Conductance and exchange coupling of two ferromagnets separated by a tunneling barrier. *Phys. Rev. B*, 39:6995–7002, Apr 1989.

[13] Kjetil M.D. Hals, Arne Brataas, and Gerrit E.W. Bauer. Thermopower and thermally induced domain wall motion in (ga, mn)as. *Solid State Commun.*, 150(11–12):461 – 465, 2010.

[14] Tiago S. Machado, Tatiana G. Rappoport, and Luiz C. Sampaio. Vortex core magnetization dynamics induced by thermal excitation. *Appl. Phys. Lett.*, 100(11):112404, 2012.

[15] Zhe Yuan, Shuai Wang, and Ke Xia. Thermal spin-transfer torques on magnetic domain walls. *Solid State Commun.*, 150(11–12):548 – 551, 2010.

[16] Gerrit E. W. Bauer, Stefan Bretzel, Arne Brataas, and Yaroslav Tserkovnyak. Nanoscale magnetic heat pumps and engines. *Phys. Rev. B*, 81:024427, Jan 2010.
[17] D.C. Ralph and M.D. Stiles. Spin transfer torques. *J. Magn. Magn. Mater.*, 320(7):1190 – 1216, 2008.
[18] S. Zhang and Z. Li. Roles of nonequilibrium conduction electrons on the magnetization dynamics of ferromagnets. *Phys. Rev. Lett.*, 93:127204, Sep 2004.
[19] C. Schieback, M. Kläui, U. Nowak, U. Rüdiger, and P. Nielaba. Numerical investigation of spin-torque using the heisenberg model. *Eur. Phys. J. B*, 59(4):429–433, 2007.
[20] Xi-guang Wang, Guang-hua Guo, Yao-zhuang Nie, Guang-fu Zhang, and Zhi-xiong Li. Domain wall motion induced by the magnonic spin current. *Phys. Rev. B*, 86:054445, Aug 2012.
[21] P. Yan, X. S. Wang, and X. R. Wang. All-magnonic spin-transfer torque and domain wall propagation. *Phys. Rev. Lett.*, 107:177207, Oct 2011.
[22] D. Hinzke and U. Nowak. Domain wall motion by the magnonic spin seebeck effect. *Phys. Rev. Lett.*, 107:027205, Jul 2011.
[23] Kwang-Su Ryu, Luc Thomas, See-Hun Yang, and Stuart Parkin. Chiral spin torque at magnetic domain walls. *Nature Nanotech.*, 8(7):527–533, 2013.
[24] Kwang-Su Ryu, See-Hun Yang, Luc Thomas, and Stuart SP Parkin. Chiral spin torque arising from proximity-induced magnetization. *Nat. Commun.*, 5, 2014.
[25] Satoru Emori, Uwe Bauer, Sung-Min Ahn, Eduardo Martinez, and Geoffrey SD Beach. Current-driven dynamics of chiral ferromagnetic domain walls. *Nature Mater.*, 12(7):611–616, 2013.
[26] R. D. McMichael, D. J. Twisselmann, and Andrew Kunz. Localized ferromagnetic resonance in inhomogeneous thin films. *Phys. Rev. Lett.*, 90:227601, Jun 2003.
[27] V. Kamberský. On the landau–lifshitz relaxation in ferromagnetic metals. *Can. J. Phys.*, 48(24):2906–2911, 1970.
[28] V. Kamberský. On ferromagnetic resonance damping in metals. *Czech. J. Phys. B*, 26(12):1366–1383, 1976.
[29] J Korringa. On the calculation of the energy of a bloch wave in a metal. *Physica*, 13(6–7):392 – 400, 1947.
[30] W. Kohn and N. Rostoker. Solution of the schrödinger equation in periodic lattices with an application to metallic lithium. *Phys. Rev.*, 94:1111–1120, Jun 1954.
[31] A I Liechtenstein, M I Katsnelson, and V A Gubanov. Exchange interactions and spin-wave stiffness in ferromagnetic metals. *J. Phys. F: Met. Phys.*, 14(7):L125, 1984.
[32] A.I. Liechtenstein, M.I. Katsnelson, V.P. Antropov, and V.A. Gubanov. Local spin density functional approach to the theory of exchange interactions in ferromagnetic metals and alloys. *J. Magn. Magn. Mater.*, 67(1):65 – 74, 1987.
[33] J. M. D.. Coey. *Magnetism and Magnetic Materials*. Cambridge University Press, 2010.

[34] Jürgen Kübler. *Theory of itinerant electron magnetism*. Internat. Ser. Mono. Phys. Oxford Univ. Press, Oxford, 2000.
[35] Neil W. Ashcroft and David N. Mermin. *Solid state physics*. Thomson Learning, Toronto, 1 edition, 1976.
[36] David Bohm and David Pines. A collective description of electron interactions. i. magnetic interactions. *Phys. Rev.*, 82:625–634, Jun 1951.
[37] J. Rusz, I. Turek, and M. Diviš. Random-phase approximation for critical temperatures of collinear magnets with multiple sublattices: Gdx compounds $(x = \mathrm{Mg}, \mathrm{Rh}, \mathrm{Ni}, \mathrm{Pd})$. *Phys. Rev. B*, 71:174408, May 2005.
[38] M. E. J. Newman and G. T. Barkema. *Monte Carlo methods in statistical physics*. Clarendon Press, 1999.
[39] M. Ruderman and C. Kittel. Indirect exchange coupling of nuclear magnetic moments by conduction electrons. *Phys. Rev.*, 96:99–102, Oct 1954.
[40] Tadao Kasuya. A theory of metallic ferro- and antiferromagnetism on zener's model. *Prog. Theor. Phys.*, 16(1):45–57, 1956.
[41] Kei Yosida. Magnetic properties of cu-mn alloys. *Phys. Rev.*, 106:893–898, Jun 1957.
[42] I. Dzyaloshinsky. A thermodynamic theory of "weak" ferromagnetism of antiferromagnetics. *J. Phys. Chem. Solid*, 4(4):241 – 255, 1958.
[43] Tôru Moriya. Anisotropic superexchange interaction and weak ferromagnetism. *Phys. Rev.*, 120:91–98, Oct 1960.
[44] Lev Davidovich Landau and E Lifshitz. On the theory of the dispersion of magnetic permeability in ferromagnetic bodies. *Phys. Z. Sowjet.*, 8:153, 1935.
[45] T.L. Gilbert. A phenomenological theory of damping in ferromagnetic materials. *IEEE Trans. Magn.*, 40(6):3443–3449, Nov 2004.
[46] S. J. Blundell. Micromagnetism and the microstructure of ferromagnetic solids, by helmut kronmüller and manfred fähnle. *Contemp. Phys.*, 52(2):157–157, 2011.
[47] William Brown. Thermal fluctuations of a single-domain particle. *Phys. Rev.*, 130:1677–1686, Jun 1963.
[48] Ryogo Kubo and Natsuki Hashitsume. Brownian motion of spins. *Prog. Theor. Phys. Supp.*, 46:210–220, 1970.
[49] M. Fähnle, R. Drautz, R. Singer, D. Steiauf, and D.V. Berkov. A fast ab initio approach to the simulation of spin dynamics. *Comp. Mater. Sci.*, 32(1):118 – 122, 2005.
[50] B. Újfalussy, B. Lazarovits, L. Szunyogh, G. M. Stocks, and P. Weinberger. *Ab initio* spin dynamics applied to nanoparticles: Canted magnetism of a finite Co chain along a Pt(111) surface step edge. *Phys. Rev. B*, 70:100404, Sep 2004.
[51] P. Hohenberg and W. Kohn. Inhomogeneous electron gas. *Phys. Rev.*, 136:B864–B871, Nov 1964.
[52] Richard M. Martin. *Electronic Structure: Basic Theory and Practical Methods (Vol 1)*. Cambridge University Press, 2004.
[53] W. Kohn and L. J. Sham. Self-consistent equations including exchange and correlation effects. *Phys. Rev.*, 140:A1133–A1138, Nov 1965.
[54] Mel Levy, John P. Perdew, and Viraht Sahni. Exact differential equation for the density and ionization energy of a many-particle system. *Phys. Rev. A*, 30:2745–2748, Nov 1984.

[55] J. F. Janak. Proof that $\frac{\partial e}{\partial n_i} = \varepsilon$ in density-functional theory. *Phys. Rev. B*, 18:7165–7168, Dec 1978.
[56] W. Kohn and L. J. Sham. Self-consistent equations including exchange and correlation effects. *Phys. Rev.*, 140:A1133–A1138, Nov 1965.
[57] I. I. Mazin, M. D. Johannes, L. Boeri, K. Koepernik, and D. J. Singh. Problems with reconciling density functional theory calculations with experiment in ferropnictides. *Phys. Rev. B*, 78:085104, Aug 2008.
[58] U von Barth and L Hedin. A local exchange-correlation potential for the spin polarized case. i. *J. Phys. C: Solid State*, 5(13):1629, 1972.
[59] S. H. Vosko, L. Wilk, and M. Nusair. Accurate spin-dependent electron liquid correlation energies for local spin density calculations: a critical analysis. *Can. J. Phys.*, 58(8):1200–1211, 1980.
[60] John P. Perdew, J. A. Chevary, S. H. Vosko, Koblar A. Jackson, Mark R. Pederson, D. J. Singh, and Carlos Fiolhais. Atoms, molecules, solids, and surfaces: Applications of the generalized gradient approximation for exchange and correlation. *Phys. Rev. B*, 46:6671–6687, Sep 1992.
[61] J. P. Perdew and Alex Zunger. Self-interaction correction to density-functional approximations for many-electron systems. *Phys. Rev. B*, 23:5048–5079, May 1981.
[62] John P. Perdew and Yue Wang. Accurate and simple analytic representation of the electron-gas correlation energy. *Phys. Rev. B*, 45:13244–13249, Jun 1992.
[63] David C. Langreth and M. J. Mehl. Beyond the local-density approximation in calculations of ground-state electronic properties. *Phys. Rev. B*, 28:1809–1834, Aug 1983.
[64] John P. Perdew, Kieron Burke, and Matthias Ernzerhof. Generalized gradient approximation made simple. *Phys. Rev. Lett.*, 77:3865–3868, Oct 1996.
[65] M. T. Czyżyk and G. A. Sawatzky. Local-density functional and on-site correlations: The electronic structure of la_2cuo_4 and $lacuo_3$. *Phys. Rev. B*, 49:14211–14228, May 1994.
[66] A. I. Liechtenstein, V. I. Anisimov, and J. Zaanen. Density-functional theory and strong interactions: Orbital ordering in mott-hubbard insulators. *Phys. Rev. B*, 52:R5467–R5470, Aug 1995.
[67] Antoine Georges, Gabriel Kotliar, Werner Krauth, and Marcelo J. Rozenberg. Dynamical mean-field theory of strongly correlated fermion systems and the limit of infinite dimensions. *Rev. Mod. Phys.*, 68:13–125, Jan 1996.
[68] A. K. Rajagopal and J. Callaway. Inhomogeneous electron gas. *Phys. Rev. B*, 7:1912–1919, Mar 1973.
[69] A H MacDonald and S H Vosko. A relativistic density functional formalism. *J. Phys. C: Solid State*, 12(15):2977, 1979.
[70] D D Koelling and B N Harmon. A technique for relativistic spin-polarised calculations. *J. Phys. C: Solid State*, 10(16):3107, 1977.
[71] Stefan Blügel, Nicole Helbig, Volker Meden, and Daniel Wortmann, editors. *Computing Solids: Models, ab-initio methods and supercomputing*, volume 74 of *Schriften des Forschungszentrums Jülich Reihe Schlüsseltechnologien / Key Technologies*. Forschungszentrum Jülich GmbH Zentralbibliothek, Verlag, Jülich, Mar 2014. The Spring School was organized by the Institute for Advanced Simulationand the Peter Grünberg Institute of the

Forschungszentrum Jülich.
[72] Warren E. Pickett. Pseudopotential methods in condensed matter applications. *Compt. Phys. Rep.*, 9(3):115 – 197, 1989.
[73] David J Singh and Lars Nordstrom. *Planewaves, Pseudopotentials, and the LAPW method*. Springer Science & Business Media, 2006.
[74] Jan Zabloudil, Robert Hammerling, László Szunyogh, and Peter Weinberger. *Electron Scattering in Solid Matter: a theoretical and computational treatise*, volume 147. Springer Science & Business Media, 2006.
[75] N Papanikolaou, R Zeller, and P H Dederichs. Conceptual improvements of the kkr method. *J. Phys. Condens. Matter.*, 14(11):2799, 2002.
[76] J. Korringa. Dispersion theory for electrons in a random lattice with applications to the electronic structure of alloys. *J. Phys. Chem. Solid*, 7(2–3):252 – 258, 1958.
[77] J. L. Beeby. The density of electrons in a perfect or imperfect lattice. *P. Roy. Soc. Lond. A Mat.*, 302(1468):113–136, 1967.
[78] J. L. Beeby. Electronic structure of alloys. *Phys. Rev.*, 135:A130–A143, Jul 1964.
[79] O. Šipr, M. Košuth, and H. Ebert. Magnetic structure of free iron clusters compared to iron crystal surfaces. *Phys. Rev. B*, 70:174423, Nov 2004.
[80] R. Podloucky, R. Zeller, and P. H. Dederichs. Electronic structure of magnetic impurities calculated from first principles. *Phys. Rev. B*, 22:5777–5790, Dec 1980.
[81] Jörg Opitz, Peter Zahn, and Ingrid Mertig. *Ab initio* calculated electronic structure of metallic nanowires and nanotubes. *Phys. Rev. B*, 66:245417, Dec 2002.
[82] B. Lazarovits, L. Szunyogh, P. Weinberger, and B. Újfalussy. Magnetic properties of finite fe chains at fcc cu(001) and cu(111) surfaces. *Phys. Rev. B*, 68:024433, Jul 2003.
[83] J. M. MacLaren, S. Crampin, and D. D. Vvedensky. Layer korringa-kohn-rostoker theory for close-spaced planes of atoms. *Phys. Rev. B*, 40:12176–12182, Dec 1989.
[84] L. Szunyogh, B. Újfalussy, and P. Weinberger. Magnetic anisotropy of iron multilayers on au(001): First-principles calculations in terms of the fully relativistic spin-polarized screened kkr method. *Phys. Rev. B*, 51:9552–9559, Apr 1995.
[85] H Ebert, D Ködderitzsch, and J Minár. Calculating condensed matter properties using the kkr-green's function method—recent developments and applications. *Rep. Prog. Phys.*, 74(9):096501, 2011.
[86] N Papanikolaou, R Zeller, and P H Dederichs. Conceptual improvements of the kkr method. *J. Phys. Condens. Matter.*, 14(11):2799, 2002.
[87] M Ogura and H Akai. The full potential korringa–kohn–rostoker method and its application in electric field gradient calculations. *J. Phys. Condens. Matter.*, 17(37):5741, 2005.
[88] P.H. Dederichs, B. Drittler, and R. Zeller. A full-potential kkr green's function method for impurities in metals. In *Symposium V – Application of Multiple Scattering Theory to Materials Science*, volume 253 of *MRS Proceedings*, 1991.

[89] Masako Ogura and Hisazumi Akai. Full-potential screened korringa-kohn-rostoker method and its applications. *J. Comput. Theor. Nanos.*, 6(12):2483–2498, 2009.
[90] Alex Zunger, S.-H. Wei, L. G. Ferreira, and James E. Bernard. Special quasirandom structures. *Phys. Rev. Lett.*, 65:353–356, Jul 1990.
[91] H Neddermeyer, L P L M Rabou, and P E Mijnarends. Photoemission investigation of the electronic structure of co 0.92 fe 0.08. *J. Phys. F: Met. Phys.*, 14(1):259, 1984.
[92] P. Soven. Coherent-Potential Model of Substitutional Disordered Alloys. *Phys. Rev.*, 156:809–813, Apr 1967.
[93] G. M. Stocks, W. M. Temmerman, and B.L. Gyorffy. Complete Solution of the Korringa-Kohn-Rostoker Coherent-Potential-Approximation Equations: Cu-Ni Alloys. *Phys. Rev. Lett.*, 41:339–343, Jul 1978.
[94] Kaoru Ohno, Keivan Esfarjani, and Yoshiyuki Kawazoe. *Computational materials science: from ab initio to Monte Carlo methods*, volume 129. Springer Science & Business Media, 2012.
[95] A J Pindor, J Staunton, G M Stocks, and H Winter. Disordered local moment state of magnetic transition metals: a self-consistent kkr cpa calculation. *J. Phys. F: Met. Phys.*, 13(5):979, 1983.
[96] J. Staunton, B.L. Gyorffy, A.J. Pindor, G.M. Stocks, and H. Winter. The "disordered local moment" picture of itinerant magnetism at finite temperatures. *J. Magn. Magn. Mater.*, 45(1):15 – 22, 1984.
[97] H. Ebert, S. Mankovsky, D. Ködderitzsch, and P. J. Kelly. *Ab Initio* calculation of the gilbert damping parameter via the linear response formalism. *Phys. Rev. Lett.*, 107:066603, Aug 2011.
[98] H. Ebert, S. Mankovsky, K. Chadova, S. Polesya, J. Minár, and D. Ködderitzsch. Calculating linear-response functions for finite temperatures on the basis of the alloy analogy model. *Phys. Rev. B*, 91:165132, Apr 2015.
[99] S. Mankovsky, D. Ködderitzsch, G. Woltersdorf, and H. Ebert. First-principles calculation of the gilbert damping parameter via the linear response formalism with application to magnetic transition metals and alloys. *Phys. Rev. B*, 87:014430, Jan 2013.
[100] M Deng, H Freyer, J Voitländer, and H Ebert. Relativistic calculation of magnetic linear response functions using the korringa–kohn–rostoker green's function method. *J. Phys. Condens. Matter.*, 13(38):8551, 2001.
[101] J Benkowitsch and H Winter. A real-space method for the calculation of the orbital susceptibility of simple metals and transition metals. *J. Phys. F: Met. Phys.*, 13(5):991, 1983.
[102] W. H. Butler. Theory of electronic transport in random alloys: Korringa-kohn-rostoker coherent-potential approximation. *Phys. Rev. B*, 31:3260–3277, Mar 1985.
[103] A Oswald, R Zeller, P J Braspenning, and P H Dederichs. Interaction of magnetic impurities in cu and ag. *J. Phys. F: Met. Phys.*, 15(1):193, 1985.
[104] O. Gunnarsson and B. I. Lundqvist. Exchange and correlation in atoms, molecules, and solids by the spin-density-functional formalism. *Phys. Rev. B*, 13:4274–4298, May 1976.

[105] O. Grotheer, C. Ederer, and M. Fähnle. *Ab initio* treatment of noncollinear spin systems within the atomic-sphere approximation and beyond. *Phys. Rev. B*, 62:5601–5608, Sep 2000.
[106] L. M. Sandratskii. Energy band structure calculations for crystals with spiral magnetic structure. *Phys. Status Solidi B*, 136(1):167–180, 1986.
[107] E. Şaşıoğlu, L. M. Sandratskii, P. Bruno, and I. Galanakis. Exchange interactions and temperature dependence of magnetization in half-metallic heusler alloys. *Phys. Rev. B*, 72:184415, Nov 2005.
[108] AR Mackintosh, OK Andersen, and M Springford. *Electrons at the Fermi surface*. Cambridge University Press, Cambridge, 1980.
[109] P. Lloyd and P.V. Smith. Multiple scattering theory in condensed materials. *Adv. Phys.*, 21(89):69–142, 1972.
[110] M. Pajda, J. Kudrnovský, I. Turek, V. Drchal, and P. Bruno. *Ab initio* calculations of exchange interactions, spin-wave stiffness constants, and curie temperatures of fe, co, and ni. *Phys. Rev. B*, 64:174402, Oct 2001.
[111] J Hamrle, O Gaier, Seong-Gi Min, B Hillebrands, Y Sakuraba, and Y Ando. Determination of exchange constants of heusler compounds by brillouin light scattering spectroscopy: application to co 2 mnsi. *J. Phys. D: Appl. Phys.*, 42(8):084005, 2009.
[112] M. Plihal, D. L. Mills, and J. Kirschner. Spin wave signature in the spin polarized electron energy loss spectrum of ultrathin fe films: Theory and experiment. *Phys. Rev. Lett.*, 82:2579–2582, Mar 1999.
[113] Stephen W Lovesey. *Theory of neutron scattering from condensed matter*. Oxford University Press, 1984.
[114] A. Conca, E. Th. Papaioannou, S. Klingler, J. Greser, T. Sebastian, B. Leven, J. Lösch, and B. Hillebrands. Annealing influence on the gilbert damping parameter and the exchange constant of cofeb thin films. *Appl. Phys. Lett.*, 104(18), 2014.
[115] U. Atxitia, D. Hinzke, O. Chubykalo-Fesenko, U. Nowak, H. Kachkachi, O. N. Mryasov, R. F. Evans, and R. W. Chantrell. Multiscale modeling of magnetic materials: Temperature dependence of the exchange stiffness. *Phys. Rev. B*, 82:134440, Oct 2010.
[116] Yuli Yin, Fan Pan, Martina Ahlberg, Mojtaba Ranjbar, Philipp Dürrenfeld, Afshin Houshang, Mohammad Haidar, Lars Bergqvist, Ya Zhai, Randy K. Dumas, Anna Delin, and Johan Åkerman. Tunable permalloy-based films for magnonic devices. *Phys. Rev. B*, 92:024427, Jul 2015.
[117] S. Mühlbauer, B. Binz, F. Jonietz, C. Pfleiderer, A. Rosch, A. Neubauer, R. Georgii, and P. Böni. Skyrmion lattice in a chiral magnet. *Science*, 323(5916):915–919, 2009.
[118] Stefan Heinze, Kirsten Von Bergmann, Matthias Menzel, Jens Brede, André Kubetzka, Roland Wiesendanger, Gustav Bihlmayer, and Stefan Blügel. Spontaneous atomic-scale magnetic skyrmion lattice in two dimensions. *Nat. Phys.*, 7(9):713–718, 2011.
[119] A. Fert and Peter M. Levy. Role of anisotropic exchange interactions in determining the properties of spin-glasses. *Phys. Rev. Lett.*, 44:1538–1541, Jun 1980.

[120] A. Crépieux and C. Lacroix. Dzyaloshinsky–moriya interactions induced by symmetry breaking at a surface. *J. Magn. Magn. Mater.*, 82(3):341 – 349, 1998.
[121] E. Y. Vedmedenko, L. Udvardi, P. Weinberger, and R. Wiesendanger. Chiral magnetic ordering in two-dimensional ferromagnets with competing dzyaloshinsky-moriya interactions. *Phys. Rev. B*, 75:104431, Mar 2007.
[122] L. Udvardi, L. Szunyogh, K. Palotás, and P. Weinberger. First-principles relativistic study of spin waves in thin magnetic films. *Phys. Rev. B*, 68:104436, Sep 2003.
[123] H. Ebert and S. Mankovsky. Anisotropic exchange coupling in diluted magnetic semiconductors: *Ab initio* spin-density functional theory. *Phys. Rev. B*, 79:045209, Jan 2009.
[124] Vikas Kashid, Timo Schena, Bernd Zimmermann, Yuriy Mokrousov, Stefan Blügel, Vaishali Shah, and H. G. Salunke. Dzyaloshinskii-moriya interaction and chiral magnetism in $3d-5d$ zigzag chains: Tight-binding model and *ab initio* calculations. *Phys. Rev. B*, 90:054412, Aug 2014.
[125] Hongxin Yang, André Thiaville, Stanislas Rohart, Albert Fert, and Mairbek Chshiev. Anatomy of dzyaloshinskii-moriya interaction at Co/Pt interfaces. *Phys. Rev. Lett.*, 115:267210, Dec 2015.
[126] M. Uchida, N. Nagaosa, J. P. He, Y. Kaneko, S. Iguchi, Y. Matsui, and Y. Tokura. Topological spin textures in the helimagnet fege. *Phys. Rev. B*, 77:184402, May 2008.
[127] C. L. Degen. Scanning magnetic field microscope with a diamond single-spin sensor. *Appl. Phys. Lett.*, 92(24), 2008.
[128] L Rondin, J-P Tetienne, T Hingant, J-F Roch, P Maletinsky, and V Jacques. Magnetometry with nitrogen-vacancy defects in diamond. *Rep. Prog. Phys.*, 77(5):056503, 2014.
[129] J-P Tetienne, T Hingant, LJ Martinez, S Rohart, A Thiaville, L Herrera Diez, K Garcia, J-P Adam, J-V Kim, J-F Roch, et al. The nature of domain walls in ultrathin ferromagnets revealed by scanning nanomagnetometry. *Nat. Commun.*, 6, 2015.
[130] XZ Yu, N Kanazawa, Y Onose, K Kimoto, WZ Zhang, S Ishiwata, Y Matsui, and Y Tokura. Near room-temperature formation of a skyrmion crystal in thin-films of the helimagnet fege. *Nature Mater.*, 10(2):106–109, 2011.
[131] N. A. Porter, J. C. Gartside, and C. H. Marrows. Scattering mechanisms in textured fege thin films: Magnetoresistance and the anomalous hall effect. *Phys. Rev. B*, 90:024403, Jul 2014.
[132] A. Szilva, M. Costa, A. Bergman, L. Szunyogh, L. Nordström, and O. Eriksson. Interatomic exchange interactions for finite-temperature magnetism and nonequilibrium spin dynamics. *Phys. Rev. Lett.*, 111:127204, Sep 2013.
[133] O. Meshcheriakova, S. Chadov, A. K. Nayak, U. K. Rößler, J. Kübler, G. André, A. A. Tsirlin, J. Kiss, S. Hausdorf, A. Kalache, W. Schnelle, M. Nicklas, and C. Felser. Large noncollinearity and spin reorientation in the novel mn_2RhSn heusler magnet. *Phys. Rev. Lett.*, 113:087203, Aug 2014.
[134] Harvey Brooks. Ferromagnetic anisotropy and the itinerant electron model. *Phys. Rev.*, 58:909–918, Nov 1940.

[135] Soshin Chikazumi and Chad D Graham. *Physics of Ferromagnetism 2e*. Number 94. Oxford University Press on Demand, 2009.
[136] P Escudier. L'anisotropie de l'aimantation: un paramètre important de l'anisotrpie magnétocristalline. *Ann. Phys. Paris*, 9:125–173, 1975.
[137] J. P. Rebouillat. High resolution automatic magnetometer using a superconducting magnet: Application to high field susceptibility measurements. *IEEE Trans. Magn.*, 8(3):630–633, Sep 1972.
[138] M T Johnson, P J H Bloemen, F J A den Broeder, and J J de Vries. Magnetic anisotropy in metallic multilayers. *Rep. Prog. Phys.*, 59(11):1409, 1996.
[139] J. H. van Vleck. On the anisotropy of cubic ferromagnetic crystals. *Phys. Rev.*, 52:1178–1198, Dec 1937.
[140] Peter Mohn. *Magnetism in the solid state: an introduction*, volume 134. Springer Science & Business Media, 2006.
[141] Patrick Bruno. Tight-binding approach to the orbital magnetic moment and magnetocrystalline anisotropy of transition-metal monolayers. *Phys. Rev. B*, 39:865–868, Jan 1989.
[142] I. V. Solovyev, P. H. Dederichs, and I. Mertig. Origin of orbital magnetization and magnetocrystalline anisotropy in *TX* ordered alloys (where *T* =fe,co and *X* =pd,pt). *Phys. Rev. B*, 52:13419–13428, Nov 1995.
[143] Till Burkert, Lars Nordström, Olle Eriksson, and Olle Heinonen. Giant magnetic anisotropy in tetragonal feco alloys. *Phys. Rev. Lett.*, 93:027203, Jul 2004.
[144] Stuart Parkin and See-Hun Yang. Memory on the racetrack. *Nature Nanotech.*, 10(3):195–198, 2015.
[145] Xindong Wang, Ding sheng Wang, Ruqian Wu, and A.J. Freeman. Validity of the force theorem for magnetocrystalline anisotropy. *J. Magn. Magn. Mater.*, 159(3):337 – 341, 1996.
[146] Xindong Wang, Ruqian Wu, Ding-sheng Wang, and A. J. Freeman. Torque method for the theoretical determination of magnetocrystalline anisotropy. *Phys. Rev. B*, 54:61–64, Jul 1996.
[147] Peter Blaha, Georg Madsen, Karlheinz Schwarz, Dieter Kvasnicka, and Joachim Luitz. WIEN2k, An Augmented Plane Wave + Local Orbitals Program for Calculating Crystal Properties, 2001.
[148] J B Staunton, S Ostanin, S S A Razee, B Gyorffy, L Szunyogh, B Ginatempo, and Ezio Bruno. Long-range chemical order effects upon the magnetic anisotropy of fept alloys from an ab initio electronic structure theory. *J. Phys. Condens. Matter.*, 16(48):S5623, 2004.
[149] Yohei Kota and Akimasa Sakuma. Relationship between magnetocrystalline anisotropy and orbital magnetic moment in l10-type ordered and disordered alloys. *J. Phys. Soc. Jpn.*, 81(8):084705, 2012.
[150] M Mizuguchi, T Kojima, M Kotsugi, T Koganezawa, K Osaka, and K Takanashi. Artificial Fabrication and Order Parameter Estimation of L 1 0 -ordered FeNi Thin Film Grown on a AuNi Buffer Layer. *J. Magn. Soc. Jpn*, 35(4):370–373, 2011.
[151] Shunsuke Fukami, Hideo Sato, Michihiko Yamanouchi, Shoji Ikeda, and Hideo Ohno. CoNi Films with Perpendicular Magnetic Anisotropy Prepared by Alternate Monoatomic Layer Deposition. *Appl. Phys. Express*,

6(7):073010, July 2013.
[152] S. H. Nie, L. J. Zhu, J. Lu, D. Pan, H. L. Wang, X. Z. Yu, J. X. Xiao, and J. H. Zhao. Perpendicularly magnetized τ-MnAl (001) thin films epitaxied on GaAs. *Appl. Phys. Lett.*, 102(15):152405, 2013.
[153] Š. Pick and H. Dreyssé. Magnetic anisotropy of transition-metal thin films. *Phys. Rev. B*, 48:13588–13595, Nov 1993.
[154] Liqin Ke and Mark van Schilfgaarde. Band-filling effect on magnetic anisotropy using a green's function method. *Phys. Rev. B*, 92:014423, Jul 2015.
[155] L. Szunyogh, B. Újfalussy, U. Pustogowa, and P. Weinberger. Overlayer-dependent magnetic moment and anisotropy of a co monolayer on cu(100). *Phys. Rev. B*, 57:8838–8841, Apr 1998.
[156] J. Kuneš and V. Kamberský. First-principles investigation of the damping of fast magnetization precession in ferromagnetic 3*d* metals. *Phys. Rev. B*, 65:212411, Jun 2002.
[157] D. Steiauf and M. Fähnle. Damping of spin dynamics in nanostructures: An *ab initio* study. *Phys. Rev. B*, 72:064450, Aug 2005.
[158] Manfred Fähnle and Daniel Steiauf. Breathing fermi surface model for noncollinear magnetization: A generalization of the gilbert equation. *Phys. Rev. B*, 73:184427, May 2006.
[159] Arne Brataas, Yaroslav Tserkovnyak, and Gerrit E. W. Bauer. Scattering theory of gilbert damping. *Phys. Rev. Lett.*, 101:037207, Jul 2008.
[160] M. Oogane and S. Mizukami. Tunnel magnetoresistance effect and magnetic damping in half-metallic heusler alloys. *Philos. T. R. Soc. A*, 369(1948):3037–3053, 2011.
[161] M. Oogane, T. Kubota, Y. Kota, S. Mizukami, H. Naganuma, A. Sakuma, and Y. Ando. Gilbert magnetic damping constant of epitaxially grown co-based heusler alloy thin films. *Appl. Phys. Lett.*, 96(25), 2010.
[162] Stéphane Andrieu, Amina Neggache, Thomas Hauet, Thibaut Devolder, Ali Hallal, Mairbek Chshiev, Alexandre M. Bataille, Patrick Le Fèvre, and Fran çois Bertran. Direct evidence for minority spin gap in the Co_2MnSi heusler compound. *Phys. Rev. B*, 93:094417, Mar 2016.
[163] S. Javad Hashemifar, Peter Kratzer, and Matthias Scheffler. Preserving the half-metallicity at the heusler alloy $co_2MnSi(001)$ surface: A density functional theory study. *Phys. Rev. Lett.*, 94:096402, Mar 2005.
[164] V. P. Antropov, M. I. Katsnelson, B. N. Harmon, M. van Schilfgaarde, and D. Kusnezov. Spin dynamics in magnets: Equation of motion and finite temperature effects. *Phys. Rev. B*, 54:1019–1035, Jul 1996.
[165] B L Gyorffy, A J Pindor, J Staunton, G M Stocks, and H Winter. A first-principles theory of ferromagnetic phase transitions in metals. *J. Phys. F: Met. Phys.*, 15(6):1337, 1985.
[166] J.C. Slonczewski. Current-driven excitation of magnetic multilayers. *J. Magn. Magn. Mater.*, 159(1–2):L1 – L7, 1996.
[167] M. Hickey and J. Moodera. Origin of intrinsic gilbert damping. *Phys. Rev. Lett.*, 102:137601, Mar 2009.
[168] Satadeep Bhattacharjee, Lars Nordström, and Jonas Fransson. Atomistic spin dynamic method with both damping and moment of inertia effects included from first principles. *Phys. Rev. Lett.*, 108:057204, Jan 2012.

[169] Pui-Wai Ma and S. Dudarev. Longitudinal magnetic fluctuations in langevin spin dynamics. *Phys. Rev. B*, 86:054416, Aug 2012.
[170] U. Atxitia and O. Chubykalo-Fesenko. Ultrafast magnetization dynamics rates within the landau-lifshitz-bloch model. *Phys. Rev. B*, 84:144414, Oct 2011.
[171] K Binder. Applications of monte carlo methods to statistical physics. *Rep. Prog. Phys.*, 60(5):487, 1997.
[172] Arthur F Voter. Introduction to the kinetic monte carlo method. In *Radiation Effects in Solids*, pages 1–23. Springer, 2007.
[173] R F L Evans, W J Fan, P Chureemart, T A Ostler, M O A Ellis, and R W Chantrell. Atomistic spin model simulations of magnetic nanomaterials. *J. Phys. Condens. Matter.*, 26(10):103202, 2014.
[174] U. Atxitia, O. Chubykalo-Fesenko, R. W. Chantrell, U. Nowak, and A. Rebei. Ultrafast spin dynamics: The effect of colored noise. *Phys. Rev. Lett.*, 102:057203, Feb 2009.
[175] B Skubic, J Hellsvik, L Nordström, and O Eriksson. A method for atomistic spin dynamics simulations: implementation and examples. *J. Phys. Condens. Matter.*, 20(31):315203, 2008.
[176] K. Uchida, S. Takahashi, K. Harii, J. Ieda, W. Koshibae, K. Ando, S. Maekawa, and E. Saitoh. Observation of the spin seebeck effect. *Nature*, 455(7214):778–781, 2008.
[177] P. Grütter. *Forces in Scanning Probe Methods*, chapter Applications of Magnetic Force Microscopy, pages 447–470. Springer Netherlands, Dordrecht, 1995.
[178] L Rondin, J-P Tetienne, S Rohart, A Thiaville, T Hingant, P Spinicelli, J-F Roch, and V Jacques. Stray-field imaging of magnetic vortices with a single diamond spin. *Nat. Commun.*, 4, 2013.
[179] XZ Yu, Y Onose, N Kanazawa, JH Park, JH Han, Y Matsui, N Nagaosa, and Y Tokura. Real-space observation of a two-dimensional skyrmion crystal. *Nature*, 465(7300):901–904, 2010.
[180] Masaya Uchida, Yoshinori Onose, Yoshio Matsui, and Yoshinori Tokura. Real-space observation of helical spin order. *Science*, 311(5759):359–361, 2006.
[181] Motohiko Ezawa. Compact merons and skyrmions in thin chiral magnetic films. *Phys. Rev. B*, 83:100408, Mar 2011.
[182] S. V. Halilov, H. Eschrig, A. Y. Perlov, and P. M. Oppeneer. Adiabatic spin dynamics from spin-density-functional theory: Application to fe, co, and ni. *Phys. Rev. B*, 58:293–302, Jul 1998.
[183] S Toth and B Lake. Linear spin wave theory for single-q incommensurate magnetic structures. *J. Phys. Condens. Matter.*, 27(16):166002, 2015.
[184] Paweł Buczek, Arthur Ernst, Patrick Bruno, and Leonid M. Sandratskii. Energies and lifetimes of magnons in complex ferromagnets: A first-principle study of heusler alloys. *Phys. Rev. Lett.*, 102:247206, Jun 2009.
[185] Corina Etz, Lars Bergqvist, Anders Bergman, Andrea Taroni, and Olle Eriksson. Atomistic spin dynamics and surface magnons. *J. Phys. Condens. Matter.*, 27(24):243202, 2015.
[186] Kh. Zakeri, Y. Zhang, J. Prokop, T.-H. Chuang, N. Sakr, W. X. Tang, and J. Kirschner. Asymmetric spin-wave dispersion on fe(110): Direct evidence of

the dzyaloshinskii-moriya interaction. *Phys. Rev. Lett.*, 104:137203, Mar 2010.
[187] Lars Bergqvist, Andrea Taroni, Anders Bergman, Corina Etz, and Olle Eriksson. Atomistic spin dynamics of low-dimensional magnets. *Phys. Rev. B*, 87:144401, Apr 2013.
[188] A. Aharoni. *Introduction to the theory of ferromagnetism*. International series of monographs on physics. Clarendon Press, 1996.
[189] David Jiles. *Introduction to magnetism and magnetic materials*. Chapman and Hall, London, New York, 1991. retirage 1994.
[190] N. L. Schryer and L. R. Walker. The motion of 180° domain walls in uniform dc magnetic fields. *J. Appl. Phys.*, 45(12):5406–5421, 1974.
[191] Yoko Yoshimura, Kab-Jin Kim, Takuya Taniguchi, Takayuki Tono, Kohei Ueda, Ryo Hiramatsu, Takahiro Moriyama, Keisuke Yamada, Yoshinobu Nakatani, and Teruo Ono. Soliton-like magnetic domain wall motion induced by the interfacial dzyaloshinskii-moriya interaction. *Nat. Phys.*, 2015.
[192] C. M. Jaworski, J. Yang, S. Mack, D. D. Awschalom, J. P. Heremans, and R. C. Myers. Observation of the spin-seebeck effect in a ferromagnetic semiconductor. *Nature Mater.*, 9:898–903, Sep 2010.
[193] K. Uchida, J. Xiao, H. Adachi, J. Ohe, S. Takahashi, J. Ieda, T. Ota, Y. Kajiwara, H. Umezawa, H. Kawai, G. E. W. Bauer, S. Maekawa, and E. Saitoh. Spin Seebeck insulator. *Nature Mater.*, 9(11):894–897, September 2010.
[194] Jiang Xiao, Gerrit Bauer, Ken-chi Uchida, Eiji Saitoh, and Sadamichi Maekawa. Theory of magnon-driven spin seebeck effect. *Phys. Rev. B*, 81:214418, Jun 2010.
[195] C. M. Jaworski, J. Yang, S. Mack, D. D. Awschalom, R. C. Myers, and J. P. Heremans. Spin-seebeck effect: A phonon driven spin distribution. *Phys. Rev. Lett.*, 106:186601, May 2011.
[196] Alexey A. Kovalev and Yaroslav Tserkovnyak. Thermomagnonic spin transfer and peltier effects in insulating magnets. *Europhys. Lett.*, 97(6):67002, 2012.
[197] Wanjun Jiang, Pramey Upadhyaya, Yabin Fan, Jing Zhao, Minsheng Wang, Li-Te Chang, Murong Lang, Kin L. Wong, Mark Lewis, Yen-Ting Lin, Jianshi Tang, Sergiy Cherepov, Xuezhi Zhou, Yaroslav Tserkovnyak, Robert N. Schwartz, and Kang L. Wang. Direct imaging of thermally driven domain wall motion in magnetic insulators. *Phys. Rev. Lett.*, 110:177202, Apr 2013.
[198] J. H. Franken, P. Möhrke, M. Kläui, J. Rhensius, L. J. Heyderman, J.-U. Thiele, H. J. M. Swagten, U. J. Gibson, and U. Rüdiger. Effects of combined current injection and laser irradiation on permalloy microwire switching. *Appl. Phys. Lett.*, 95(21):212502, 2009.
[199] P. Möhrke, J. Rhensius, J.-U. Thiele, L.J. Heyderman, and M. Kläui. Tailoring laser-induced domain wall pinning. *Solid State Commun.*, 150(11–12):489 – 491, 2010.
[200] J. Prokop, W. X. Tang, Y. Zhang, I. Tudosa, T. R. F. Peixoto, Kh. Zakeri, and J. Kirschner. Magnons in a ferromagnetic monolayer. *Phys. Rev. Lett.*, 102:177206, Apr 2009.
[201] M. Pratzer, H. J. Elmers, M. Bode, O. Pietzsch, A. Kubetzka, and R. Wiesendanger. Atomic-scale magnetic domain walls in quasi-one-dimensional fe nanostripes. *Phys. Rev. Lett.*, 87:127201, Aug 2001.

[202] Anders Bergman, Andrea Taroni, Lars Bergqvist, Johan Hellsvik, Björgvin Hjörvarsson, and Olle Eriksson. Magnon softening in a ferromagnetic monolayer: A first-principles spin dynamics study. *Phys. Rev. B*, 81:144416, Apr 2010.
[203] Koichi Momma and Fujio Izumi. *VESTA3* for three-dimensional visualization of crystal, volumetric and morphology data. *J. Appl. Crystallogr.*, 44(6):1272–1276, Dec 2011.
[204] Peng Yan and Gerrit E. W. Bauer. Magnonic domain wall heat conductance in ferromagnetic wires. *Phys. Rev. Lett.*, 109:087202, Aug 2012.
[205] F. Schlickeiser, U. Ritzmann, D. Hinzke, and U. Nowak. Role of entropy in domain wall motion in thermal gradients. *Phys. Rev. Lett.*, 113:097201, Aug 2014.
[206] X. S. Wang and X. R. Wang. Thermodynamic theory for thermal-gradient-driven domain-wall motion. *Phys. Rev. B*, 90:014414, Jul 2014.
[207] Gen Tatara. Thermal vector potential theory of magnon-driven magnetization dynamics. *Phys. Rev. B*, 92:064405, Aug 2015.
[208] Se Kwon Kim and Yaroslav Tserkovnyak. Landau-lifshitz theory of thermomagnonic torque. *Phys. Rev. B*, 92:020410, Jul 2015.
[209] Peter J Metaxas, Joao Sampaio, André Chanthbouala, Rie Matsumoto, Abdelmadjid Anane, Albert Fert, Konstantin A Zvezdin, Kay Yakushiji, Hitoshi Kubota, Akio Fukushima, et al. High domain wall velocities via spin transfer torque using vertical current injection. *Sci. Rep.*, 3, 2013.
[210] Ioan Mihai Miron, Thomas Moore, Helga Szambolics, Liliana Daniela Buda-Prejbeanu, Stéphane Auffret, Bernard Rodmacq, Stefania Pizzini, Jan Vogel, Marlio Bonfim, Alain Schuhl, et al. Fast current-induced domain-wall motion controlled by the rashba effect. *Nature Mater.*, 10(6):419–423, 2011.
[211] J. Torrejon, G. Malinowski, M. Pelloux, R. Weil, A. Thiaville, J. Curiale, D. Lacour, F. Montaigne, and M. Hehn. Unidirectional thermal effects in current-induced domain wall motion. *Phys. Rev. Lett.*, 109:106601, Sep 2012.
[212] T Koyama, K Ueda, K-J Kim, Y Yoshimura, D Chiba, K Yamada, J-P Jamet, A Mougin, A Thiaville, S Mizukami, S Fukami, N Ishiwata, Y Nakatani, H Kohno, K Kobayashi, and T Ono. Current-induced magnetic domain wall motion below intrinsic threshold triggered by walker breakdown. *Nature Nanotech.*, 2012.
[213] P. Chureemart, R. F. L. Evans, and R. W. Chantrell. Dynamics of domain wall driven by spin-transfer torque. *Phys. Rev. B*, 83:184416, May 2011.
[214] Soo-Man Seo, Kyoung-Whan Kim, Jisu Ryu, Hyun-Woo Lee, and Kyung-Jin Lee. Current-induced motion of a transverse magnetic domain wall in the presence of spin hall effect. *Appl. Phys. Lett.*, 101(2), 2012.
[215] Kevin Garello, Ioan Mihai Miron, Can Onur Avci, Frank Freimuth, Yuriy Mokrousov, Stefan Blügel, Stéphane Auffret, Olivier Boulle, Gilles Gaudin, and Pietro Gambardella. Symmetry and magnitude of spin-orbit torques in ferromagnetic heterostructures. *Nature Nanotech.*, 8(8):587–593, August 2013.
[216] See-Hun Yang, Kwang-Su Ryu, and Stuart Parkin. Domain-wall velocities of up to 750 m s−1 driven by exchange-coupling torque in synthetic

antiferromagnets. *Nature Nanotech.*, advance online publication, February 2015.
[217] Guoqiang Yu, Pramey Upadhyaya, Kin L. Wong, Wanjun Jiang, Juan G. Alzate, Jianshi Tang, Pedram Khalili Amiri, and Kang L. Wang. Magnetization switching through spin-hall-effect-induced chiral domain wall propagation. *Phys. Rev. B*, 89:104421, Mar 2014.
[218] A. V. Khvalkovskiy, V. Cros, D. Apalkov, V. Nikitin, M. Krounbi, K. A. Zvezdin, A. Anane, J. Grollier, and A. Fert. Matching domain-wall configuration and spin-orbit torques for efficient domain-wall motion. *Phys. Rev. B*, 87:020402, Jan 2013.
[219] PPJ Haazen, E Murè, JH Franken, Reinoud Lavrijsen, HJM Swagten, and Bert Koopmans. Domain wall depinning governed by the spin hall effect. *Nature Mater.*, 12(4):299–303, 2013.
[220] Xiao-Liang Qi and Shou-Cheng Zhang. Topological insulators and superconductors. *Rev. Mod. Phys.*, 83:1057–1110, Oct 2011.
[221] R. B. Laughlin. Quantized hall conductivity in two dimensions. *Phys. Rev. B*, 23:5632–5633, May 1981.
[222] Y. Aharonov and D. Bohm. Significance of electromagnetic potentials in the quantum theory. *Phys. Rev.*, 115:485–491, Aug 1959.
[223] B. D. Josephson. The discovery of tunneling supercurrents. *Science*, 184(4136):527–530, 1974.
[224] Albert Fert, Vincent Cros, and João Sampaio. Skyrmions on the track. *Nature Nanotech.*, 8(3):152–156, 2013.
[225] A. N. Bogdanov and U. K. Rößler. Chiral symmetry breaking in magnetic thin films and multilayers. *Phys. Rev. Lett.*, 87:037203, Jun 2001.
[226] Junichi Iwasaki, Masahito Mochizuki, and Naoto Nagaosa. Current-induced skyrmion dynamics in constricted geometries. *Nature Nanotech.*, 8(10):742–747, 2013.
[227] UK Rößler, AN Bogdanov, and C Pfleiderer. Spontaneous skyrmion ground states in magnetic metals. *Nature*, 442(7104):797–801, 2006.
[228] T.H.R. Skyrme. A unified field theory of mesons and baryons. *Nuclear Physics*, 31:556 – 569, 1962.
[229] T. H. R. Skyrme. A non-linear field theory. *P. Roy. Soc. Lond. A Mat.*, 260(1300):127–138, 1961.
[230] AN Bogdanov and DA Yablonskii. Thermodynamically stable" vortices" in magnetically ordered crystals. the mixed state of magnets. *Zh. Eksp. Teor. Fiz*, 95:182, 1989.
[231] A. Bogdanov and A. Hubert. Thermodynamically stable magnetic vortex states in magnetic crystals. *J. Magn. Magn. Mater.*, 138(3):255 – 269, 1994.
[232] M. V. Berry. Quantal phase factors accompanying adiabatic changes. *P. Roy. Soc. Lond. A Mat.*, 392(1802):45–57, 1984.
[233] Y. Onose, T. Ideue, H. Katsura, Y. Shiomi, N. Nagaosa, and Y. Tokura. Observation of the magnon hall effect. *Science*, 329(5989):297–299, 2010.
[234] Krishna Kumar, Kai Sun, and Eduardo Fradkin. Chiral spin liquids on the kagome lattice. *Phys. Rev. B*, 92:094433, Sep 2015.
[235] Lifa Zhang, Jie Ren, Jian-Sheng Wang, and Baowen Li. Topological magnon insulator in insulating ferromagnet. *Phys. Rev. B*, 87:144101, Apr 2013.

[236] Ryo Matsumoto and Shuichi Murakami. Theoretical prediction of a rotating magnon wave packet in ferromagnets. *Phys. Rev. Lett.*, 106:197202, May 2011.
[237] Ryo Matsumoto and Shuichi Murakami. Rotational motion of magnons and the thermal hall effect. *Phys. Rev. B*, 84:184406, Nov 2011.
[238] Alexander Mook, Jürgen Henk, and Ingrid Mertig. Magnon hall effect and topology in kagome lattices: A theoretical investigation. *Phys. Rev. B*, 89:134409, Apr 2014.
[239] V. De Alfaro, S. Fubini, and G. Furlan. A new classical solution of the yang-mills field equations. *Phys. lett. B*, 65(2):163 – 166, 1976.
[240] Riccardo Hertel and Claus M. Schneider. Exchange explosions: Magnetization dynamics during vortex-antivortex annihilation. *Phys. Rev. Lett.*, 97:177202, Oct 2006.

Acta Universitatis Upsaliensis

Digital Comprehensive Summaries of Uppsala Dissertations from the Faculty of Science and Technology 1383

Editor: The Dean of the Faculty of Science and Technology

A doctoral dissertation from the Faculty of Science and Technology, Uppsala University, is usually a summary of a number of papers. A few copies of the complete dissertation are kept at major Swedish research libraries, while the summary alone is distributed internationally through the series Digital Comprehensive Summaries of Uppsala Dissertations from the Faculty of Science and Technology. (Prior to January, 2005, the series was published under the title "Comprehensive Summaries of Uppsala Dissertations from the Faculty of Science and Technology".)

Distribution: publications.uu.se
urn:nbn:se:uu:diva-287415

ACTA
UNIVERSITATIS
UPSALIENSIS
UPPSALA
2016